



THESIS APPROVED BY

4/26/18  
Date



Elton Jeffrey North, Ph.D., Chair



Victoria Roche, Ph.D.



Alekha Dash, Ph.D.



James Fletcher, Ph.D.



Gail M. Jensen, Ph.D., Dean



TITLE OF THESIS

DESIGN, SYNTHESIS AND EVALUATION OF NOVEL ANTIMYCOBACTERIAL  
COMPOUNDS TARGETING THE MMPL3 TRANSPORTER PROTEIN

---

By  
POOJA V HEGDE

---

A THESIS

Submitted to the faculty of the Graduate School of the Creighton University in  
Partial Fulfilment of the Requirements for the degree of Master of Science in the  
Department of Pharmaceutical Sciences

Omaha, NE

(April, 5<sup>th</sup>, 2018)

© Pooja V. Hegde, 2018

## ABSTRACT

Tuberculosis (TB) is an airborne infectious disease caused by *Mycobacterium tuberculosis* (*M. tb*). TB is one of the leading causes of death in developing countries. Current TB therapy requires a minimum six-month treatment and is associated with increasing drug resistance and decreased patient compliance. Therefore, new anti-TB compounds with novel mechanisms of action that have activity against resistant strains and can potentially reduce treatment duration are urgently needed. Mycolic acids are the primary lipid components in the mycobacterial cell wall and are responsible for mycobacterial cell wall integrity, permeability and virulence. Mycobacterial membrane protein large 3 (MmpL3) is an essential transporter responsible for the translocation of mycolic acids to the outer membrane. Published indole-2-carboxamides with suggested MmpL3 inhibition showed good potency, against whole-cell *M. tb*, yet had poor aqueous solubility. **This project hypothesizes that bioisosteric replacement of the indole ring, will maintain anti-tubercular activity with improved aqueous solubility leading to enhanced pharmacokinetics.** The project focuses on retaining the required pharmacophore and increasing the molecular heteroatom percentage by reducing lipophilic atoms. The designed and synthesized indole bioisosteres are pyrrole, mandelic acid and imidazole, coupled to lipophilic head groups ensuring anti-tubercular activity. In addition to minimum inhibitory concentration (MIC) determination, the active compounds were subjected to *in vitro* ADMET assays, including aqueous solubility, permeability and metabolic

stability toward mouse liver S9 fractions, to determine their suitability for further *in vivo* preclinical evaluation.

Lead compounds had improved pharmacokinetics over their indole-2-carboxamide analogs while their potency against mycobacteria varied. It was observed that an improvement in the aqueous solubility negatively impacted the anti-tubercular potency. Pyrrole analogs were found to be the best with respect to activity and had an improved solubility, permeability and were metabolically stable.

***Dedicated to my parents, Mr. Venkatesh Hegde, Mrs. Janavi Hegde, my grandparents, Mr. Madhav Bhandarkar and Mrs. Shanta Hegde and my sister Priyanka Hegde***

## **Acknowledgements**

I would like to express my gratitude to my advisor, Dr. Elton Jeffrey North for the continuous support and guidance throughout my Master's program. I am thankful to him for being my advisor and mentoring me to develop a research mind-set. I would also like to extend my gratitude to my committee members, Dr. Victoria Roche, Dr. James Fletcher and Dr. Alekha Dash, for their valuable suggestions on my research and thesis writing. I would like to thank Dr. Somnath Singh for his support and guidance throughout my stay at Creighton University in his capacity as the program director. I would also like thank Dr. Chauhan, for guiding me with my project. I am grateful for the financial assistance provided by the School of Pharmacy and Health Professions.

I am also thankful to Dr. Amit Pandya, Dan Munt and Dr. Pavan Prathipati for teaching me the operations of instruments, for their valuable suggestions and inputs. My heartfelt thanks to Dawn Trojanowski, Taunya Plater and entire administrative staff of the Department of Pharmacy Sciences for their support and assistance throughout my Master's program. I would also like to thank Dr. Mary Jackson and her research team from Colorado State University for their help with the microbial testing.

Lastly, I cannot thank my family enough, my parents, Mr. Venkatesh Hegde, Mrs. Janavi Hegde, my grandparents, Mr. Madhav Bhandarkar and Mrs. Shanta Hegde and my sister Priyanka Hegde, for their constant love, support, and belief in me. My closest friends: Siddhi Kale, Trupti Dhumal, Tejas Shanbhag, Asmita Gawde, Sugandh Pandey and Chinmay Dighe for always being there for me and making my stay away from family easier. Finally, I would like to thank Prajakta Waghmare, Tasneem Arsiwala, Rachna Nayak, Deepal Vora, Bishal Misra, Aayushi Laliwala and Shambhavi Borde for making Omaha memorable and a place I could call my home away from home.

## **Table of Contents**

Abstract	iii
Acknowledgements	vi
Table of contents	vii
List of Figures	ix
List of Tables	xiv
List of equations	xvi
List of abbreviations	xvii
<b>Chapter 1: Introduction</b>	<b>1</b>
1.1. Background	2
1.2. Drug resistant <i>M. tb</i> and current treatment	2
1.3. Types of mycobacteria	7
1.4. The mycobacterial cell wall	8
1.5. The role of MmpL3 protein	12
1.6. The medicinal chemistry of MmpL3 inhibitors	13
1.7. Summary	31
1.8. Scope and specific aims of my project	32
<b>Chapter 2: Design, synthesis and microbiological evaluation of novel anti-tubercular agents</b>	<b>34</b>
2.1. Introduction	35
2.2. Drawbacks of previous series of Ureas and ICs	35
2.3. Design of new series	38
2.4. Synthetic Scheme and mechanism of synthesis	41
2.5. Microbiological assessment	43
2.6. Conclusion	51

2.7.	Experimental	53
2.7.1	Methods and instrumentation	53
2.7.2	General synthetic method for coupling	54
2.7.3	(1 <i>R</i> ,2 <i>R</i> ,3 <i>R</i> ,5 <i>S</i> )-(-)-Isopinocampheyl-pyrrole-2-carboxamide	54
2.7.4	Cyclooctyl-pyrrole-2-carboxamide	55
2.7.5	2-Adamantyl-2-phenyl-2-hydroxy-ethanamide	55
2.7.6	4-(trans-methyl)-cyclohexyl-pyrrole-2-carboxamide	55
2.7.7	Cycloheptyl-pyrrole-2-carboxamide	55
2.7.8	Cyclooctyl-2-Phenyl-2-hydroxyl ethanamide	56
2.7.9	(1 <i>R</i> ,2 <i>R</i> ,3 <i>R</i> ,5 <i>S</i> )-(-)-Isopinocampheyl-2-Phenyl-2-hydroxyl ethanamide	56
2.7.10	Cycloheptyl-2-Phenyl-2-hydroxyl ethanamide	56
2.7.11	Trans-4-methyl-cyclohexyl-2-Phenyl-2-hydroxyl ethanamide	57
2.7.12	1-Adamantyl-2-Phenyl-2-hydroxyl ethanamide	57
2.7.13	1-Adamantyl-pyrrole-2-carboxamide	57
2.7.14	2-Adamantyl-pyrrole-2-carboxamide	57
2.7.15	2-Adamantyl-2-phenyl-2 <i>R</i> -hydroxy-ethanamide	58
2.7.16	Cyclooctyl-2-Phenyl-2 <i>R</i> -hydroxyl ethanamide	58
2.7.17	(1 <i>R</i> ,2 <i>R</i> ,3 <i>R</i> ,5 <i>S</i> )-(-)-Isopinocampheyl-2-Phenyl-2 <i>R</i> -hydroxyl ethanamide	58
2.7.18	Cycloheptyl-2-Phenyl-2 <i>R</i> -hydroxyl ethanamide	59
2.7.19	Trans-4-methyl-cyclohexyl-2-Phenyl-2 <i>R</i> hydroxyl ethanamide	59
2.7.20	1-Adamantyl-2-Phenyl-2 <i>R</i> -hydroxyl ethanamide	589
2.7.21	2-Adamantyl-2-phenyl-2 <i>S</i> -hydroxy-ethanamide	59
2.7.22	Cyclooctyl-2-Phenyl-2 <i>S</i> -hydroxyl ethanamide	60
2.7.23	(1 <i>R</i> ,2 <i>R</i> ,3 <i>R</i> ,5 <i>S</i> )-(-)-Isopinocampheyl-2-Phenyl-2 <i>S</i> hydroxyl ethanamide	60
2.7.24	Cycloheptyl-2-Phenyl-2 <i>S</i> -hydroxyl ethanamide	60
2.7.25	Trans-4-methyl-cyclohexyl-2 <i>S</i> -Phenyl-2-hydroxyl ethanamide	61
2.7.26	1-Adamantyl-2-Phenyl-2 <i>S</i> -hydroxyl ethanamide	61

2.7.27	4-(trans-methyl)-cyclohexyl-imidazole-2-carboxamide	61
2.7.28	(1 <i>R</i> ,2 <i>R</i> ,3 <i>R</i> ,5 <i>S</i> )-(-)-Isopinocampheyl-pyrrole-2-carboxamide	61
2.7.29	Cyclooctyl-imidazole-2-carboxamide	62
2.7.30	Cycloheptyl-imidazole -2-carboxamide	62
2.7.31	1-Adamantyl-imidazole -2-carboxamide	62
2.7.32	2-Adamantyl-imidazole -2-carboxamide	62
2.7.33	MIC testing	63
<b>Chapter 3: Pharmacokinetic assays of active novel compounds</b>		<b>65</b>
3.1.	Introduction	66
3.2.	Pharmacokinetic assays	66
3.3.	Solubility assay	70
3.4.	Permeability assay	80
3.5.	Protein binding assay	89
3.6.	Metabolic stability assay	96
3.7.	Experimental section	102
3.7.1.	Materials and instrumentation	102
3.7.2.	Kinetic solubility determination	102
3.7.3.	PAMPA permeability determination	103
3.7.4.	Human plasma protein binding	104
3.7.5.	S9 metabolic stability testing	105
<b>Chapter 4: Summary and future perspectives</b>		<b>106</b>
4.1.	Conclusion	107
4.2.	Global perspectives	111
4.3.	Future perspectives	112
4.3.1	Human metabolic stability testing	112
4.3.2	Toxicity studies for active compounds	112
4.3.3	MmpL3 binding assay	114
4.3.4	Prodrugs and substituted analogs	115
4.3.5	Formulation and delivery systems	118

**References**

**120**

**Appendix**

**126**

## LIST OF FIGURES

Figure 1	Sites of action for targeting mycobacteria	5
Figure 2	Structural classes of mycolic acids found in <i>M. tuberculosis</i>	9
Figure 3	Mycolic acid biosynthetic pathway	11
Figure 4	Urea and Indole-2-carboxamide as classes of MmpL3 Pharmacophore	14
Figure 5	Bioisosteric replacement from urea to indole-2-carboxamide, while retaining the pharmacophore	23
Figure 6	Summary of the pharmacophore required to act at the MmpL3	35
Figure 7	Dose response pharmacokinetics for North 2 and 21 when dosed to mice	37
Figure 8	Imidazole, a bioisostere of benzene	38
Figure 9	Design of novel scaffolds	39
Figure 10	Structures of the head groups which showed best activities in previous classes of MmpL3 inhibitors	40
Figure 11	Coupling mechanism	43
Figure 12	A representation of the four fundamental pathways of drug movement and modification in the body, the ADME processes	67
Figure 13	Method used for kinetic aqueous solubility testing	71
Figure 14	Serial dilution	72
Figure 15	LC chromatogram of standard-6 of compound <b>98</b>	73
Figure 16	Plot of area ratio v/s actual compound concentration for <b>98</b>	74

Figure 17	Closer molecular packing seen in chirally pure compounds	79
Figure 18	Drug passive diffusion from donor to acceptor plates through an artificial membrane in PAMPA setup	82
Figure 19	An example of a phosphatidylcholine, a type of phospholipid in lecithin	82
Figure 20	Plot of area ratio as a function of compound concentration for <b>95</b>	84
Figure 21	Equilibrium dialysis experiment for human plasma protein binding assay	91
Figure 22	Free drug crossing dialysis membrane and drug concentrations in both chambers	91
Figure 23	Plot of area ratio as a function of compound concentration for <b>89</b>	93
Figure 24	Plot of ln (peak area) v/s time for compound <b>95</b>	99
Figure 25	Potential compound for synthesis with a reduced cLogP as compared to an IC with the same head group	112
Figure 26	Different solubilizing groups that can be added to the indole scaffold	117
Figure 27	Example of a solubilizing groups on IC	118
Figure 28	Open ring ICs	119
Figure 29	Phosphate prodrug of mandelic acid analog activation by phosphatase	120
Figure 30	Chemical and 3D structure of cyclodextrins	121
Figure 31	Proton NMR spectra for compound <b>89</b> (Pyrrole-2-carboxamide)	128
Figure 32	Carbon NMR spectra for compound <b>89</b>	129

Figure 33	HPLC chromatogram and parameters for compound <b>89</b>	130
Figure 34	Mass spectra for compound <b>89</b>	131
Figure 35	Proton NMR spectra for compound <b>112</b> (Imidazole-2-carboxamide)	132
Figure 36	Carbon NMR spectra for compound <b>112</b>	133
Figure 37	HPLC chromatogram and parameters for compound <b>112</b>	134
Figure 38	Mass spectra for compound <b>112</b>	135
Figure 39	Proton NMR spectra for compound <b>103</b> (Racemic mandelic acid)	136
Figure 40	Carbon NMR spectra for compound <b>103</b>	137
Figure 41	Mass spectra for compound <b>103</b>	138
Figure 42	Proton NMR spectra for compound <b>121</b> (R-(-)-mandelic acid)	139
Figure 43	Carbon NMR spectra for compound <b>121</b>	140
Figure 44	Mass spectra for compound <b>121</b>	141
Figure 45	Proton NMR spectra for compound <b>122</b> (S-(+)-mandelic acid)	142
Figure 46	Carbon NMR spectra for compound <b>122</b>	143
Figure 47	Mass spectra for compound <b>122</b>	143
Figure 48	2D NMR for North <b>89</b>	146

## LIST OF TABLES

Table 1	MmpL proteins and their functions	13
Table 2	Effects of different substitutions at N-1 on the MIC	16
Table 3	Structures and MICs of the phenyl adamantyl-ureas	18
Table 4	Structures and MICs of the phenyl-adamantyl-phenyl-ureas	19
Table 5	<i>In vitro</i> whole cell anti-TB activity and cLogP of 1-(1-adamantyl)-3-heteroaryl ureas	20
Table 6	MIC values for compounds with modifications on the urea linker	22
Table 7	IC derivatives studied for activity profiles by testing MIC	26
Table 8	MIC and cLogP values of IC Analogs	28
Table 9	MIC and cLogP Values of IC Analogs	30
Table 10	Activity of pyrrole-2-carboxamides against mycobacteria	46
Table 11	Activity of imidazole-2-carboxamides against mycobacteria	47
Table 12	Activity of racemic mixture of mandelic acid analogs against mycobacteria	49
Table 13	Activity of S-Mandelic acid analogs against mycobacteria	49
Table 14	Activity of R-Mandelic acid analogs against mycobacteria	50
Table 15	Actual and calculated concentrations, AUC and area ratios for compound <b>98</b>	73
Table 16	Results for the kinetic aqueous solubility assay	77
Table 17	Actual and calculated concentrations, AUC and area ratios for compound <b>95</b>	84

Table 18	Acceptor, donor and drug equilibrium concentrations of active compounds that have been used for the calculation of the apparent permeability ( $P_e$ ) and the fraction retained in the membrane (R)	87
Table 19	Actual and calculated concentrations, AUC and area ratios for compound <b>89</b>	90
Table 20	Percentage of compound bound to plasma proteins, unbound and bound concentrations of compounds tested for protein binding	96
Table 21	Time, peak areas and natural logs of peak areas for compound <b>95</b>	98
Table 22	Half-lives of compounds over time after incubating with S9 fraction	100
Table 23	A summary of <i>M. tb</i> MIC, cLog P, solubility, plasma protein binding, half-life, $P_e$ , and fraction retained in the membrane (R) for active compounds from the mini-series	109
Table 24	Melting point table	147

## LIST OF EQUATIONS

Equation 1	Apparent permeability ( $P_e$ ) calculation	86
Equation 2	Compound retention in the membrane ( $R$ ) calculation	86
Equation 3	Equation for calculation of the elimination rate constant ( $k$ ) for first- order reactions	94
Equation 4	Equation for calculation of half-life, for first-order reactions	94

## LIST OF ABBREVIATIONS

WHO: World Health Organization

TB: Tuberculosis

*M. tb*: *Mycobacterium tuberculosis*

MIC: Minimum inhibitory concentration

MDR-TB: Multi-drug resistant TB

XDR-TB: Extensively-drug resistant TB

FDA: Food and Drug Administration

MB: Multibacillary

cLog P: Calculated log P

GI: gastrointestinal

TMM: Trehalose Monomycolate

ROS: Reactive oxygen species

SAR: Structure activity relationship

CFU: Colony Forming Units

TLC: Thin Layer Chromatography

NMR: Nuclear Magnet Resonance

HPLC: High Performance Liquid Chromatography

LC: Liquid Chromatography

IC: Indole-2-carboxamide

MmpL: Mycobacterial membrane protein large

ADME: Absorption, Distribution, Metabolism and Elimination

TEA: Triethylamine

NAD: Nicotinamide Adenine Dinucleotide

TMS: Tetramethylsilane

ESI: Electrospray Ionization

MS: Mass Spectrometry

m/z: Mass to charge

PC: Pyrrole-2-carboxamides

DMSO: Dimethylsulfoxide

Log P: The log transformed partition coefficient

PDA: Photo Diode Array

AUC: Area under the Curve

USP: United States Pharmacopoeia

COPD: Chronic Obstructive Pulmonary Disease

CF: Cystic Fibrosis

PAMPA: Parallel Artificial Membrane Permeation Assay

PVDF: Polyvinylidene Fluoride

PBS: Phosphate Buffer Solution

$P_e$ : Apparent permeability

R: Fraction of the compound that is retained in the membrane

Ln: Natural log

## **Chapter 1: Introduction**

## 1.1. **Background**

Tuberculosis (TB) is an airborne infectious disease caused by *Mycobacterium tuberculosis* (*M. tb*) that predominantly affects the lungs and upper respiratory tract. It causes sickness in millions of people each year and in 2015 was one of the top 10 causes of death worldwide, ranking above HIV/AIDS as one of the leading causes of death from an infectious disease.[1] In 2016, 10.4 million people were infected with TB, and 1.7 million died from the disease.[2, 3] TB can be caused by strains of *M. tb* that are resistant to currently available drugs for the treatment of the disease.[4] Therefore, there is a critical need to develop novel anti-TB agents to combat the prevalent TB infections and threat of growing TB resistance.

## 1.2. **Drug resistant *M. tb* and current treatment**

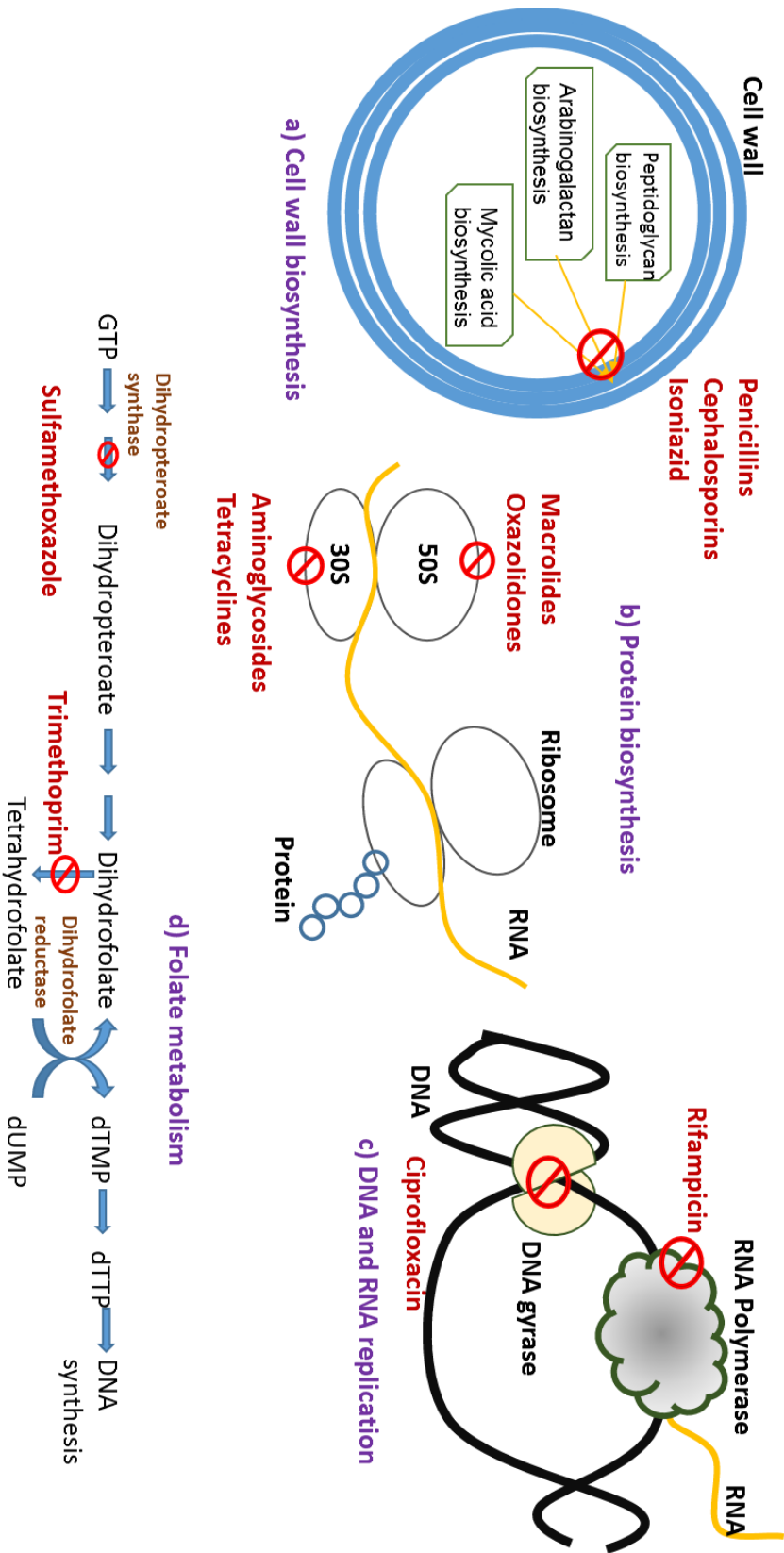
Currently, four first-line drugs are being used against *M. tb* infections. These drugs namely, isoniazid, rifampicin, ethambutol and pyrazinamide, will be described in detail shortly.[5] Microbiologically, drug resistant TB strains are classified based on their antibacterial sensitivity patterns. These classifications of TB resistance include: multi-drug-resistant (MDR) *M. tb* that are resistant to at least isoniazid and rifampicin; extensively drug-resistant (XDR) *M. tb* that are resistant to isoniazid and rifampicin as well as any fluoroquinolone and at least one second-line injectable drug (capreomycin, kanamycin, amikacin); and totally drug-resistant bacteria, where the *M. tb* strain is resistant to the first-line agents as well as the second-line agents.[6] To treat the multi-drug resistant and the extensively-drug

resistant strains and to improve therapy for the drug susceptible strains, new anti-TB compounds, with novel mechanisms of action which may i) shorten current treatment regimens against drug-susceptible *M. tb* strains and ii) be effective against drug-resistant *M. tb* strains, need to be synthesized and studied.

Epidemiologically, drug-resistance in TB can be classified into three categories based on the origination of drug resistance: primary, acquired, and initial.[7] Primary resistance occurs when previously untreated patients are infected by drug-resistant *M. tb*, mainly due to an outside source of resistant bacilli. Acquired resistance occurs in patients who initially have drug-susceptible *M. tb* that later become resistant because of inadequate, inappropriate or irregular treatment or, more importantly, because of patient nonadherence to treatment protocols.[8] Initial resistance occurs when patients deny previous treatment but their prior drug use history cannot be verified. This category consists of true primary resistance and an unknown amount of undisclosed acquired resistance.[9] In the case of acquired resistance, *M. tb* is believed to develop resistance by spontaneous chromosomal mutations.[8] According to a multicenter research conducted in India, the rates of acquired resistance were consistently higher than the rates of initial drug resistance.[7]

*M. tb* presents challenges for antibacterial treatment because it is a slow growing bacterium that can exist in an actively growing phase as well as a dormant or latent phase. The treatment, for both active and dormant bacteria, requires a six-month minimum treatment with the first two months of 'intensive phase' administration of four first-line drugs: isoniazid, rifampicin, pyrazinamide and

ethambutol or streptomycin which target the actively growing bacteria. The later four-month 'continuation phase' treatment kills the dormant bacteria and consists of the two most effective anti-TB drugs isoniazid and rifampicin.[10] Each of these drugs target different microbiological sites and have different mechanisms of action to prevent growth of the mycobacterium.[11] Classically, antibiotics exert pharmacologic action by selectively targeting biochemical differences between mammalian cells and bacterial cells. The four main biochemical targets in bacteria include, cell-wall biosynthesis, protein biosynthesis, DNA and RNA replication, and folate metabolism (Figure 1).



**Figure1:** Sites of action for targeting mycobacteria (Modified from C. Walsh, *Nat. Rev. Microbiol.*, **2003**, 1, 65-70[2])

Mechanisms of action for the currently marketed first-line anti-TB drugs (isoniazid, rifampicin, ethambutol, pyrazinamide and streptomycin) are summarized below. Isoniazid (INH) is one of the most widely used anti-TB drugs, since it also kills the dormant *M. tb*, for the susceptible strains.[12] INH penetrates the host cell and diffuses across the membrane easily and hence shows a good pharmacokinetic profile.[13] INH is a prodrug and must be activated by *M. tb* catalase-peroxidase enzyme KatG, the activation of isoniazid produces oxygen-derived free radicals (superoxide, hydrogen peroxide, etc.) and the INH free radical. This INH free radical covalently binds with nicotinamide adenine dinucleotide (NAD<sup>+</sup>). This is the active form of INH and inhibits the reductase InhA.[14] These free radicals inhibit the formation of mycolic acids of the bacterial cell wall, causing DNA damage and, subsequently, the death of the bacillus.[6] Rifampicin (RIF) acts as an inhibitor of protein synthesis. It inhibits the gene transcription of mycobacteria by blocking the DNA-dependent RNA polymerase, which prevents the bacillus from synthesizing messenger RNA and protein, causing cell death.[12, 13] Ethambutol (EMB) acts as a cell wall biosynthesis inhibitor by preventing the synthesis of arabinogalactan, which is an important polysaccharide on the mycobacterial cell wall. EMB inhibits the arabinosyltransferase enzyme encoded by the *embB* gene, which mediates the polymerization of arabinose into arabinogalactan and thus causes weakening of the mycobacterial cell wall and eventually cell death.[13] The mechanism of action of pyrazinamide (PYR) is not well understood but it is hypothesized to act at the level of mycolic acid biosynthesis.[15] It is a prodrug and requires to be converted

to pyrazinoic acid inside the bacterial cell.[15] The accumulation of pyrazinoic acid decreases the intracellular pH to levels that cause the inactivation of enzymes- such as fatty acid synthase I, which plays a fundamental role in synthesizing fatty acids-and, consequently, the impairment of mycolic acid biosynthesis and cell death.[6] Streptomycin acts against the mycobacterial species through their binding to the 30S ribosomal subunit, which affects polypeptide synthesis, ultimately resulting in inhibition of translation hence preventing protein biosynthesis.[6]

*M. tb* is slow growing and exists as both, active and dormant forms, hence multi-drug therapy is preferred, since it targets both the forms and hinders various steps involved in mycobacterial growth and replication. In addition, combination therapy prevents the rise of resistant strains by attacking multiple targets at once. The long duration of treatment promotes poor patient tolerability of the current regimens and represents important challenges in existing medication. Most of the anti-tubercular drugs have a wide spectrum of adverse effects due to which patient compliance is reduced, which is the major cause of development of drug-resistant strains of mycobacterium.[16]

### **1.3. Types of mycobacteria**

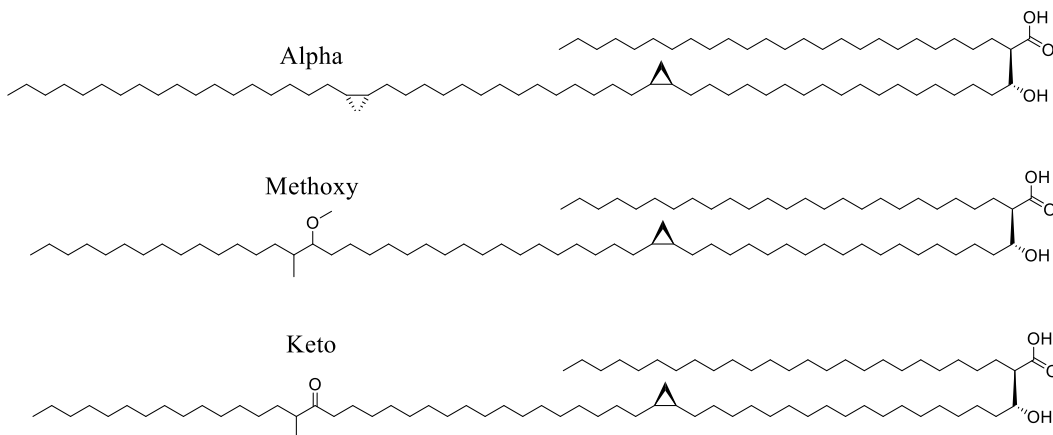
Mycobacteria are aerobic, non-motile organisms that appear positive with acid-fast alcohol stains.[17] A variety of mycobacterial species are found in nature and they are broadly classified as tuberculous mycobacteria and non-tuberculous mycobacteria (NTM). Under the microscope, NTM and *M. tb* appear quite similar. *M. chelonae* is an atypical fast-growing mycobacteria that is a rare cause of human

infection. In 1996, clinically important NTM, including *M. kansasii*, *M. genavense*, *M. marinum*, *M. simiae*, *M. scrofulaceum*, *M. szulgai*, *M. avium*, *M. haemophilum*, *M. intracellulare*, *M. malmoense*, *M. ulcerans*, *M. xenopi*, *M. abscessus*, *M. chelonae*, *M. fortuitum*, and (rarely) *M. smegmatis* were noted.[18] Although over 150 different species of NTM have been described thereafter. NTM are typically opportunistic pathogens that infect patients with structural lung disorders, such as chronic obstructive pulmonary disease (COPD) and cystic fibrosis (CF). Similar to TB, NTM infections can occur throughout the body. The most commonly described attributable human infections are pulmonary infections, lymphadenitis, and skin and soft tissue infections.[19] The pulmonary infections are most commonly due to *M. avium* complex (MAC), *M. kansasii*, and the *M. abscessus* complex (MABSC).[20] Historically, among the whole panel of mycobacteria described above, *M. tb* was found to cause the majority of the human infections in developing nations. However, recently, it has been found that the cases of human infection due to the NTM species are drastically increasing.[20] NTM related death numbers are rising and are unevenly distributed in the United States.[21] The prevalence of diseases caused by NTM was reported to be between 1.6 and 1.8 per 100,000 population in the 1980s, but recent North American studies have reported a higher prevalence of 14.1 per 100,000. [22]

#### **1.4. The mycobacterial cell wall**

The mycobacterial cell wall consists of several layers including the plasma membrane, a peptidoglycan layer, a mycolic acid layer and an arabinogalactan polysaccharide layer.[23] Due to these layers, the mycobacterial cell wall is not

easily permeated. The mycobacterial cell wall contains large alpha-alkylated  $\beta$ -hydroxylated fatty acids called mycolic acids. Three distinct structural classes of mycolic acids are found in *M. tb*, as shown below in Figure 2.[24] The mycolic acids have varying functions based on the structural class that they belong to.

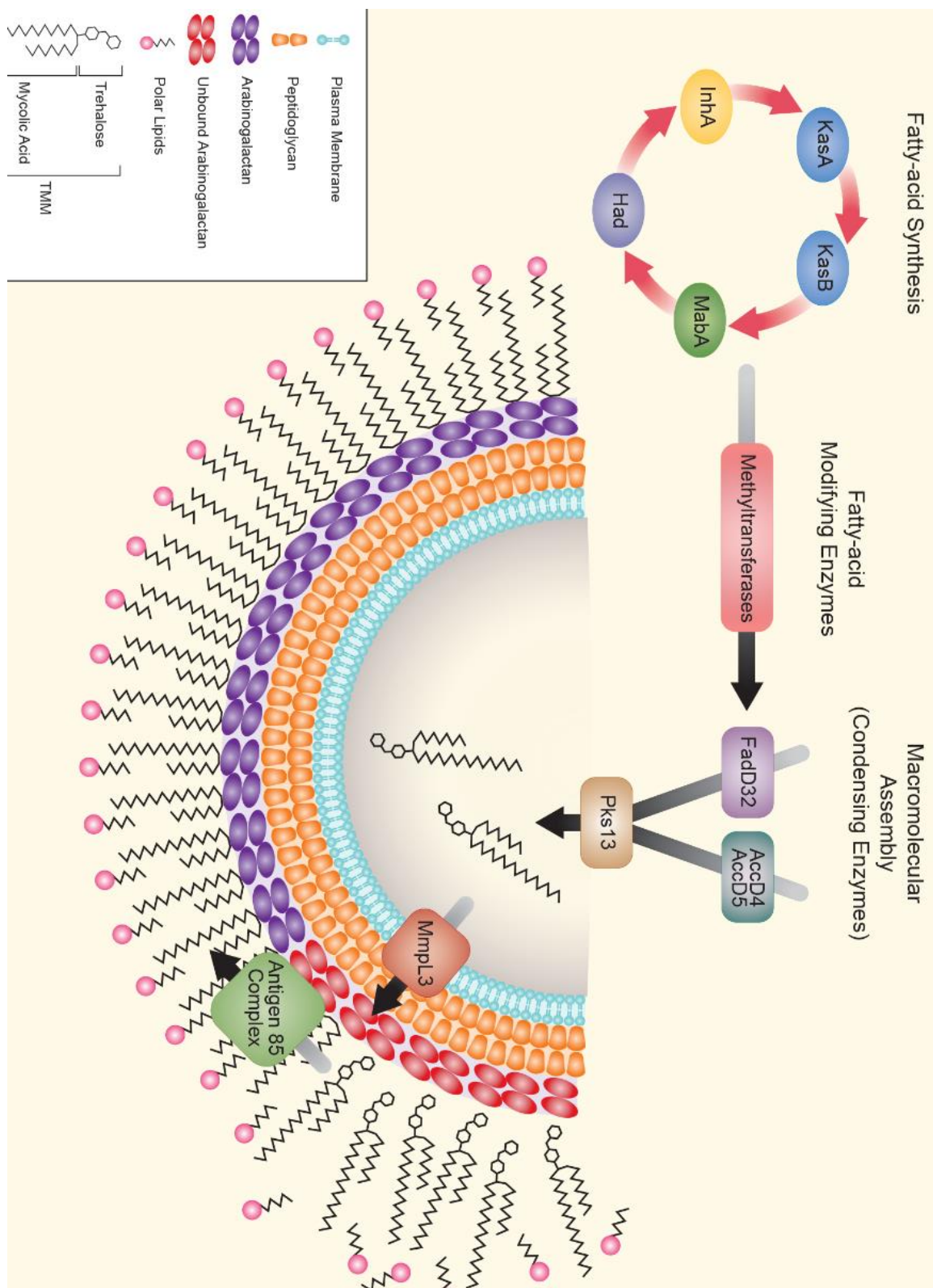


**Figure 2:** Structural classes of mycolic acids found in *M. tuberculosis*

Mycolic acids are unique to mycobacteria and are the primary lipid constituents of the mycobacterial cell wall and contribute to outer membrane permeability and integrity as well as virulence.[25, 26] The mycolic acid biosynthetic pathway is described herein and shown in Figure 3. The saturated  $\alpha$ -alkyl chain ( $C_{22} - C_{26}$ ) and the long meromycoloyl chain ( $C_{40} - C_{60}$ ) are synthesized by the fatty-acid synthase-I (FAS-I) and fatty-acid synthase-II (FAS-II) complexes, respectively.[24] The fatty acid modifying enzymes, such as desaturases, dehydratases/isomerases, and methyl transferases, add additional functional groups to the meromycoloyl chain. These fatty acid modifying enzymes, introduce double bonds, cyclopropyl, methoxy and keto functionalities which are essential,

since the mycolic acids are characterized into sub-classes based on these functional groups, as seen in Figure 2.[24] Once the  $\alpha$ -chain is carboxylated by acyl-CoA carboxylases (AccD4 or AccD5) and the meromycoloyl chain is adenylated by FadD32, the activated  $\alpha$ - and meromycoloyl chains are coupled together via Claisen condensation by acyl-AMP ligase, FadD32 and polyketide synthase, Pks13 which form the macromolecular assembly. [27] The product is a mycolic acid coupled to trehalose which is then shuttled to the periplasm as a trehalose monomycolate (TMM) by MmpL3, a fatty acid transporter protein (referred to as the third mycobacterial membrane protein large – MmpL3). Once TMM has been shuttled extracellularly, it is attached to the arabinogalactan layer or to another molecule of trehalose monomycolate (TMM) to form the free lipid trehalose dimycolate (TDM) by the antigen 85 complex.[14] This improves the strength and integrity of the cell wall. The mycolic acid biosynthetic pathway, described above, is shown in Figure 3.

The mycolic acid biosynthetic pathway contains many essential mycobacterial targets that can be exploited by novel chemotherapeutic intervention. Isoniazid (INH) is a current front-line anti-TB drug, which acts to inhibit the mycolic acid biosynthetic pathway through InhA inhibition, validating the importance of this pathway and its clinical utility as a target for anti-tubercular therapy.[26, 28] Since one of the most powerful anti-TB agent acts to inhibit the same pathway as our putative target, which is the MmpL3 transporter protein, it justifies the discovery and development of MmpL3 inhibitors.



**Figure 3:** Mycolic acid biosynthetic pathway (*Curr. Pharm. Des.*, 2014, 58(11), 6413-23)[14]

### 1.5. The role of MmpL3 protein

Mycobacterial species have a lipid rich, hydrophobic cell wall, which is substantially thicker than most other bacteria.[17] Mycobacteria are impermeable to hydrophilic nutrients and resistant to disinfectants and many antibiotics due to the thickness and lipophilic composition of the cell wall.[23] In case of the drug susceptible strains, the agents that target unique sites than the front-line anti-TB drugs, may lead to combination therapy improving duration of action and shorten the treatment. [29] MmpL3 is an essential transporter protein and an interesting novel target for synthetic chemical inhibitors to disrupt cell-wall biosynthesis.

MmpL proteins belong to the RND (resistance, nodulation and cell division) family of proteins and are involved in the transport of various compounds across the cell wall. The *M. tb* genome codes for twelve MmpL proteins.[30] Only MmpL3 is essential for TB viability since it plays an important role in the mycobacterial cell wall biosynthetic pathway, responsible for the bacteria's viability.[4] MmpL11 coordinates the transport of mono-meromycolyl diacylglycerol and mycolate ester wax.[31] MmpL5 and MmpL7 are involved in drug efflux and MmpL8 has been shown to transfer sulfolipid-1 (SL-1) to the cell envelope.[31] Recently, MmpL10 was shown to be involved in the translocation of acylated trehaloses.[32] Among all the MmpL proteins, MmpL3 has been studied the most as a possible target of anti-mycobacterial drugs since MmpL3 protein is essential. Mycolic acid transport is important for the cell wall synthesis, growth and development of *M. tb*, the inhibition of this step can prevent the growth of *M. tb*. Table 1 summarizes the functions of MmpL subtypes.

**Table 1:** MmpL proteins and their functions [31]

Sub-type of MmpL protein	Function
MmpL3	Translocation of mycolic acids in the form of TMM from their production site in the cytoplasm into the cell envelope
MmpL5, MmpL7	Involved in drug efflux
MmpL8	Transfers SL-1 to the cell envelope
MmpL10	Involved in the translocation of acylated trehaloses
MmpL11	Co-ordinates the transport of monomeromycolyl diacylglycerol and mycolate ester wax

MmpL3 is a membrane associated protein, and contains 12 transmembrane (TM) domains and two non-TM loops, L1 and L2 of sizes 151 and 142 amino acids, respectively. The crystal structure of the protein has not yet been confirmed due to its large and lipophilic molecular structure. With the help of docking studies, it was hypothesized that the residues lining the putative inhibitor binding site are serine 288 and 325, aspartate 640, arginine 259 and tyrosine 252 residues.[33] Other hydrophobic residues may be isoleucine 248, 256, 291 and 292, valine 278, 285 and 643, alanine 281, phenylalanine 644 and proline 330.[33]

### 1.6. The medicinal chemistry of MmpL3 inhibitors

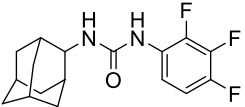
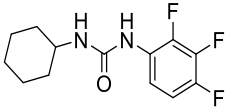
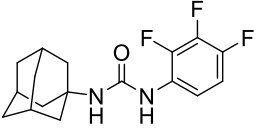
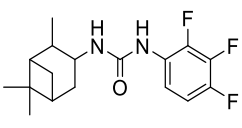
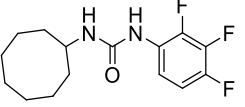
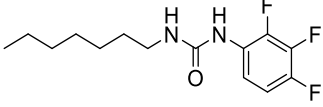
Generally, there are two major classes of MmpL3 inhibitors possessing the same pharmacophore requirements. These classes include:



## SAR: Structure-Activity Relationship

Different aliphatic substituents such as cyclohexyl, cyclooctyl, n-octyl, n-heptyl, adamantyl and other substituents were evaluated on N-1 (R<sub>1</sub>), keeping the aryl substituent on N-3 constant as 2, 3, 4-trifluorophenyl group (as shown in Table 2). The maximum potency was obtained when the saturated bulky group on N-1 was a 2-adamantyl ring (Table 2: **1**, MIC = 0.01 µg/mL). As bulky aliphatic rings are reduced in number of carbons, as shown with the cyclohexyl analog (Table 2: **4**, MIC = 12.5 µg/mL), MIC values are significantly reduced. However, when lipophilicity and bulkiness of cyclohexane is increased, anti-tubercular potency is significantly improved as seen with isopinocampheyl group **5** (MIC = 0.02 µg/mL). Uncyclized aliphatic straight chains, such as n-heptyl, were also found to be detrimental for activity (Table 2: **6**). Hence, it was observed that bulky cyclic aliphatic groups had the best MIC values.

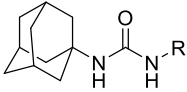
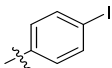
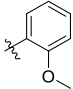
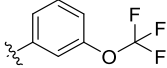
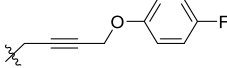
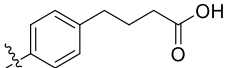
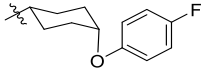
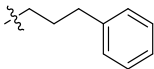
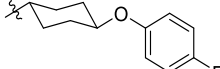
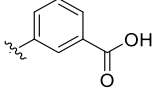
**Table 2:** Effects of different substitutions at N-1 on the MIC.[35]

No.	Compound	<i>M. tb</i> MIC ( $\mu\text{g/mL}$ )	No.	Compound	<i>M. tb</i> MIC ( $\mu\text{g/mL}$ )
1		0.01	4		12.5
2		0.4	5		0.02
3		0.8	6		6

When the aromatic ring on N-3 is a benzene ring and the saturated ring on N-1 is a 1-adamantane ring it forms a 1-(1-adamantyl)-3-phenyl urea. The 1-(1-adamantyl)-3-phenyl urea with substituents on the phenyl group were evaluated for their anti-tubercular activity (Table 3 and 4). The halogenated substituents, as shown with the 4-iodo (Table 3: **7**, MIC = 0.6  $\mu\text{g/mL}$ ) and 3-trifluoromethoxy (Table 3: **8**, MIC = 0.2  $\mu\text{g/mL}$ ) groups were found to be most active, whereas compounds with ionizable carboxylic acid groups showed significantly reduced MIC values, (Table 3: **9**, **11**). Substituents on the para and meta positions of the phenyl ring (Table 3: **7**, **8**) had varied effects on the potency of the compound, but had MIC values below 11  $\mu\text{g/mL}$ , whereas the ortho substituents resulted in a significant loss of potency (Table 3: **12**). This loss of activity could be due to increased steric

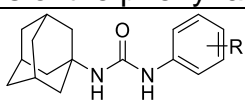
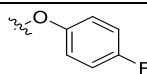
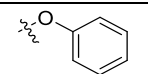
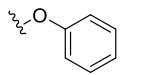
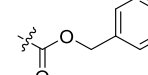
hindrance resulting in a non-bioactive conformation (with an exception for fluorine, due to its small size). [35] Compounds in which the aromatic group of adamantyl phenyl ureas were attached to the urea moiety via nonaromatic linker groups, such as short alkanes or alkynes, retained activity (Table 3: **10, 13**) whereas cyclohexyl spacer groups (Table 3: **14, 15**) in either the cis or trans configuration in which the phenyl groups were attached by an ether linkage essentially lost all activity. This could suggest that the binding site cannot accommodate bulky spacer groups. Bulky spacer groups may cause steric hindrance which might affect the binding of the molecule to the site of action.[35]

**Table 3:** Structures and MICs of the phenyl adamantyl-ureas [35]

					
No.	R	<i>M. tb</i> MIC (µg/mL)	No.	R	<i>M. tb</i> MIC (µg/mL)
7		0.6	12		30
8		0.2	13		0.7
9		36	14		>20
10		0.7	15		>39
11		7.8			

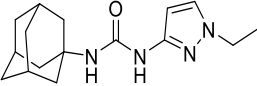
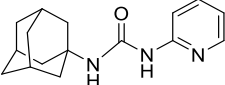
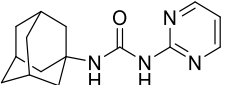
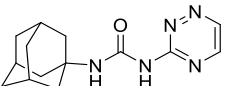
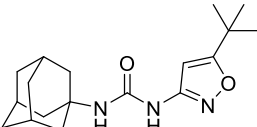
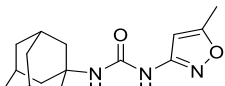
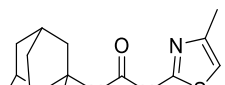
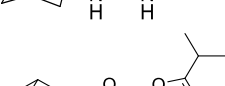
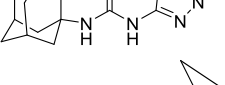
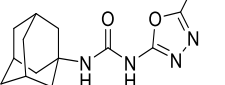
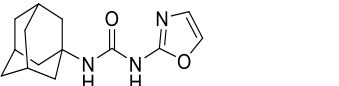
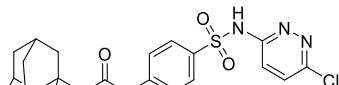
The attachment of a second phenyl ring to the phenyl adamantyl ureas via an ether linkage led to compounds with MIC values below 1 µg/mL (Table 4: **16**, **17**). The activity depended on the position of attachment on the phenyl ring. Moving the phenoxy substituent from the para position to the meta position resulted in decreased activity (Table 4: **17**, **18**). However, the presence of an ester linker between the two phenyl ring decreases the steric bulk, hence improving activity (Table 4: **19**).

**Table 4:** Structures and MICs of the phenyl-adamantyl-phenyl-ureas[35]

					
No	R	<i>M. tb</i> MIC ( $\mu\text{g/mL}$ )	No.	R	<i>M. tb</i> MIC ( $\mu\text{g/mL}$ )
<b>16</b>	para 	0.6	<b>18</b>	meta 	3.4
<b>17</b>	para 	0.01	<b>19</b>	meta 	0.3

Calculated LogP (cLogP) is the theoretical logarithm of the octanol:water partition coefficient and is often used as an aqueous solubility surrogate. Compounds with low hydrophilicities and therefore high LogP typically have high aqueous solubility values. However, these compounds have poor permeability because they are not lipophilic enough to diffuse across the cell membrane. Typical cLogP values for the urea class were ranging from 3.51 for compound **1** to 3.86 for compound **6**. The high cLogP value corresponds to low aqueous solubility, for compound **1**, it was found to be less than 0.1  $\mu\text{g/mL}$ , which in turn negatively affects their pharmacokinetic profile.[36] Hence in order to overcome the problems posed by the phenyl-adamantyl ureas, a new series of 1-adamantyl-3-heteroaryl ureas, with reduced cLogP values were synthesized by replacing the phenyl substituent of the original series with pyridines, pyrimidines, triazines, oxazoles, isoxazoles, oxadiazoles, pyrazoles and aromatic sulfonamides (Table 5). These aromatic rings were designed with reduced cLogP values which could potentially increase aqueous solubility. [26]

**Table 5:** *In vitro* whole cell anti-TB activity and cLogP of 1-(1-adamantyl)-3-heteroaryl ureas[36]

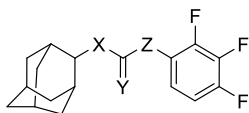
No.	Compound	<i>M. tb</i> MIC ( $\mu\text{g/mL}$ )	Solubility ( $\mu\text{g/mL}$ )	cLogP
20		25	$10.5 \pm 0.1$	2.9
21		200	$1.4 \pm 0.2$	3.2
22		200	$6.9 \pm 1.5$	2.6
23		200	$6.8 \pm 0.3$	2.1
24		0.10	$22.7 \pm 2.2$	5.3
25		6.25	$25.5 \pm 2.8$	4.0
26		1.56	$1.5 \pm 0.2$	4.7
27		1.56	$10.1 \pm 4.0$	3.9
28		3.13	$4.8 \pm 2.6$	3.4
29		12.5	$14.9 \pm 2.7$	3.5
30		25	$20.7 \pm 0.2$	3.6
31		25	$27.3 \pm 0.9$	3.1

The pyridines, pyrimidines and triazines (Table 5: **20, 21, 22, 23**) were found to have poor anti-TB activity. Pyrimidine analogs were also evaluated and it was observed that on substituting an additional nitrogen in the 2-pyrimidinyl analog (Table 5: **22**) poor anti-TB activity was retained. Also, introduction of a third nitrogen did not enhance anti-TB activity (Table 5: **23**). The pyrimidine analogs showed an enhancement in solubility, but showed a loss in their anti-TB potency. Heteroaryl rings such as oxazoles, isoxazoles, oxadiazoles and pyrazoles were modified to modulate MIC and solubility, the ethyl substituted pyrazoles (Table 5: **20**) were found to be active. Pyrazole and pyrimidine rings, both are two nitrogen containing rings, but the size of the ring differs. The 6-membered pyrimidine ring was found to be inactive as compared to the 5- membered pyrazole ring, which was slightly active. To help increase the solubility of adamantyl ureas, oxazole and isoxazole rings were introduced (Table 5: **24, 25, 29**). Introduction of an alkyl group to the 5-position of the isoxazole showed increased activity, but decreased solubility (Table 5: **24**). Addition of a bulkier lipophilic group at the 5-position such as the tertiary butyl group enhanced potency over the 5-methyl analogs (Table 5: **24, 25**). To increase solubility of the isoxazole series, a more polar oxadiazole ring was substituted and increasing substituent lipophilicity in the 5-position of the oxadiazole ring, with isopropyl and cyclopropyl groups (Table 5: **27, 28**), increased anti-TB activity. The sulfonamide antibiotics, which have ionizable groups in the para position of the phenyl ring, have shown clinical utility against gram positive bacterial infections.[36] Hence, enhancement of solubility of the ureas, by introduction of ionizable groups, was evaluated by designing and synthesizing the

sulfonamide series (Table 5: **30**, **31**). The sulfonamide and pyridine series had good solubility but failed to have substantial activity against *M. tb*.<sup>[36]</sup> The first generation of ureas were found to be highly potent, but had poor ADME (Absorption, Distribution, Metabolism and Excretion) properties. On the other hand, the heteroaryl urea series resulted in an enhancement of solubility, which could result in improved absorption, but showed a loss of antimicrobial potency and hence they were further modified. Hence, it was observed that, 5 membered heteroaryl rings were found to be active and lipophilic substituents on the 5 position of the ring, resulted in enhancement of potency.

Modifications on the urea core established the essentiality of the two H-bond donors and one H-bond acceptor pharmacophore points. Changing the urea group to a thio-urea results in lowered activity (Table 6: **32**). Methylation of one of the nitrogens (Table 6: **34**) of the urea linker reduces potency whereas methylation of both the nitrogens (Table 6: **35**) results in complete loss of anti-tubercular activity, which is due to the loss of H-donating character of the pharmacophore. Removal of one NH through carbamate replacement for the urea as seen with **33**, resulted in similar MIC as mono-methylated urea (Table 6: **34**)

**Table 6:** MIC values for compounds with modifications on the urea linker<sup>[36]</sup>



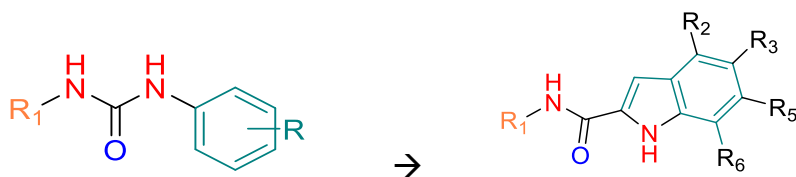
No.	X	Y	Z	<i>M. tb</i> MIC( $\mu\text{g/mL}$ )
<b>1</b>	NH	O	NH	0.01
<b>32</b>	NH	S	NH	0.8
<b>33</b>	O	O	NH	6
<b>34</b>	NH	O	NMe	6
<b>35</b>	NMe	O	NMe	12

Hence, it was observed that bulky aliphatic groups were required for binding at the hydrophobic pocket of the protein. The aromatic ring was essential for activity and addition of ionizable groups or heteroatoms, to the aromatic ring, in most cases, resulted in significant loss of antimicrobial potency. The urea linker, which consists of two H-bond donors and one H-bond acceptor, is essential for making H-bonds with the serine residue of the MmpL3 binding pocket.

#### Bioisosteric replacement:

Isosteres are functional groups that have similar electronic and steric (size) properties, and therefore, similar physicochemical properties. Bioisosteres are isosteres which, when exchanged for one another, result in similar biological activities. [37]

Bioisosteric replacement from the 1-phenyl urea core to an indole-2-carboxamide core results in potent anti-mycobacterial compounds with the same pharmacophore but with low cytotoxicity against mammalian cells.[37, 38] The only difference is that one of the hydrogen bond donors has been changed from a urea NH to an indole NH as shown in Figure 5.[37]



**Figure 5:** Bioisosteric replacement from urea to indole-2-carboxamide, while retaining the pharmacophore

The indole-2-carboxamides (IC) are the results of the bioisosteric replacements

on the urea based compounds and was identified as highly potent scaffold for *M. tb* by whole-cell phenotypic *M. tb* MIC testing. The pharmacophore points (Figure 5) for the ICs are described below and are similar to the urea series:

- a) A bulky aliphatic group (R1) on N-1
- b) The nitrogen is a part of the indole-ring, which serves as an aromatic ring and the N can act as an H-donor (NH)
- c) The carboxamide nitrogen which acts as an H-donor (NH)
- d) A H-bond acceptor, the O of the carbonyl

Like the urea-based compounds, these compounds have a bulky aliphatic ring, an aromatic ring, 2 NH groups (which serve as H-donors) linked by a carbonyl group (urea-like linkage) where the oxygen is the essential H-acceptor.

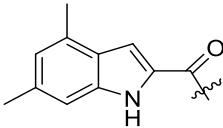
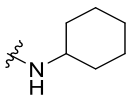
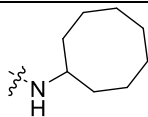
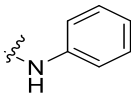
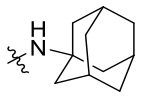
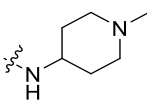
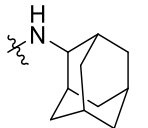
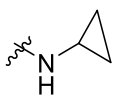
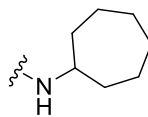
### IC SAR

The SAR for the IC series was determined from a number of synthetic IC analogs consisting of modifications to all portions of the compound, including the substituents on the amide nitrogen, indole ring and introduction of heteroaromatic indole analogs. The SAR observations are described as follows.

The 4, 6-dimethyl-1H-indole-2-carboxamide scaffold was studied by modifying the aliphatic group on the amide nitrogen (Table 7). The cyclohexyl group when aromatized to a benzene ring, anti-*M. tb* activity reduced (Table 7: **36**, **37**). Methylation on the indole nitrogen, exemplified by **52** (Table 9: **52**) resulted in loss of one H-donor of the pharmacophore and hence resulted in loss of activity. On replacing the cyclohexyl group with nitrogen containing cycloaliphatic groups,

as shown by the methylpiperidine analog (Table 7: **38**), activity was lost. Ring constriction from cyclohexyl to cyclopropyl (Table 7: **39**), led to a complete loss of activity whereas ring expansion to cycloheptyl (Table 7: **43**) and cyclooctyl (Table 7: **40**), increased activity. Interestingly, 1-adamantyl (Table 7: **41**) and 2-adamantyl analogs had equal potency with MIC values of 0.12 µg/mL, which was not the case with the urea based series where the 2-adamantyl analogs were consistently 10-fold more potent than 1-adamantyl analogs. This could imply that a large hydrophobic pocket may be present in the target binding site within proximity of the amide moiety, which can accommodate such bulky groups as above.

**Table 7:** IC derivatives studied for activity profiles by testing MIC. [39]

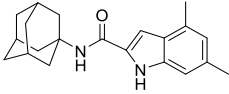
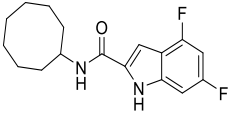
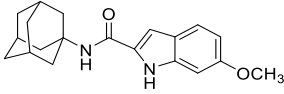
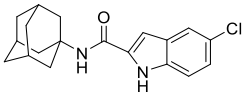
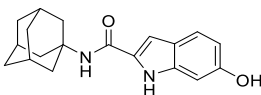
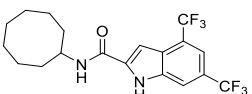
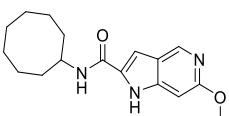
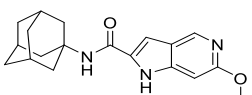
					
No.	R	<i>M. tb</i> MIC (μM)	No.	R	<i>M. tb</i> MIC (μM)
<b>36</b>		0.93	<b>40</b>		0.013
<b>37</b>		3.8	<b>41</b>		0.012
<b>38</b>		448	<b>42</b>		0.012
<b>39</b>		561	<b>43</b>		0.055

Various substitutions on the indole ring were investigated for their anti-TB potency (Table 8). Generally, the 4,6-dimethyl substituents on the indole ring, exemplified by **41** (Table 8), resulted in compounds that were among the most potent anti-TB activity with sub-μg/mL MIC values. Replacement of the 4,6-dimethyl groups (Table 7: **40**) with 4,6-difluoro- (Table 8: **44**) or 4,6-ditrifluoromethyl-substituents (Table 8: **48**) resulted in a 2.5- to 4-fold drop in activity compared to their dimethyl- counterparts. The mono-substituted IC with a methoxy substituent at the 6<sup>th</sup> position yielded a potent compound (Table 8: **45**, MIC: 0.77 μM). The more polar 6-hydroxy substituent (Table 8: **48**) resulted in

reduction of activity.[40] Introduction of a chlorine atom at C-5 position (Table 8: **47**) resulted in a 2-fold decrease as compared to the 6-methoxy analog (Table 8: **45**).

This class of compounds was highly lipophilic, as observed from their cLogP values, shown in Table 8. In order to increase the aqueous solubility of these compounds, which might further improve absorption and subsequently bioavailability, nitrogen groups were introduced and the 5-aza-6-methoxyindoles (Table 8: **49**, **50**) were synthesized and evaluated. In the 5-aza-6-methoxyindoles, the benzene ring of the indole nucleus was replaced with a pyridine ring (Table 8: **50**, MIC: 1.5  $\mu\text{M}$ ), this resulted in a 2-fold decrease in activity as compared to the 6-methoxy IC analogs (Table 8: **45**, MIC: 0.77  $\mu\text{M}$ ). This suggests that the extra heteroatoms may interfere with the binding of the compound to the hydrophobic pocket of the receptor. From the data trends discussed thus far, the higher the lipophilicity of the compound the more active it is. This can be inferred by comparing the MICs and the cLogP values of the compounds in Table 8.

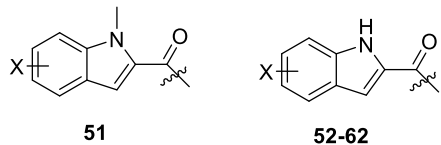
**Table 8:** MIC and cLogP values of IC Analogs. [39]

No.	Compound	<i>M. tb</i> MIC ( $\mu\text{M}$ )	cLogP
41		0.012	3.57
44		0.10	3.47
45		0.77	2.47
46		0.38	3.16
47		13	2.21
48		0.04	5
49		6.6	2.41
50		1.5	1.85

With the exception of compound **51**, compounds possessing mono-substitution such as a methyl group at position C-4 of the indole moiety (Table 9: **52**, **53**) retained anti-tubercular activity as seen with the cycloheptyl (Table 9: **52**, MIC = 0.93  $\mu\text{M}$ ) and cyclooctyl (Table 9: **53**, MIC = 0.11  $\mu\text{M}$ ) analogs. The following SAR discussion is regarding compounds with the cyclooctyl head group found in Table 9. Moving the C-4 methyl (Table 9: **53**, MIC = 0.11  $\mu\text{M}$ ) to the C-5 position (Table 9: **60**, MIC = 0.88  $\mu\text{M}$ ) reduced potency slightly. The more polar 4-aminoindole (Table 9: **51**, MIC = 20  $\mu\text{M}$ ) and 5-aminoindole (Table 9: **61**, MIC = 80

$\mu\text{M}$ ) derivatives showed significant decrease in activity. In the case of the C-6 position, mixed results were obtained as the compound (Table 9: **54**, MIC = 0.09  $\mu\text{M}$ ) with the more lipophilic bromo group was only slightly more active than its close analog possessing the 6-methyl group (Table 9: **56**, MIC 0.11  $\mu\text{M}$ ). Lastly, 4,6-dichloroindoles were evaluated and were found to be highly potent with MIC values of 0.11 – 0.12  $\mu\text{M}$ , regardless of the bulky aliphatic head group (cyclooctyl **57**, 1-adamantyl **58**, N-(1R,2R,3R,5S)-(-)-isopinocampheyl **59**). The noncyclic derivatives (Table 9: **62**) were found to be inactive which could be due to (a) linear substituents are less able to contact the surrounding nonpolar residues, (b) their flexibility may play a disfavoring entropic role, and (c) they can bump against aromatic residues, which restricts access to this sub pocket, of the MmpL3 protein.

[33]

**Table 9:** MIC and cLogP Values of IC Analogs. [41]

Analogue	x	R	<i>M. tb</i> MIC ( $\mu$ M)	cLogP
<b>51</b>	4,6-dimethyl		450	3.53
<b>52</b>	4-methyl		0.93	4.54
<b>53</b>	4-methyl		0.11	5.10
<b>54</b>	6-methyl		0.11	5.10
<b>55</b>	4-amino		20	3.44
<b>56</b>	6-Br		0.09	5.56
<b>57</b>	4,6-dichloro		0.011	6.16
<b>58</b>	4,6-dichloro		0.011	5.67
<b>59</b>	4,6-difluoro		0.012	5.74
<b>60</b>	5-methyl		0.88	5.10
<b>61</b>	5-amino		80	3.44
<b>62</b>	4,6-dimethyl		59	3.82

The SAR of these analogues leads to the following considerations for anti-TB activity: at N-1 (amide nitrogen): lipophilic and bulky substituents are preferred for potent anti-TB activity whereas non-bulky and/or polar substituents lead to loss of the activity. The bulky head groups are required to be linked to the indole ring by a carboxamide linkage at the 2 position of the indole ring for retaining the anti-TB activity. An unsubstituted indole nitrogen (N-2) is necessary for the anti-mycobacterial activity. Mono and di substitutions on the indole ring were well tolerated with lipophilic groups and detrimental with hydrophilic groups. Bioisosteric replacement of the indole ring to a nitrogen containing a 5-aza-indole ring was detrimental to anti-*M. tb* activity.

### 1.7. **Summary**

*M. tb* is constantly growing resistant to medication that is currently used for treatment of TB. Novel compounds with a new mechanism of action may improve treatment options against the resistant strains and also help in improving treatment against the susceptible strains. MmpL3 is a novel and essential target involved in mycobacterial cell wall construction, specifically mycolic acid transport involved in the biosynthetic pathway. Since mycolic acid is a fatty acid, it has a lipophilic structure and hence the inhibitors of the protein are also required to have a lipophilic structure in order to have affinity for the protein. These molecules have extremely low aqueous solubility and hence dissolve in the body fluids to a lower extent causing low absorption and hence low oral bioavailability.

The classes of urea-based analogs and ICs were studied in detail. The basic pharmacophore and SARs were revealed and the compounds were optimized to

achieve highly potent compounds. But, the ADME profiles of these MmpL3 inhibitors were found to be poor. In most cases, any structural modification that was made on the molecule to improve hydrophilicity, and thus the pharmacokinetic profile, was shown to generally take a heavy toll on the potency of the compound.

### **1.8. Scope and specific aims of my project**

This project involves design and synthesis of novel compounds based on the pharmacophore and SAR information obtained through literature. The poor aqueous solubility of the ureas and ICs has significant consequences on their pharmacokinetic profiles. In addition, there is a gap in current research related to compounds acting at the MmpL3 transporter protein of mycobacteria. This project aims to bridge that gap. The urea series when modified from the phenyl ureas to the heteroaryl compounds, showed lead compounds with sub  $\mu\text{g/mL}$  potency and were observed to have improved aqueous solubility by at least 22- fold. This project takes an adoptive approach in increasing the heteroatom percentage of the IC series to maintain anti-TB activity and improve aqueous solubility.

The specific aims to support this hypothesis are

1. Design, synthesis and characterization of compounds forming novel bioisosteric scaffolds

The new series of compounds are designed and synthesized with the pharmacophore points required for anti-mycobacterial activity. These series of compounds are designed so as to possess improved pharmacokinetic properties over their urea and indole analogs.

2. Evaluating the compounds for physicochemical, anti-TB activity and *in vitro* pharmacokinetic parameters

The improvement in pharmacokinetic profiles will be studied by *in vitro* assays including solubility, permeability, protein binding and metabolic stability testing.

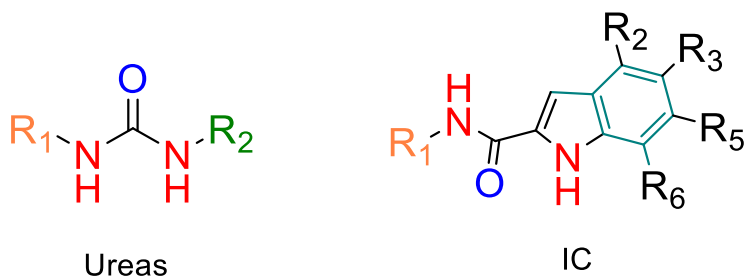
**Chapter 2: Design, synthesis and microbiological evaluation of novel anti-tubercular agents**

## 2.1. Introduction

Mycobacteria have a unique set of transporter proteins which are a part of the mycolic acid biosynthetic pathway, known as MmpL3 proteins. A crystal structure of MmpL3 is yet to be solved, therefore structure-based drug design is currently unavailable.[30] The previous classes of compounds (ureas and the ICs) tested for their whole-cell *M. tb* activity, were found to have good MIC values in the sub- $\mu\text{g/mL}$  range. Based on the pharmacophore and SAR of the previous series, ligand-based drug design was employed to discover novel anti-tubercular agents with improved physicochemical and pharmacokinetic profiles. Structural modifications and bioisosteric replacements on the ureas and ICs generates newer series of compounds which can be further studied for their microbiological activity and pharmacokinetic parameters.

## 2.2. Drawbacks of Previous Series of Ureas and ICs

The pharmacophore requirements of compounds to act at the MmpL3 protein were determined from the previous classes of compounds. The pharmacophore for both the series was the same and it can be summarized as follows:



**Figure 6:** Summary of the pharmacophore required to act at the MmpL3 protein

- A bulky aliphatic group ( $\text{R}_1$ ) on one nitrogen

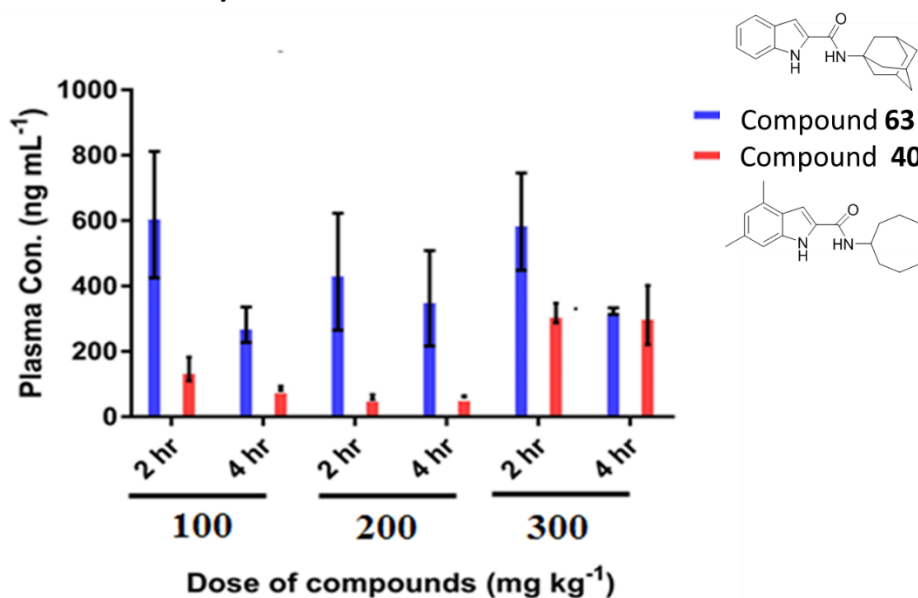
- b) Two hydrogen bond donors (NH)
- c) A hydrogen bond acceptor (O of carbonyl)
- d) An aromatic ring (R<sub>2</sub> for ureas and indole ring for ICs)

Previously developed series of ureas and ICs had potent anti-tuberculosis activity, however they had undesirable pharmaceutical properties, particularly high lipophilicity and poor solubility.[26, 42] All of the phenyl ureas and indoles showed poor aqueous solubility which was less than 4 µg/mL. Most of the compounds from the urea and IC series have MIC values in the sub-µg/mL range and poor aqueous solubility below 1 µg/mL. [35, 36, 41, 43, 44]. The hetero-aromatic ureas did improve solubility while maintaining sub µg/mL potency, however they were poorly absorbed and were not found to be efficacious in mouse models.[45]

Two ICs, namely 1-adamantyl-indole-2-carboxamide (**40**) and cyclooctyl-4, 6-dimethyl- indole-2-carboxamide (**63**), that are bioavailable and are efficacious in a mouse model of *M. abscessus* infection were tested *in vivo* using infected mouse models. Compounds **40** and **63** were formulated with 20% cyclodextrin at three different concentration (100 mg/kg, 200 mg/kg and 300 mg/kg) and administered PO for three consecutive days drug plasma concentration were quantified at the two and four hour time points after the last dose. Two and four hour time points were chosen for analysis, based on studies carried out previously to find time required for achieving C<sub>max</sub>. [41, 46, 47] A plot of plasma concentration versus time was plotted for all three doses and is represented in Figure 7. It was determined that compound **63** achieved maximum plasma concentration of approximately 600 ng/mL at two hours for both the 100 mg/kg and 300 mg/kg

doses. Compound **40** had lower plasma concentrations, below 200 ng/mL, at 100 and 200 mg/kg doses. At 300 mg/kg dose plasma concentrations at approximately  $318 \pm 30$  ng/mL were achieved. Hence, these compounds were found to have low plasma concentrations even at high doses. We hypothesize that this decreased absorption is a result of poor aqueous solubility of the compound. If these results are extrapolated to humans, the doses required may be excessive and hence the pill burden may be high. Thus, the purpose of this study is to design and develop analogs that maintain anti-tuberculosis activity but have improved *in vitro* pharmacokinetic (PK) properties and aqueous solubility which is an important physicochemical property.

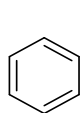
## Dose proportionality of the pharmacokinetics



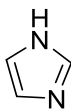
**Figure 7:** Dose response pharmacokinetics for compounds **40** and **63** when dosed to mice (Manuscript: Indole-2-carboxamides are Active against an Acute *Mycobacterium abscessus* Infection Mouse Model, under review with Antimicrobial Agents & Chemotherapy)[47]

### 2.3. Design of new series

Bioisosterism has always been and is still utilized in drug design and development to introduce diverse structural changes that are expected to enhance specific properties while maintaining desired biological activity.[48] Bioisosteric modifications can enhance potency, improve the lipophilicity/hydrophilicity balance, improve pharmacokinetic properties, reduce affinity for metabolizing enzymes, and/or improve therapeutic indexes.[49] For example, as shown in Figure 8, the benzene and imidazole both are aromatic rings and both could engage in Van der Waals interactions when bound to proteins. However, they are different in size, shape, electronic distribution, polarity, lipophilicity, hydrogen bond formation capacity and pKa.[51] The similarities between the two result in similar biological effect and their differences help in modulating the pharmacokinetics.

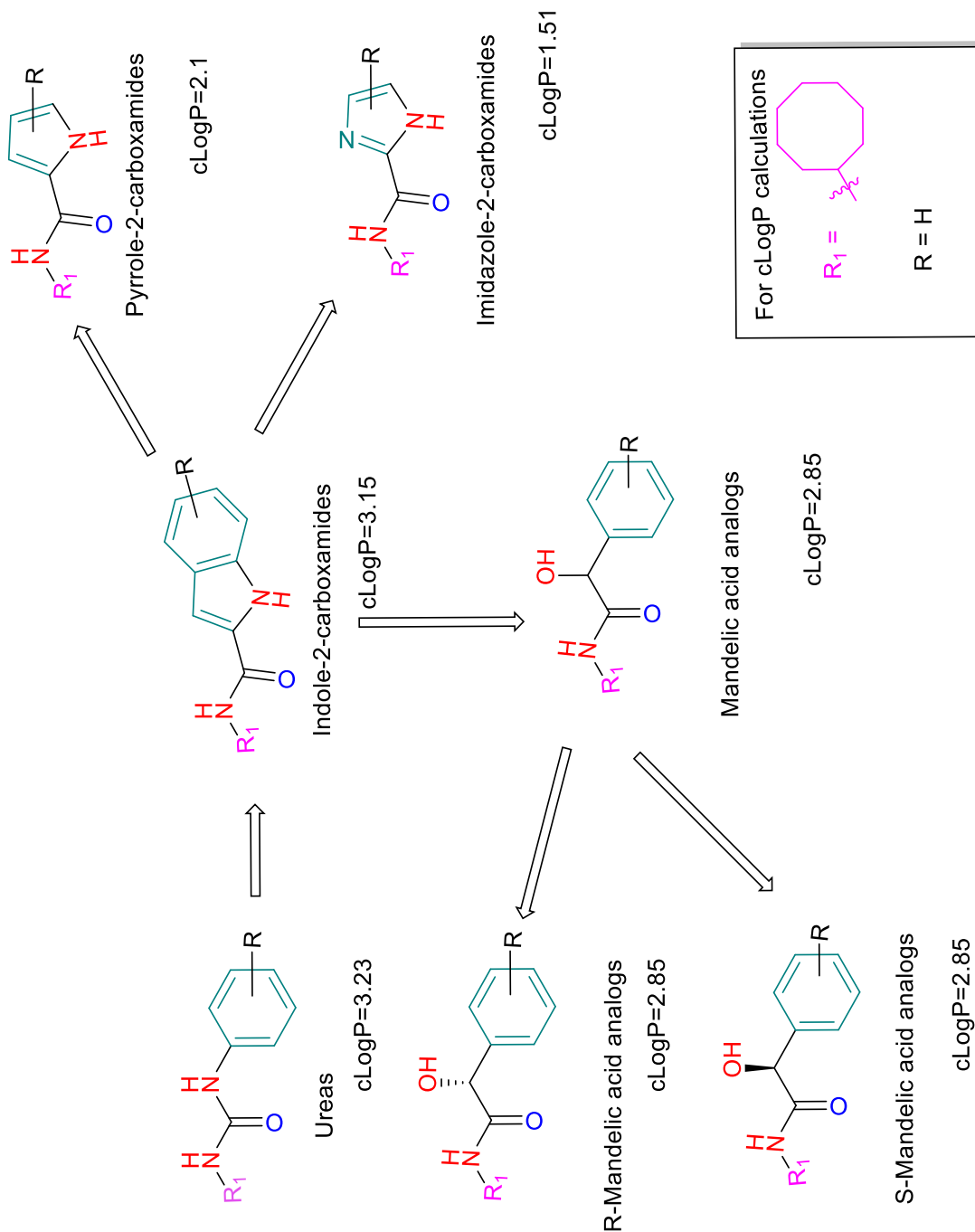


Benzene



Imidazole

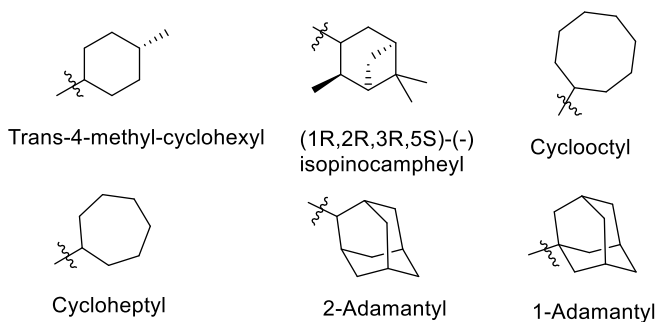
**Figure 8:** Imidazole, a bioisostere of benzene



**Figure 9:** Design of novel scaffolds

In this study, we used rational bioisosteric replacements for the indole group of the ICs in five miniseries (pyrrole, imidazole, racemic and pure R and S enantiomeric forms of mandelic acid) in order to increase polarity, as evidenced by

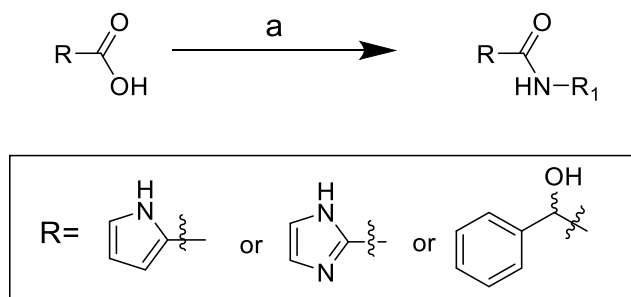
a reduced cLogP value, which should help increase solubility while maintaining good anti-tuberculosis activity (Figure 9). The cLogP values are aqueous solubility surrogates and lower values indicate a potential enhancement in aqueous solubility. The first series designed resulted from removal of the benzene ring on the indole ring yielding a less lipophilic pyrrole as evidenced by a reduced cLogP from 3.15 of the indole to 2.1. In order to further increase polarity, introduction of a second nitrogen to the pyrrole ring lead to the design of an imidazole-based series, further decreasing cLogP to 1.51. To expand chemical space of this series and test the identity of the indole NH H-donor pharmacophore point, mandelic acid analogs with an OH H-donor, were also designed with a cLogP value of 2.85. In addition, modifications were also made to the bulky aliphatic portions to optimize anti-tubercular efficacy. The bulky aliphatic groups chosen to form a mini-series with head groups that showed best anti-*M. tb* activity in the previous classes, including cyclooctyl, cycloheptyl, 1-adamantyl, 2-adamantyl, trans-4-methyl-cyclohexyl and (1*R*,2*R*,3*R*,5*S*)-(-)-isopinocampheyl groups were used as the head groups (Figure 10). A total of 30 compounds belonging to 5 different series were synthesized and evaluated for *in vitro* antimicrobial efficacy and physicochemical properties.



**Figure 10:** Structures of the head groups which showed best activities in previous classes of MmpL3 inhibitors

#### 2.4. Synthetic Scheme and mechanism of synthesis

The synthesis for all the designed compounds was carried out according to Scheme 1. The coupled products were synthesized using standard HOBt/EDC coupling conditions. Thirty compounds were synthesized.

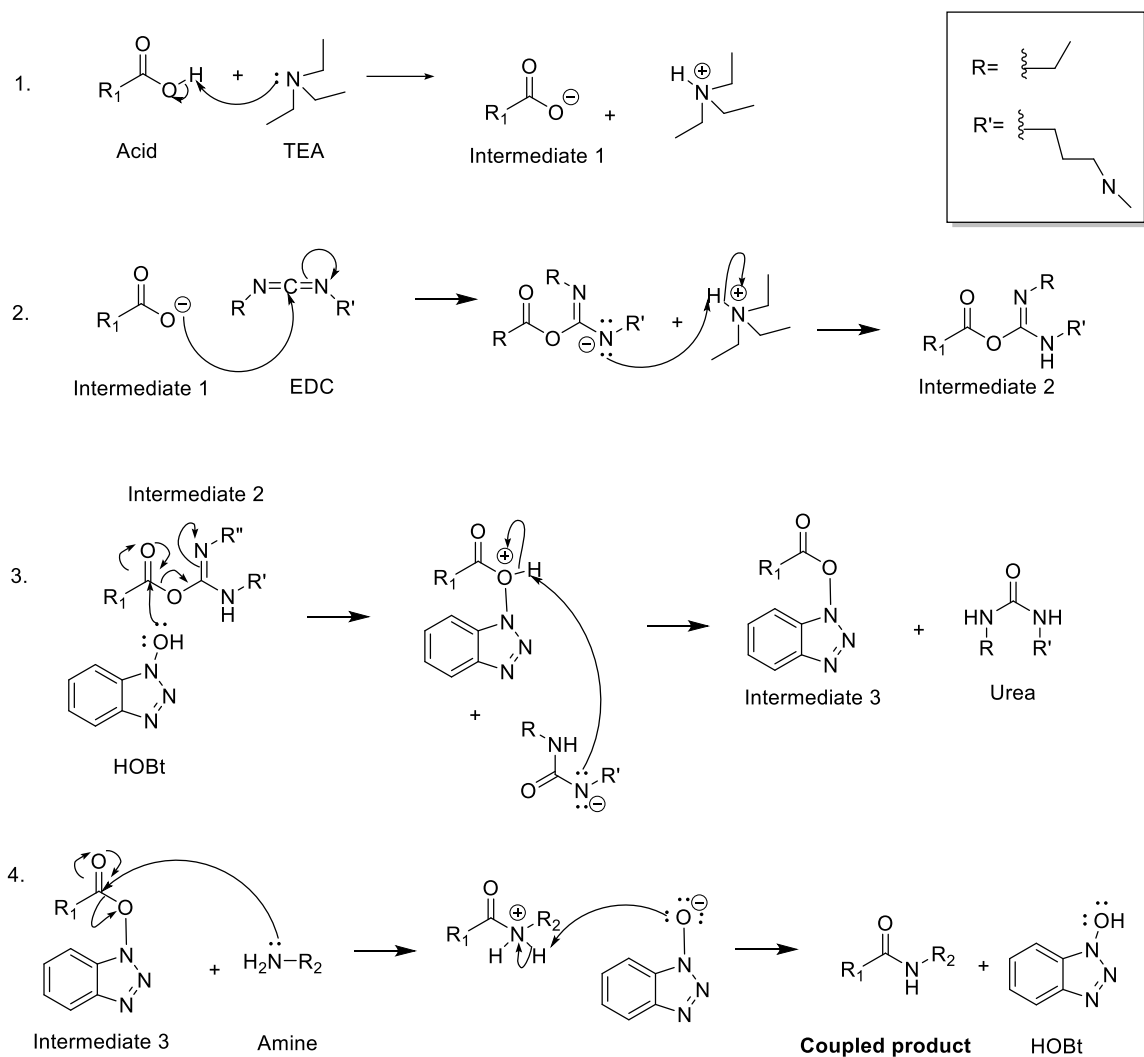


**Scheme 1.** Synthesis of coupled compounds. Reagents and conditions: a) HOBt, EDC, TEA, amine, DMF, r.t., overnight.

Each compound in the series was characterized by determining its molecular mass, structural connectivity and purity. Proton and carbon NMR were used to confirm structural connectivity, molecular weight was confirmed by mass spectroscopy. HPLC with UV/vis detection was used to determine purity for the pyrrrole-2-carboxamides and the imidazole-2-carboxamides. The mandelic acid analogs had poor UV/vis absorbance, therefore elemental analysis was conducted

on these to confirm purity of compounds. Characterization data for representative compounds, which are compounds **89** (pyrrole-2-carboxamide), **103** (racemic mandelic acid analog), **112** (imidazole-2-carboxamide), **121** (R- mandelic acid analog) and **122** (S- mandelic acid analog) can be found in the appendix.

The mechanism for the coupling reaction is shown in Figure 11. The reaction takes place via 4 steps and the formation of intermediates in each reaction is required for the beginning of the next reaction. The reaction begins with step 1 which is an acid base reaction where TEA accepts a proton from the carboxylic acid. Step 2 is an addition reaction where the nucleophilic carboxylate anion attacks the electrophilic carbon in the carbodiimide functional group on EDC. After charge neutralization through an acid base reaction with the protonated TEA, step 3 proceeds through an addition-elimination reaction where the nucleophilic hydroxyl group on HOBt attacks the electrophilic carbonyl carbon on intermediate two. Intermediate 3 undergoes an addition-elimination reaction where the nucleophilic amino group attacks the electrophilic carbonyl carbon on intermediate three.



**Figure 11:** Coupling reaction mechanism.

## 2.5. Microbiological assessment

Phenotypic whole-cell minimum inhibitory concentration (MIC) screening against *M. tb* is a routine initial assessment of antimicrobial efficacy. The MIC is the lowest concentration of drug required to prevent bacterial growth. The following series of compounds were tested against three mycobacterial strains, (*M. tuberculosis*, *M. abscessus* and *M. smegmatis*) to gain insight on mycobacterial

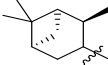
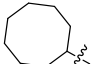
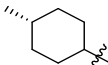
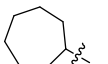
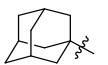
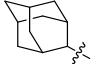
spectrum of activity. MIC testing is carried out by our collaborators at Colorado State University.

Series 1: Pyrrole-2-carboxamides: The first approach to increase aqueous solubility was the reduction in the number of lipophilic carbon atoms on the indole ring. This will also help determine the essentiality of the benzene group on an indole ring. The synthesis for the unsubstituted pyrrole-2-carboxamide (PC) series was carried out according to Scheme 1 and high yields ranging between 80-90% were obtained. Six unsubstituted PCs were synthesized and are shown in Table 10.

Compound **88**, with the (1*R*, 2*R*, 3*R*, 5*S*)-(-) isopinocampheyl head group, had the best activity amongst the series against all three mycobacterial strains, however, it was most active against *M. tb* with an MIC value of 2 µg/mL. Compound **88**, also had the highest cLogP in the series and hence a higher lipophilicity as compared to the other compounds in this mini-series, this may be one of the reasons for its high activity against the mycobacteria. The trans-4-methyl cyclohexyl analog (compound **96**) showed higher activity against *M. abscessus* (MIC: 16 µg/mL) as compared to *M. tb*, but was inactive against *M. smegmatis* (MIC: >32 µg/mL). Compound **89**, the cyclooctyl analog, has equal activity against all three mycobacterial strains (MIC: 32 µg/mL). Compounds **98**, **104** and **105** were equally active against *M. tb* and *M. abscessus*, but inactive against *M. smegmatis*. Overall, *M. tb* and *M. abscessus* were found to be more susceptible to this series of compounds as compared to *M. smegmatis*. Compounds **96** and **98** both have seven carbon containing head groups, however compound **96**, with the trans-4-

methyl cyclohexyl group was found to be more active against *M. abscessus* (MIC: 16 µg/mL) as compared to compound **98**, with the cycloheptyl ring (MIC: 32 µg/mL). Compounds **88** and **96**, with substituted cyclohexyl rings as their head groups had the best activity against *M. abscessus* which could be due to their better binding interactions at the MmpL3 pocket of *M. abscessus*. Both the adamantyl group and the isopinocampheyl group are 13 carbon rings, however, compound **88**, with the isopinocampheyl head group was found to be more active as compared to the adamantyl analogs (compounds **104** and **105**). Therefore, rearranging the carbon atom reduced the potency against *M. abscessus* by 2-fold and the potency against *M. tb* by 16-fold. Hence, it was observed that the (1*R*, 2*R*, 3*R*, 5*S*)-(-) isopinocampheyl head group was best tolerated amongst this series. All compounds from this series were found to be active against *M. tb* with MIC values of 32 µg/mL or below.

**Table 10:** Activity of pyrrole-2-carboxamides against mycobacteria

No.	R	MIC ( $\mu\text{g/mL}$ )			cLogP
		<i>M. abscessus</i>	<i>M. tb</i>	<i>M. smeg.</i>	
88		16	2	16	2.21
89		32	32	32	2.1
96		16	32	>32	1.6
98		32	32	>32	1.68
104		32	32	>32	1.55
105		32	32	>32	1.73

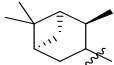
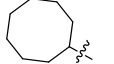
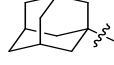
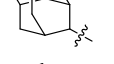
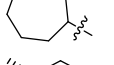
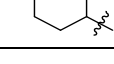
Series 2: Imidazole-2-carboxamides: The second approach to enhance solubility was to introduce a heteroatom in the pyrrole ring generating a more polar bioisostere of pyrrole. A decrease in the ratio of carbon: heteroatom is expected to enhance the aqueous solubility of the compounds.

The synthesis for the unsubstituted imidazole-2-carboxamide series was carried out according to Scheme 1 and high yields ranging between 80-90% were observed. Six unsubstituted imidazole-2-carboxamides were synthesized.

On testing these compounds for their anti-mycobacterial potency, the following results were observed (Table 11). All the compounds from this series were inactive against *M. tb* and *M. smegmatis* with MICs greater than 32  $\mu\text{g/mL}$ . However, compounds **106** and **109**, with the (1*R*, 2*R*, 3*R*, 5*S*)-(-) isopinocampheyl

and the 1-adamantly head groups, respectively, were active against *M. abscessus*, with an MIC of 32 µg/mL. The cLogP of all the compounds reduced significantly, rendering them unable to penetrate the lipophilic mycobacterial cell wall and bind at the MmpL3 transporter. Hence, the addition of an extra heteroatom to the aromatic ring, proved to be detrimental for anti-mycobacterial activity. Since none of the compounds from this series were active against *M. tb* these weren't evaluated further.

**Table 11:** Activity of imidazole-2-carboxamides against mycobacteria

No.	R	MIC (µg/mL)			cLogP
		<i>M. abscessus</i>	<i>M. tb</i>	<i>M. smeg.</i>	
106		32	>32	>32	1.62
108		>32	>32	>32	1.51
109		32	>32	>32	1.09
110		>32	>32	>32	0.95
111		>32	>32	>32	1.14
112		>32	>32	>32	1.00

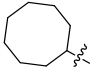
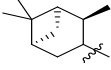
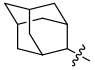
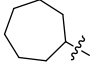
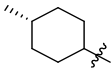
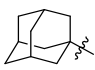
Series 3: Mandelic acid analogs: A single S-mandelic acid based camphane analog was published and it was found to have excellent anti-mycobacterial activity.[52] Hence a mandelic acid analog series was designed to determine and expand SAR. This series is expected to significantly enhance the aqueous solubility of compounds as observed from the cLogP values for these.

The synthesis for the mandelic acid derivatives series was carried out according to Scheme 1 with low yields ranging between 15-30% were observed. The low yields observed may be due to the free benzylic hydroxyl group which may act as a nucleophile and. Protecting groups, such as silyl ethers, may be used in the future to protect the free hydroxyl group and prevent it from participating in the coupling reaction and hence increase yields of the reaction. Eighteen mandelic acid derivatives were synthesized comprising six racemates (Table 12) and 12 chirally pure analogs (Tables 13 and 14).

MIC values for the mandelic acid racemates are shown in Table 12. All of these were found to be inactive against *M. smegmatis* with MICs above 32 µg/mL. *M. abscessus* was more susceptible to this class of compounds, as compared to *M. tb* and *M. smegmatis*. Compounds **77** (cyclooctyl analog) and **78** ((1*R*, 2*R*, 3*R*, 5*S*)-(-) isopinocampheyl analog) were found to be inactive against all three strains, whereas compounds **101** (cycloheptyl analog), **102** (trans-4-methyl cyclohexyl analog) and **103** (1-adamantyl analog) were active only against *M. abscessus* with an MIC of 32 µg/mL. The most promising compound from this series, was the 2-adamantyl substituted mandelic acid, **95**, with an MIC of 16 µg/mL against *M. abscessus* and an MIC of 32 µg/mL against *M. tb*. In this mini-series, compounds with the 13-carbon adamantyl head groups (compounds **95** and **103**) were found to be active against *M. abscessus*, as opposed to compounds with the 13-carbon isopinocampheyl head group (compound **78**) which were inactive. Hence, rearranging the carbon atoms resulted in a reduction of potency. Since, compound

**95** was the only compound in the series which had activity against *M. tb*, it was further evaluated for its *in vitro* pharmacokinetic properties.

**Table 12:** Activity of racemic mixture of mandelic acid analogs against mycobacteria

No.	R	MIC ( $\mu\text{g/mL}$ )			cLogP
		<i>M. abscessus</i>	<i>M. tb</i>	<i>M. smeg.</i>	
<b>77</b>		>32	>32	>32	2.85
<b>78</b>		>32	>32	>32	2.96
<b>95</b>		16	32	>32	2.47
<b>101</b>		32	>32	>32	2.43
<b>102</b>		32	>32	>32	2.34
<b>103</b>		32	>32	>32	2.29

**Table 13:** Activity of S-Mandelic acid analogs against mycobacteria

No.	R	MIC ( $\mu\text{g/mL}$ )			cLogP
		<i>M. abscessus</i>	<i>M. tb</i>	<i>M. smeg.</i>	
118		>32	>32	>32	2.85
120		>32	>32	>32	2.96
122		>32	>32	>32	2.29
124		>32	>32	>32	2.47
127		>32	>32	>32	2.34
128		>32	>32	>32	2.43

**Table 14:** Activity of R-Mandelic acid analogs against mycobacteria

No.	R	MIC ( $\mu\text{g/mL}$ )			cLogP
		<i>M. abscessus</i>	<i>M. tb</i>	<i>M. smeg.</i>	
117		>32	>32	>32	2.85
119		>32	>32	>32	2.96
121		>32	>32	>32	2.29
123		>32	>32	>32	2.47
125		>32	>32	>32	2.43
126		>32	>32	>32	2.34

On testing the pure chiral compounds for their anti-mycobacterial potency, the following results were observed (Table 13 and 14). None of the compounds in

this series was found to be active. In this series of compounds, one NH of the IC series, which is a H-bond donor, has been replaced by OH, which is also a H-bond donor. However, this seems to be detrimental to the anti-mycobacterial activity of this compounds. This indicates that a more specific H-bond donor, is required for enhanced binding at the receptor. Further discussion about the activity of these compounds can be found in the next chapter along with the aqueous solubility patterns.

Amongst the currently marketed first line anti-*M. tb* drugs, isoniazid and ethambutol have the lowest and the highest MIC values, respectively. The MIC for isoniazid is 0.02-0.08 µg/mL, whereas for ethambutol it is 3-5 µg/mL.[53, 54] Most of the novel compounds described in this project have MIC values of 32 µg/mL or higher, which are high and further optimization is warranted. Despite having improved cLogP values, all the novel compounds showed a large reduction in *M. tb* MIC values compared to ureas and ICs. This suggests that a decrease in the size of the aromatic ring and addition of polar heteroatoms to the aromatic ring are not well tolerated by the molecular target and are thus detrimental to anti-TB activity. Only compounds with an MIC of 32 µg/mL or below, against *M. tb*, were further studied for their pharmacokinetic parameters and the compounds with MIC above that, were considered to be inactive and were only assayed for their kinetic solubility.

The mycobacterial cell wall is highly lipophilic and the MmpL3 proteins are situated in the mycobacterial membrane. For the compounds to bind to the receptor on the MmpL3 protein, they need to pass through the lipophilic cell wall.

Since these novel compounds have decreased lipophilicity suggesting a reduction of mycobacterial cell wall permeability, this may be one of the reasons for the reduction in MIC values. However, since these compounds do fulfil the pharmacophore requirements of MmpL3 inhibitors, they are assumed to bind to MmpL3 if they can reach this target.

## 2.6. **Conclusion**

A one-step reaction synthesis Scheme was utilized to produce thirty different final products. The yields were greater than 80% for all of PC and the imidazole-2-carboxamides but poor yields of less than 30% were observed for the all the mandelic analogs. The primary reason for the low yields of the mandelic acid analogs is most likely due to the free hydroxyl group which is an additional nucleophilic site. The anti-mycobacterial activity of all the mini-series reduced significantly as compared to their urea and IC counterparts. However, seven active compounds (*M. tb* MIC  $\leq$  32  $\mu\text{g/mL}$ ) were identified from these mini-series. Six out of these active compounds were the PCs, with all six of the head groups tested, and one of these active compounds was the 2-adamantyl racemic mandelic acid analog and these compounds were further evaluated for their *in vitro* pharmacokinetic parameters, as explained in the next chapter.

## **Experimental**

### **2.7.1 - Methods and instrumentation**

All glassware was dried in a 150°C oven overnight. All chemicals, solvents, and glassware were purchased from either Fisher Scientific (Pittsburg, Pennsylvania) or Sigma Aldrich (St. Louis, Missouri). TLC plates, silica gel columns (100, 50, 25, and 10g), and C18 columns (30g) were purchased from Biotage® (Charlotte, North Carolina). The chemical reactions were tracked using fluorescent silica gel-coated TLC plates and the separated components were visualized using UV light (254 nm) or I<sub>2</sub> condensation. Compounds were purified using flash-column chromatography on a Biotage Isolera™ with either silica gel or C18 silica. Mass spectra were acquired on an Agilent 1200 / AB Sciex® API 5500 QTrap LC/MS/MS, using electrospray ionization and a single quadrupole analyzer. All <sup>1</sup>H and <sup>13</sup>C NMR spectra were obtained on an Ascend™ 400 MHz Bruker spectrometer, and chemical shifts were reported relative to TMS. Analytical HPLC was determined on an Agilent 1260 Infinity Quaternary LC system equipped with an Acquity BEH C18 column (1.7 μm), flow rate of 1 mL/min and a gradient of solvent A (water with 0.1% formic acid) and solvent B (acetonitrile with 0.1% formic acid): 0-2.5 min 20% A; 2.5-8.0 min 80-30% B (linear gradient); 8.0-9.0 min 30-20% B (linear gradient); 9-10 min 80% A. UV absorbance at 254 nm and 280 nm was used as the detection method. All compounds were found to have >95% purity with the described analytical methods. Elemental analysis was conducted on mandelic acid analogs and all compounds were found to be within 0.4% of the calculated values for the proposed formula except compounds **78, 95, 101, 103,**

**119, 124** which were found to be within 0.8% of the calculated values, without accounting for the water for hydration, since special precautions were taken to ensure the submission of an anhydrous sample.

**2.7.2 - General synthetic method for coupling:** Aromatic carboxylic acid (1 eq) was added to hydroxybenzotriazole (HOBT, 1 eq), 1-ethyl-3-(3-dimethylaminopropyl) carbodiimide (EDC, 1.2 eq) and trimethylamine (TEA, 1.5 eq) and stirred in dimethyl formamide (DMF, 10 mL used per 100 mg of acid) for 15 minutes at room temperature. The bulky amine (1 eq) was added to the reaction mixture and stirred under N<sub>2</sub> atmosphere overnight. The reaction mixture was diluted in water and extracted with ethyl acetate. The organic layer was removed and evaporated under reduced pressure. The crude product was purified using flash chromatography. For the mandelic acid analogs, the gradient used was 0 - 40% of ethyl acetate in hexane, whereas the PCs and imidazole-2-carboxamides eluted with a gradient of 25 - 55% of ethyl acetate in hexane.

**2.7.3 – (1*R*,2*R*,3*R*,5*S*)-(-)-Isopinocampheyl-pyrrole-2-carboxamide (88):** 370 mg (75%) of off-white powder; <sup>1</sup>H NMR (CDCl<sub>3</sub>) δ = 0.91(d, *J* = 10 Hz, 1H), 1.09 (s, 3H), 1.15 (d, *J* = 7 Hz, 3H), 1.24 (s, 3H), 1.53-1.63 (m, 4H), 1.83-1.90 (m, 2H), 1.97-2.01 (m, 1H), 2.42-2.48 (m, 1H), 2.63-2.70 (m, 1H), 4.39-4.48 (m, 1H), 5.68-5.70 (m, 1H) the nitrogen proton of the pyrrole ring, 6.23-6.25 (m, 1H) C-4 proton of pyrrole ring, 6.52-6.54 (m, *J* = 1 Hz, 1H) pyrrole C3-H, 6.91-6.93 (m, *J* = 1 Hz, 1H,) C-5 proton of the pyrrole ring; <sup>13</sup>C NMR (CDCl<sub>3</sub>) δ = 19.73, 22.37, 27.01, 34.38, 36.41, 37.43, 40.61, 45.55, 46.71, 46.79, 106.95 pyrrole C2, 108.74 pyrrole

C3, C4, 120.04 pyrrole C5, 159.39 carbonyl carbon; ESI-MS calculated for C<sub>15</sub>H<sub>22</sub>N<sub>2</sub>O: 247.7, found: 247.1 [M+H]<sup>+</sup>.

**2.7.4 – Cyclooctyl-pyrrole-2-carboxamide (89):** 259 mg (58%) of white powder; <sup>1</sup>H NMR (CDCl<sub>3</sub>) δ = 1.54-1.73 (m, 12H), 1.87-1.94 (m, 2H), 3.49-3.50 (d, *J* = 5 Hz, 1H), 4.12-4.18 (m, 1H), 5.75-5.76 (m, 1H) the nitrogen proton of the pyrrole ring, 6.21-6.24 (d, *J* = 7 Hz, 1H,) C-4 proton of pyrrole ring, 6.48-6.50 (d, *J* = 7 Hz, 1H) pyrrole C3-H, 6.89- 6.91 (t, *J* = 5 Hz, 1H) C-5 proton of the pyrrole ring; <sup>13</sup>C NMR (CDCl<sub>3</sub>) δ = 23.68, 25.46, 27.34, 32.59, 49.34, 107.99 pyrrole C2, 109.78 pyrrole C3, C4, 121.07 pyrrole C5, 159.91 carbonyl carbon; ESI-MS calculated for C<sub>13</sub>H<sub>20</sub>N<sub>2</sub>O: 221.3, found: 220.9 [M+H]<sup>+</sup>.

**2.7.5– 2-Adamantyl-2-phenyl-2-hydroxy-ethanamide(95):** 701 mg (62%) of white powder; <sup>1</sup>H NMR (CDCl<sub>3</sub>) δ = 1.42-1.46 (m, 1H), 1.55-1.56 (m, 1H), 1.59 (s, 1H), 1.61-1.63 (m, 2H), 1.70-1.71 (m, 2H), 1.76-1.89 (m, 8H), 3.48-3.49 (m, 2H), 3.65 (d, *J* = 3 Hz, 1H), 4.01-4.05 (m, 1H), 5.04 (d, *J* = 3 Hz, 1H), 6.34 (bs, 1H), 7.32-7.43 (m, 5H); <sup>13</sup>C NMR (CDCl<sub>3</sub>) δ = 14.21, 21.07, 26.98, 27.06, 31.77, 31.84, 36.92, 37.01, 37.40, 53.45, 60.42, 126.76, 128.69, 139.81; ESI-MS calculated for C<sub>18</sub>H<sub>23</sub>NO<sub>2</sub>: 287.4, found: 286.1 [M+H]<sup>+</sup>.

**2.7.6– 4-(trans-methyl)-cyclohexyl-pyrrole-2-carboxamide (96):** 397 mg (96%) of off-white powder; <sup>1</sup>H NMR (CDCl<sub>3</sub>) δ = 0.91 (d, *J* = 6 Hz, 3H), 1.03-1.26 (m, 4H), 1.31-1.41 (m, 1H), 1.72-1.77 (m, 2H), 2.00-2.07 (m, 2H), 3.81-3.91 (m, 1H), 5.67 (s, 1H) pyrrole N-H, 6.20-6.22 (m, 1H) pyrrole C4-H, 6.49-6.51 (m, *J* = 1 Hz, 1H) pyrrole C3-H, 6.89-6.91 (m, *J* = 1Hz, 1H) pyrrole C5-H, 9.63 (s, 1H); <sup>13</sup>C NMR (CDCl<sub>3</sub>) δ = 22.20, 32.00, 33.43, 33.88, 48.37, 108.04 pyrrole C2, 109.74 pyrrole

C3, C4, 121.04 pyrrole C5, 160.21 carbonyl carbon; ESI-MS calculated for C<sub>12</sub>H<sub>18</sub>N<sub>2</sub>O: 206.3, found: 207.3 [M+H]<sup>+</sup>.

**2.7.7 - Cycloheptyl- pyrrole-2-carboxamide (98):** 155 mg (38%) of white powder; <sup>1</sup>H NMR (CDCl<sub>3</sub>) δ = 1.52-1.54 (m, 4H), 1.57 (s, 7H), 1.97-1.20 (m, 2H), 4.08-4.15 (m, 1H), 5.75 (s, 1H) pyrrole N-H, 6.22-6.24 (m, 1H) pyrrole C4-H, 6.48-6.50 (sextet, *J* = 1 Hz, 1H) pyrrole C3-H, 6.89-6.91 (m, *J* = 1 Hz, 1H) pyrrole C5-H, 9.27 (s, 1H); <sup>13</sup>C NMR (CDCl<sub>3</sub>) δ = 24.12, 28.06, 35.37, 105.70; ESI-MS calculated for C<sub>12</sub>H<sub>18</sub>N<sub>2</sub>O: 206.3, found: 207.0 [M+H]<sup>+</sup>.

**2.7.8 - Cyclooctyl-2-Phenyl-2-hydroxyl ethanamide (77):** 178 mg (17%) of white powder; <sup>1</sup>H NMR (CDCl<sub>3</sub>) δ = 1.41-1.56(m, 13H), 1.69-1.81 (m, 2H), 3.55 (d, *J* = 4 Hz, 1H), 3.93-4.02 (m, *J* = 5 Hz, 1H), 4.97 (d, *J* = 4 Hz, 1H), 5.89-5.91 (m, 1H), 7.31-7.40 (m, 5H); <sup>13</sup>C NMR (CDCl<sub>3</sub>) δ = 23.56, 25.37, 27.12, 32.22, 49.73, 74.09, 126.88, 128.69, 128.96, 139.73, 170.67; ESI-MS calculated for C<sub>16</sub>H<sub>23</sub>NO<sub>2</sub>: 261.2, found: 262.1 [M+H]<sup>+</sup>.

**2.7.9 - (1*R*,2*R*,3*R*,5*S*)-(-)-Isopinocampheyl-2-Phenyl-2-hydroxyl ethanamide (78):** 93 mg (8%) of white powder; <sup>1</sup>H NMR (CDCl<sub>3</sub>) δ = 0.77-0.82 (m, 1H), 1.01-1.02 (m, 3H), 1.03 (s, 1H), 1.05 (s, 1H), 1.20 (s, 3H), 1.38-1.51 (m, 1H), 1.64-1.81 (m, 2H), 1.89-1.94 (m, 1H), 2.34-2.41 (m, 1H), 2.48-2.57 (m, 1H), 4.04 (s, 1H), 4.19-4.27 (m, 1H), 4.96 (s, 1H), 6.21-6.25 (m, 1H), 7.33-7.41 (m, 5H); <sup>13</sup>C NMR (CDCl<sub>3</sub>) δ = 20.71, 23.34, 28.01, 35.26, 36.77, 38.42, 41.53, 46.08, 47.68, 48.03, 74.13, 126.93, 128.89, 139.81, 171.42; ESI-MS calculated for C<sub>16</sub>H<sub>23</sub>NO<sub>2</sub>: 287.4, found: 288.3 [M+H]<sup>+</sup>.

**2.7.10 - Cycloheptyl-2-Phenyl-2-hydroxyl ethanamide (101):** 789 mg (69%) of white powder;  $^1\text{H}$  NMR ( $\text{CDCl}_3$ )  $\delta$  = 1.30-1.61 (m, 12H), 1.79-1.92 (m, 2H), 2.88 (s, 2H), 2.95 (s, 2H), 3.63 (d,  $J$  = 4 Hz, 1H), 3.90-3.98 (m,  $J$  = 5 Hz, 1H), 4.98 (d,  $J$  = 4 Hz, 1H), 5.93-5.99 (m, 1H), 7.31-7.40 (m, 5H);  $^{13}\text{C}$  NMR ( $\text{CDCl}_3$ )  $\delta$  = 23.93, 24.02, 27.84, 31.45, 34.93, 34.94, 36.50, 50.71, 74.09, 126.88, 128.65, 128.92, 139.70, 162.55, 170.74; ESI-MS calculated for  $\text{C}_{15}\text{H}_{21}\text{NO}_2$ : 247.3, found: 270.1  $[\text{M}+\text{Na}]^+$  .

**2.7.11 – Trans-4-methyl-cyclohexyl-2-Phenyl-2-hydroxyl ethanamide (102):** 469 mg (45%) of white powder;  $^1\text{H}$  NMR ( $\text{CDCl}_3$ )  $\delta$  = 0.87 (d,  $J$  = 6 Hz, 3H), 0.95-1.15 (m, 5H), 1.23-1.33 (m, 1H), 1.35-1.71 (m, 2H), 1.85-1.93 (m, 2H), 3.62-3.71 (m, 1H), 3.78 (d,  $J$  = 4 Hz, 1H), 4.94 (d,  $J$  = 4 Hz, 1H), 5.97 (bs, 1H), 7.29-7.37 (m, 5H);  $^{13}\text{C}$  NMR ( $\text{CDCl}_3$ )  $\delta$  = 14.13, 22.11, 22.66, 31.59, 32.96, 33.70, 48.72, 74.07, 126.88, 128.84, 139.70, 171.27; ESI-MS calculated for  $\text{C}_{15}\text{H}_{21}\text{NO}_2$ : 247.3, found: : 270.2  $[\text{M}+\text{Na}]^+$  .

**2.7.12 – 1-Adamantyl-2-Phenyl-2-hydroxyl ethanamide (103):** 534 mg (45%) of white powder;  $^1\text{H}$  NMR ( $\text{CDCl}_3$ )  $\delta$  = 1.58 (s, 6H), 1.86-1.87 (m, 6H), 1.99 (s, 3H), 3.63 (bs, 1H), 4.81 (s, 1H), 5.55 (s, 1H), 7.24-7.31 (m, 5H);  $^{13}\text{C}$  NMR ( $\text{CDCl}_3$ )  $\delta$  = 29.37, 36.22, 41.43, 52.24, 74.09, 126.88, 128.59, 128.92, 140.00, 171.02 ; ESI-MS calculated for  $\text{C}_{18}\text{H}_{23}\text{NO}_2$ : 287.4, found: 308.0  $[\text{M}+\text{Na}]^+$  .

**2.7.13 - 1-Adamantyl-pyrrole-2-carboxamide (104):** 317 mg (65%) of white powder,  $^1\text{H}$  NMR ( $\text{CDCl}_3$ )  $\delta$  = 1.58 (s, 1H), 1.71 (s, 6H), 2.10 (s, 9H), 5.54 (s, 1H) pyrrole N-H, 6.19-6.21 (m, 1H) pyrrole C4-H, 6.43-6.45 (m,  $J$  = 1 Hz, 1H) pyrrole C3-H, 6.87-6.89 (m,  $J$  = 1 Hz, 1H) pyrrole C5-H;  $^{13}\text{C}$  NMR ( $\text{CDCl}_3$ )  $\delta$  = 29.52, 30.94,

36.38, 41.97, 52.06, 107.75 pyrrole C2, 109.63 pyrrole C3, C4, 120.83 pyrrole C5, 160.25 carbonyl carbon; ESI-MS calculated for C<sub>15</sub>H<sub>20</sub> N<sub>2</sub>O : 244.5, found: 245.1 [M+H]<sup>+</sup> .

**2.7.14 - 2-Adamantyl-pyrrole-2-carboxamide (105):** 297 mg (61%) of white powder, <sup>1</sup>H NMR (CDCl<sub>3</sub>) δ = 1.56 (s, 2H), 1.67 (s, 1H), 1.71 (s, 1H), 1.77 (s, 2H), 1.83 (s, 1H), 1.89 (s, 8H), 2.01 (s, 2H), 4.19-4.23 (m, 1H), 6.17 (s, 1H) pyrrole N-H, 6.23-6.25 (m, 1H) pyrrole C4-H, 6.54-6.55 (m, 1H) pyrrole C3-H, 6.90-6.91 (m, J = 6 Hz, 1H) pyrrole C5-H; <sup>13</sup>C NMR (CDCl<sub>3</sub>) δ = 27.13, 27.25, 32.04, 32.14, 37.15, 37.54, 53.05, 109.76, 121.03; ESI-MS calculated for C<sub>15</sub>H<sub>20</sub> N<sub>2</sub>O : 244.5, found: 245.1 [M+H]<sup>+</sup> .

**2.7.15 - 2-Adamantyl-2-phenyl-2R-hydroxy-ethanamide (123):** 501 mg (30%) of white powder; <sup>1</sup>H NMR (CDCl<sub>3</sub>) δ = 1.17-1.82 (m, 14H), 3.94-3.97 (m, 1H), 4.97 (s, 1H), 6.29 (bs, 1H), 7.24-7.44 (m, 5H); <sup>13</sup>C NMR (CDCl<sub>3</sub>) δ = 27.05, 31.76, 37.00, 53.44, 74.16, 127.47, 128.97, 139.79, 171.09; ESI-MS calculated for C<sub>18</sub>H<sub>23</sub>NO<sub>2</sub>: 287.4, found: 286.1 [M+H]<sup>+</sup> .

**2.7.16 - Cyclooctyl-2-Phenyl-2R-hydroxyl ethanamide (117):** 643 mg (41%) of white powder; <sup>1</sup>H NMR (CDCl<sub>3</sub>) δ = 1.18-1.75 (m, 14H), 3.87-3.95 (m, J = 4 Hz, 1H), 4.91 (s, 1H), 5.87 (bs, 1H), 7.24-7.46 (m, 5H); <sup>13</sup>C NMR (CDCl<sub>3</sub>) δ = 23.55, 25.35, 27.11, 32.19, 49.71, 74.07, 126.74, 128.93, 139.69, 170.71; ESI-MS calculated for C<sub>16</sub>H<sub>23</sub>NO<sub>2</sub>: 261.2, found: 262.2 [M+H]<sup>+</sup> .

**2.7.17 - (1R,2R,3R,5S)-(-)-Isopinocampheyl-2-Phenyl-2R-hydroxyl ethanamide (119):** 717 mg (42%) of oily liquid; <sup>1</sup>H NMR (CDCl<sub>3</sub>) δ =

0.72 (d,  $J = 10$  Hz, 1H), 0.95-0.97 (m, 5H), 1.14 (s, 3H), 1.17-1.21 (t,  $J = 7$  Hz, 1H), 1.39-1.45 (m, 1H), 1.53-1.61 (quintet,  $J = 8$  Hz, 1H), 1.71 (t,  $J = 6$  Hz, 1H), 1.85-1.89 (m, 1H), 2.29-2.35 (m, 1H), 2.46-2.53 (m, 1H), 4.16-4.24 (m, 1H), 4.94 (s, 1H), 5.85 (bs, 1H), 7.24-7.35 (m, 5H);  $^{13}\text{C}$  NMR ( $\text{CDCl}_3$ )  $\delta = 14.21, 21.08, 23.33, 27.99, 35.29, 36.92, 38.39, 41.48, 46.24, 48.12, 60.4341, 74.09, 126.87, 128.91, 139.73, 171.44$ ; ESI-MS calculated for  $\text{C}_{16}\text{H}_{23}\text{NO}_2$ : 287.4, found: 288.1  $[\text{M}+\text{H}]^+$ .

**2.7.18 - Cycloheptyl-2-Phenyl-2R-hydroxyl ethanamide (125):** 368 mg (21%) of white powder ;  $^1\text{H}$  NMR ( $\text{CDCl}_3$ )  $\delta = 0.74-1.04$  (m, 1H), 1.19 (s, 1H), 1.23-1.52 (m, 10H), 1.72-1.84 (m, 2H), 3.41-3.69 (m, 1H), 3.83-3.92 (m,  $J = 5$ Hz, 1H), 4.91 (s, 1H), 5.85-5.92 (m, 1H), 7.24-7.47 (m, 5H);  $^{13}\text{C}$  NMR ( $\text{CDCl}_3$ )  $\delta = 24.02, 27.83, 34.94, 50.72, 74.08, 126.89, 129.25, 139.67, 170.73$ ; ESI-MS calculated for  $\text{C}_{15}\text{H}_{21}\text{NO}_2$ : 247.3, found: 248.1  $[\text{M}+\text{H}]^+$ .

**2.7.19 – Trans-4-methyl-cyclohexyl-2-Phenyl-2R hydroxyl ethanamide (126):** 341 mg (23%) of white powder;  $^1\text{H}$  NMR ( $\text{CDCl}_3$ )  $\delta = 0.89$  (d,  $J = 7$  Hz, 3H), 0.99-1.85 (m, 4H), 1.26-1.36 (m, 1H), 1.67-1.74 (m, 2H), 1.87-1.97 (m, 2H), 3.67-3.77 (m, 1H), 5.00 (s, 1H), 5.80-5.82 (m, 1H), 7.36-7.42 (m, 5H);  $^{13}\text{C}$  NMR ( $\text{CDCl}_3$ )  $\delta = 22.19, 31.85, 32.89, 33.72, 73.99, 126.81, 128.31, 128.63, 139.89, 171.65$ ; ESI-MS calculated for  $\text{C}_{15}\text{H}_{21}\text{NO}_2$ : 247.34, found: 248.2  $[\text{M}+\text{H}]^+$ .

**2.7.20 - 1-Adamantyl-2-Phenyl-2R-hydroxyl ethanamide (121):** 281 mg (16%) of white powder ;  $^1\text{H}$  NMR ( $\text{CDCl}_3$ )  $\delta = 1.64$  (s, 6H), 1.93 (s, 6H), 2.03-2.05 (m, 3H), 3.99 (s, 1H), 4.83 (s, 1H), 5.84 (s, 1H), 7.29-7.36 (m, 5H);  $^{13}\text{C}$  NMR ( $\text{CDCl}_3$ )

$\delta$  = 29.39, 36.29, 41.62, 52.28, 74.13, 126.81, 128.45, 128.63, 140.07, 171.29;  
ESI-MS calculated for  $C_{18}H_{23}NO_2$ : 287.4, found: 286.1  $[M+H]^+$  .

**2.7.21 — 2-Adamantyl-2-phenyl-2S-hydroxy-ethanamide (124):** 308 mg (18%)  
of white powder ;  $^1H$  NMR ( $CDCl_3$ )  $\delta$  = 0.87-1.91 (m, 10H), 3.78-3.93 (m, 1H),  
5.23-5.40 (m, 1H), 6.04-6.19 (m, 1H), 7.28-7.44 (m, 5H) ;  $^{13}C$  NMR ( $CDCl_3$ )  $\delta$  =  
26.89, 31.57, 36.92, 37.34, 53.11, 73.28, 126.88, 127.48, 128.84, 129.13, 135.36,  
137.81, 165.56, 171.80; ESI-MS calculated for  $C_{18}H_{23}NO_2$ : 247.71,  
found: 248.1  $[M+H]^+$  .

**2.7.22 - Cyclooctyl-2-Phenyl-2S-hydroxyl ethanamide (118):** 426 mg (27%) of  
transparent oily liquid;  $^1H$  NMR ( $CDCl_3$ )  $\delta$  = 1.38-1.74 (m, 12H), 3.82-3.91 (m, 1H),  
4.83-4.86 (m, 2H), 6.74-6.76 (m, 1H), 7.24-7.47 (m, 5H);  $^{13}C$  NMR ( $CDCl_3$ )  $\delta$  =  
23.56, 25.35, 27.11, 32.19, 49.70, 60.43, 74.07, 126.88, 127.46, 128.84, 139.69,  
170.30; ESI-MS calculated for  $C_{16}H_{23}NO_2$ : 261.2, found: 262.1  $[M+H]^+$  .

**2.7.23 - (1R,2R,3R,5S)-(-)-Isopinocampheyl-2-Phenyl-2S-hydroxyl ethanamide (120):** 537 mg (31%) of white powder;  $^1H$  NMR ( $CDCl_3$ )  $\delta$   
= 0.80 (d,  $J$  = 10 Hz, 1H), 1.04 (s, 3H), 1.07 (d,  $J$  = 7 Hz, 2H), 1.23 (s, 3H), 1.39-  
1.45 (m, 1H), 1.74-1.83 (m, 2H), 1.91-1.96 (m, 1H), 2.36-2.43 (m, 1H), 2.52-2.59  
(m, 1H), 3.94 (s, 1H), 4.22-4.30 (m, 1H), 4.99 (s, 1H), 6.18-6.20 (m, 1H), 7.33-7.41  
(m, 5H);  $^{13}C$  NMR ( $CDCl_3$ )  $\delta$  = 20.71, 23.34, 28.01, 35.26, 36.77, 38.42, 41.53,  
46.08, 47.68, 48.03, 74.13, 126.93, 128.89, 139.81, 171.42 ; ESI-MS calculated  
for  $C_{16}H_{23}NO_2$ : 287.4, found: 288.3  $[M+H]^+$  .

**2.7.24 - Cycloheptyl-2-Phenyl-2S-hydroxyl ethanamide (128):** 366 mg (21%) of white powder;  $^1\text{H}$  NMR ( $\text{CDCl}_3$ )  $\delta$  = 1.26-1.57 (m, 11H), 1.75-1.83 (m, 2H), 3.78-3.87 (m,  $J$  = 4 Hz, 1H), 4.50 (s, 1H), 4.84 (s, 1H), 6.54 (bs, 1H), 7.27-7.34 (m, 5H);  $^{13}\text{C}$  NMR ( $\text{CDCl}_3$ )  $\delta$  = 23.99, 27.89, 34.82, 50.36, 73.98, 126.74, 125.31, 128.59, 139.98, 171.21; ESI-MS: calculated for  $\text{C}_{15}\text{H}_{21}\text{NO}_2$  247.34; found: 248.1  $[\text{M}+\text{H}]^+$  .

**2.7.25 - Trans-4-methyl-cyclohexyl-2S-Phenyl-2-hydroxyl ethanamide (127):** 373 mg (25%) of off- white powder ;  $^1\text{H}$  NMR ( $\text{CDCl}_3$ )  $\delta$  = 0.79-0.82 (m, 3H), 0.90-1.09 (m, 4H), 1.18-1.27 (m, 1H), 1.58-1.65 (m, 2H), 1.78-1.89 (m, 2H), 3.37-3.67 (m, 2H), 4.91 (s, 1H), 5.75 (bs, 1H), 7.24-7.37 (m, 5H);  $^{13}\text{C}$  NMR ( $\text{CDCl}_3$ )  $\delta$  = 22.12, 31.85, 32.99, 33.71, 48.79, 74.09, 126.93, 129.26, 139.65, 171.18; ESI-MS calculated for  $\text{C}_{15}\text{H}_{21}\text{NO}_2$ : 247.3, found: 248.2  $[\text{M}+\text{H}]^+$  .

**2.7.26 - 1-Adamantyl-2-Phenyl-2S-hydroxyl ethanamide (122):** 446 mg (26%) of white powder;  $^1\text{H}$  NMR ( $\text{CDCl}_3$ )  $\delta$  = 1.64 (s, 6H), 1.92-1.93 (m, 6H), 2.04 (s, 3H), 4.12 (s, 1H), 4.81 (s, 1H), 5.94 (s, 1H), 7.30-7.36 (m, 5H);  $^{13}\text{C}$  NMR ( $\text{CDCl}_3$ )  $\delta$  = 29.39, 36.26, 41.42, 52.09, 74.12, 126.84, 128.39, 128.76, 140.11, 171.23; ESI-MS calculated for  $\text{C}_{18}\text{H}_{23}\text{NO}_2$ : 287.39, found: 286.0  $[\text{M}+\text{H}]^+$  .

**2.7.27- 4-(trans-methyl)-cyclohexyl- imidazole -2-carboxamide (112):** 364 mg (88%) of white powder  $^1\text{H}$  NMR ( $\text{CDCl}_3$ )  $\delta$  = 0.91 (d,  $J$  = 7 Hz, 3H), 1.04-1.14 (m, 2H), 1.24-1.39 (m, 3H), 1.69-1.78 (m, 2H), 2.00-2.06 (m, 2H), 3.49-3.50 (m, 1H), 3.81-3.90 (m,  $J$  = 4 Hz, 1H), 7.11 (s, 1H) imidazole C4-H, 7.16 (s, 1H) imidazole C5-H;  $^{13}\text{C}$  NMR ( $\text{CDCl}_3$ )  $\delta$  = 22.24, 31.86, 32.91, 33.95, 48.64, 118.75 imidazole

C2, 129.28 imidazole C4, 141.51 imidazole C5, 157.89 carbonyl carbon; ESI-MS calculated for C<sub>11</sub>H<sub>17</sub>N<sub>3</sub>O: 207.3, found: 208.1 [M+H]<sup>+</sup> .

**2.7.28 – (1R,2R,3R,5S)-(-)-Isopinocampheyl-imidazole-2-carboxamide (106):**

440 mg (89%) of off-white powder; <sup>1</sup>H NMR (CDCl<sub>3</sub>) δ = 0.88-0.98 (m, 1H), 1.02 (s, 2H), 1.08 (d, *J* = 7 Hz, 2H), 1.18 (s, 2H), 1.65-1.71 (m, 1H), 1.78-1.82 (m, 1H), 1.91-1.95 (m, 1H), 1.97-2.02 (m, 1H), 2.34-2.41 (m, 1H), 2.52-2.59 (m, 1H), 4.34-4.42 (m, 1H), 7.12 (s, 1H) imidazole C5-H, 7.19 (s, 2H) imidazole C5-H; <sup>13</sup>C NMR (CDCl<sub>3</sub>) δ = 20.83, 23.45, 28.05, 35.12, 36.61, 38.54, 41.57, 45.54, 47.81, 48.04, 119.45 imidazole C2, 129.30 imidazole C4, 141.42 imidazole C5, 158.52 carbonyl carbon; ESI-MS calculated for C<sub>14</sub>H<sub>21</sub>N<sub>3</sub>O: 247.3, found: 248.2 [M+H]<sup>+</sup> .

**2.7.29 – Cyclooctyl-imidazole-2-carboxamide (108):**

422 mg (96%) of off-white powder; <sup>1</sup>H NMR (CDCl<sub>3</sub>) δ = 1.46-1.89 (m, 11H), 4.06-4.14 (m, *J* = 4 Hz, 1H), 7.15 (s, 1H), 7.19 (s, 2H) imidazole C4-H and C5-H; <sup>13</sup>C NMR (CDCl<sub>3</sub>) δ = 23.76, 25.49, 27.17, 31.87, 141.63 imidazole C4, C5, 151.71 carbonyl carbon; ESI-MS calculated for C<sub>12</sub>H<sub>19</sub>N<sub>3</sub>O: 221.3, found: 222.1 [M+H]<sup>+</sup> .

**2.7.30 - Cycloheptyl- imidazole -2-carboxamide (109):**

397 mg (96%) of white powder; <sup>1</sup>H NMR (CDCl<sub>3</sub>) δ = 1.25 (s, 1H), 1.51-1.72 (m, 14H), 1.98-2.05 (m, 1H), 4.06-4.15 (m, 1H), 7.11-7.12 (m, 1H) imidazole C4-H, 7.13-7.14 (m, 1H) imidazole C5-H; <sup>13</sup>C NMR (CDCl<sub>3</sub>) δ = 24.12, 28.09, 30.96, 34.94, 50.74, 141.22 imidazole C4, C5, 157.23 carbonyl carbon; ESI-MS calculated for C<sub>11</sub>H<sub>17</sub>N<sub>3</sub>O: 207.2, found: 208.2 [M+H]<sup>+</sup> .

**2.7.31 - 1-Adamantyl- imidazole -2-carboxamide (110):** 365mg (75%) of white powder ;  $^1\text{H}$  NMR ( $\text{CDCl}_3$ )  $\delta$  = 1.56 (s, 1H), 1.59 (s, 3H), 1.72 (s, 4H), 2.12 (s, 7H), 3.49 (d,  $J$  = 6 Hz, 1H), 7.09 (m, 1H) imidazole C4-H, 7.11-7.13 (m, 1H) imidazole C5-H;  $^{13}\text{C}$  NMR ( $\text{CDCl}_3$ )  $\delta$  = 22.56, 29.45, 36.31, 41.55, 52.44, 119.27 imidazole C2, 129.27 imidazole C4, 141.94 imidazole C5, 158.17 carbonyl carbon; ESI-MS calculated for  $\text{C}_{14}\text{H}_{19}\text{N}_3\text{O}$ : 245.3, found: 246.1  $[\text{M}+\text{H}]^+$

**2.7.32 - 2-Adamantyl- imidazole -2-carboxamide (111):** 362mg (74%) of white powder;  $^1\text{H}$  NMR ( $\text{CDCl}_3$ )  $\delta$  = 1.19 (s, 1H), 1.49 (s, 6H), 1.65 (t,  $J$  = 3 Hz, 3H), 2.04-2.08 (m, 2H), 2.16 (m, 2H), 7.28-7.32 (m, 2H) imidazole C4-H and C5-H;  $^{13}\text{C}$  NMR ( $\text{CDCl}_3\text{-d}$ )  $\delta$  = 27.11, 27.19, 31.83, 32.04, 37.14, 37.49, 53.47, 118.81 imidazole C2, 129.69 imidazole C4; ESI-MS calculated for  $\text{C}_{14}\text{H}_{19}\text{N}_3\text{O}$ : 245.3, found: 245.9  $[\text{M}+\text{H}]^+$  .

**2.7.33 - MIC testing.** MIC testing is performed by microbroth dilution method using Mueller Hinton (MH) broth (Cation Adjusted) to the calcium and magnesium ion concentration recommended in the CLSI standard M7-A7 (Becton Dickinson). MIC testing also is performed by microbroth dilution method using 7H9 broth (Sigma-Aldrich). The justification for use of both MH and 7H9 broth for compound screening is anti-mycobacterial compounds have shown to display different MIC activity depending on the broth that is used in the MIC assay. Rapid growing NTMs are grown on 7H11 agar plates (Sigma-Aldrich) for 3 days at 35-37°C in ambient air (depending on bacterial strain). Slow growing (SG) NTMs are grown on agar 7H11 plates (Sigma-Aldrich) for 21-30 days at 37°C in ambient air. The CFUs are taken from the agar plates and placed in either MH or 7H9 broth with 0.05% tween-80 and grown at 35-37°C in ambient air until the optical density (OD) absorbance taken after 3 days (RGM) or 12 (SG) of growth is an (OD) 0.08 - 0.1 (0.5 McFarland Standard). The bacterial cell suspensions are then confirmed by preparing them in saline, matching the (OD) 0.08 - 0.1 (0.5 McFarland Standard). The broth (MH or 7H9) 180 µL is added to the first column in the 96-well plates. Then 100 µL of the broth (MH or 7H9) is added to the other columns in the 96 well plate. Compounds are made using 1.28 mg/mL in DMSO and used immediately for test range 32-0.062 µg/mL and 20 µL of compound added to the first column of wells and 100 µL serially diluted. Finally, 100 µL NTM cell suspension is added in all the wells except the media only control wells. QC agents specific for each organism 1) bacteria only negative control 2) media only negative control 3) (CLA) clarithromycin positive drug control 4) optional E. coli control. RGMs are assayed

for ODs on day 3, and SL on day 12. After that, the plate is assayed by using the Resazurin Microtiter Assay Plate method as recommended by the Clinical and Laboratories Standards Institute. Briefly, the method uses the addition of resazurin (7-Hydroxy-3H-phenoxazin-3-one 10-oxide) to the MIC 96 well plate. Resazurin is a blue dye, itself weakly fluorescent until it is irreversibly reduced to the pink colored and highly red fluorescent resorufin.

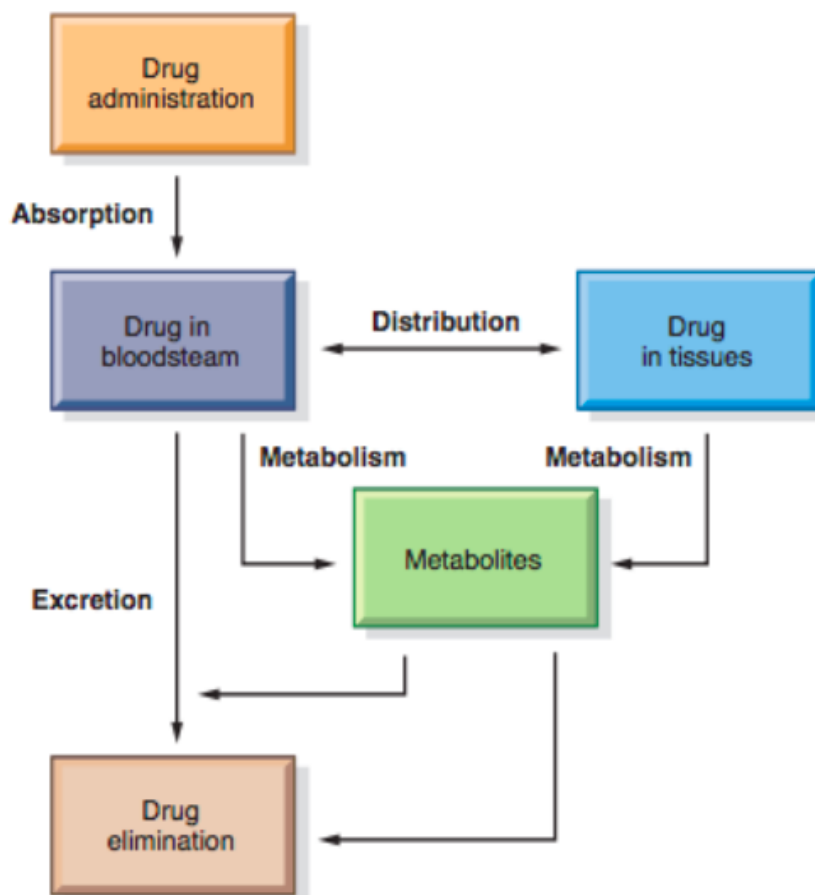
## **Chapter 3: Pharmacokinetic assays of active novel compounds**

### **3.1. Introduction**

In addition to the microbiological efficacy, an important aspect of drug discovery and development is the physicochemical and pharmacokinetic profiles that have influence on a drug's absorption, distribution and metabolism. These assays, presented in this chapter include aqueous solubility, permeability and plasma protein binding, all of which are important parameters before a compound will proceed to further preclinical development.

### **3.2. Physicochemical and pharmacokinetic assays**

Common pharmacokinetic parameters of a drug are absorption, distribution, metabolism and excretion (ADME). ADME profiles help to predict drug entering the body (A), repositioning throughout the body (D), altering within the body (M) and exiting the body (E) as shown in Figure 12.[55] Optimization of ADME profiles of therapeutics is crucial for clinical, as well as commercial, success of these drugs. [56]. Drug candidates might fail during development because of numerous reasons and poor PK and ADME profiles is one of the major reasons for its failure.[57] *M. tb* infections are prevalent in poor and rural areas of the world, therefore it is important that new anti-*M. tb* chemotherapy to be orally bioavailable. This project focuses on oral administration and the ADME profiles required.



**Figure 12:** A representation of the four fundamental pathways of drug movement and modification in the body, the ADME processes. [58]

Absorption of a compound is affected by many factors, however aqueous solubility and membrane permeability are two common determinants medicinal chemists employ to evaluate a compound's viability for further preclinical testing. A compound with poor solubility will most likely poorly dissolve in gastrointestinal fluid after oral administration, therefore has little chance of permeating across the gut wall. For compounds intended for oral administration, a high aqueous solubility accompanied by a high membrane permeability is desirable. As per FDA guidelines, for a compound to be used as an active pharmaceutical ingredient in a

solid- oral dosage form an aqueous solubility of 30 to 100 mg/mL is desirable.[59] Human plasma protein binding patterns and metabolic stability influence a compound's distribution and metabolic profile. Highly protein bound drugs have longer half- lives, since low concentrations of drug are freely available for being metabolized by the metabolic enzymes. High protein binding is also beneficial since it lowers free drug concentration results in reduced side effects. Low plasma protein binding, on the other hand, leads to higher free plasma fraction causing an increase in volume of distribution and a shorter elimination half-life. Compounds susceptible to GI and/or liver metabolic mechanisms tend to have short half-lives leading to potential multiple doses per day, which is not a desirable characteristic for an oral drug. Metabolic stability data should be taken in consideration and influence dosage regimen. Half-lives of about 12-18 hours are desirable for compounds designed for once a day dosing. The assays conducted for this project are the aqueous solubility and permeability which may influence the absorption patterns of compounds. Plasma protein binding assay and metabolic stability assay using mouse liver enzymes are also conducted which may influence the bioavailability, the distribution and metabolism patterns of compounds.

### **3.3. Solubility assay**

Solubility represents an important parameter during pharmaceutical research and development, where it translates directly into their pharmacokinetics, pharmacodynamics and toxicodynamics.[60] Buffered water is the solvent of choice for pharmaceutical formulations.[61] Aqueous solubility is a critical factor as drug substances have to be dissolved before they can be absorbed.[57] Poorly

soluble compounds can dramatically reduce productivity in drug discovery and development. Potential complications arising from low aqueous solubility are:

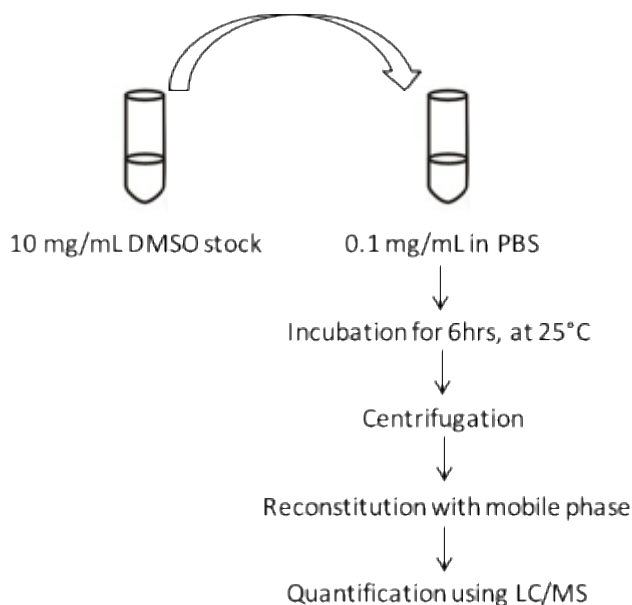
- Compound precipitation during:
  - serial dilutions in buffer
  - biochemical assays
  - functional assays
  - cell-based assays
- Reduced target specificity
- Low bioavailability in animal studies [62]

Aqueous solubility can be measured as 'thermodynamic' aqueous solubility or as 'kinetic' aqueous solubility. The thermodynamic solubility of a compound is defined as the maximum quantity of the compound which can be completely dissolved at a given temperature and pressure in a given amount of solvent, and is in equilibrium with the solution phase.[63] Kinetic solubility measures a precipitation rate rather than solubility.[63] Thermodynamic aqueous solubility testing requires pure crystalline forms of compounds and a larger amount of compound is needed for the assay as compared to kinetic aqueous solubility testing.[64] Hence, during drug discovery, kinetic aqueous solubility testing is preferred since compounds are available in a small amount and it is difficult to maintain consistency between the batches. Kinetic approaches do not necessarily involve a long incubation period with thorough agitation and assays can be completed quickly and efficiently.[57]. Kinetic solubility offers a high-throughput method with relatively small amount of compound, especially useful in the early

discovery phases.[60] Thermodynamic solubility is typically performed during the latter stages of drug discovery or early development, and may help to design formulation strategies for *in vivo* studies. For this project we have used the kinetic aqueous solubility assay. Kinetic solubility has two distinguishing characteristics: (a) the compound initially is fully dissolved in an organic solvent (e.g., DMSO) then added to the aqueous buffer, and (b) equilibrium is not reached between the compound dissolved in solution and undissolved compound.[64] Thermodynamic solubility is distinguished by (a) the addition of aqueous solvent directly to solid crystalline material and (b) establishment of equilibrium between the dissolved and undissolved material.[64] Long mixing time is applied to ensure equilibrium (e.g., 24–72 hours) for thermodynamic solubility assay.[57] Kinetic solubility in general tends to be higher than thermodynamic solubility.[64] This is because the presence of DMSO helps enhance solubility and supersaturation of the solution occurs due to a non-equilibrium state.

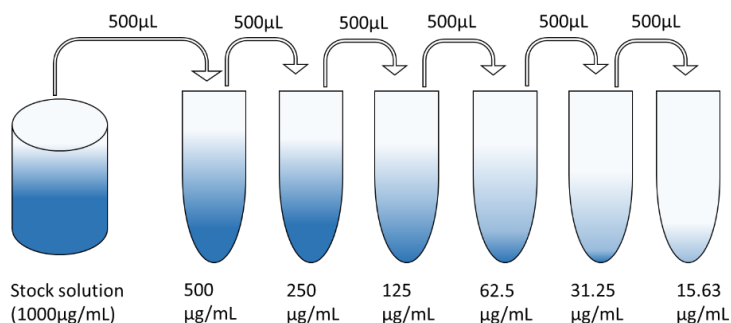
As mentioned above, in this project we used the kinetic aqueous solubility assay to determine the solubility of compounds described in chapter 2. The procedure followed for the kinetic aqueous solubility testing is described with respect to the sample preparation and the solubility calculations. As shown in Figure 13, DMSO stock solutions of compounds are prepared. Aliquots of the stock solutions are diluted in a physiologically relevant buffer (phosphate buffered saline (PBS)) at pH 7.4. The diluted compound-buffer samples were left for 6 hours at room temperature to allow for maximum dissolution without compound degradation. Aliquots from the samples were collected and centrifuged to separate

undissolved particles. The supernatant was further diluted four times with a solution of internal standard prepared in 50: 50 of methanol and water. Compound concentration in this diluted solution was quantified using LC-MSMS. The assay was conducted in triplicates for each sample and the solubility of the compound was reported as mean  $\pm$  SD.



**Figure 13:** Method used for kinetic aqueous solubility testing. [36]

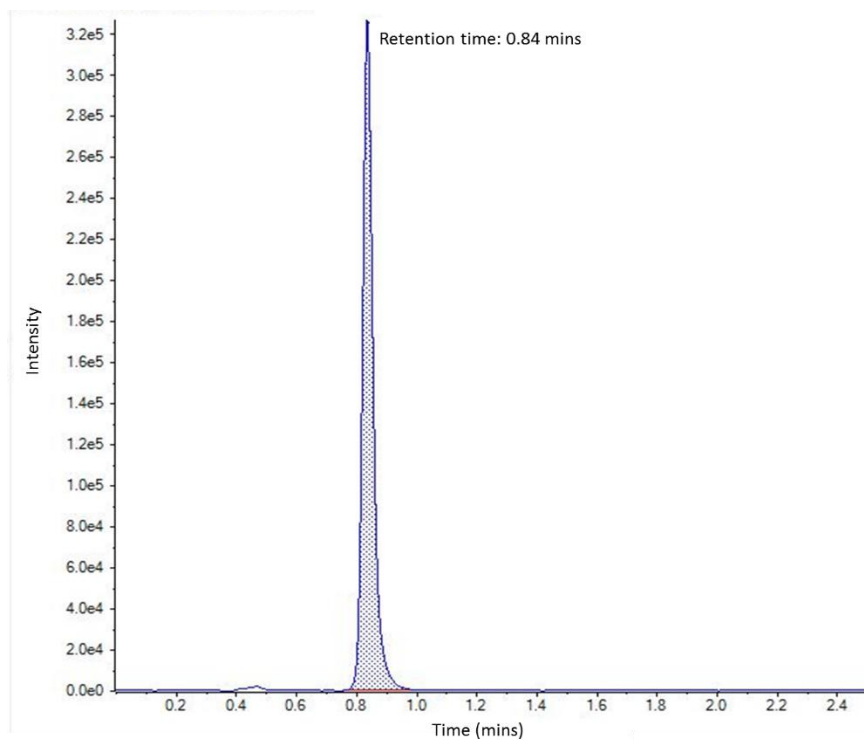
Calibration curves are used to understand the instrumental response to an analyte and predict the concentration in an unknown sample. Generally, a set of standard samples are made at various concentrations with a range that includes the unknown of interest and the instrumental response at each concentration is recorded.[65] Serial dilution was used for the preparation of standard samples (Figure 14). The data obtained by quantification of standard samples is then plotted to obtain an equation of the linear data, so that unknown concentrations can be predicted.



**Figure 14:** Serial dilution

An internal standard is a substance added in a constant amount to a sample, blank, and standard in an analysis. The internal standard can compensate for both systematic and random errors.[66] For example, if there are any fluctuations in the instrument that cause random errors in the measurement, these fluctuations are expected to be the same for both the internal standard and the analyte and thus the ratio of signals does not change. For systematic errors, such as effects of the solvent, as long as the effect is equal for both the standard and the analyte, the ratio is again unaffected.[66] Warfarin was used as the internal standard for these experiments.

The solubility calculations for a representative compound, **98**, are described herein as an example. The observed values for the areas under the curve (AUC) and the area ratios of the sample and the internal standard for **98** are shown in Table 17. An example of a LC chromatogram of standard-6 solution of **98**, containing 250 ng/mL of compound **98**, with a retention time of 0.84 minutes is shown in Figure 15 and the area of the peak is tabulated in Table 15 below.



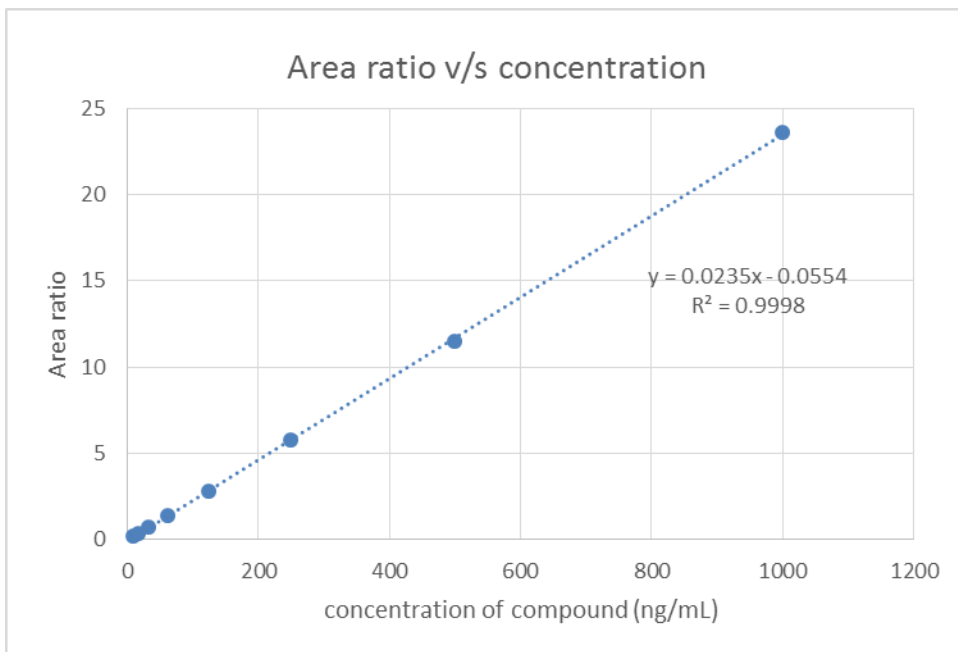
**Figure 15:** LC chromatogram of standard-6 (250 ng/mL) of compound **98**

**Table 15:** Concentrations, AUC and area ratios for compound **98**

Sample Name	AUC for compound	AUC for internal standard	Area ratio	Actual concentration (ng/mL)
Standard-1	26393	127483	0.207	7.82
Standard-2	48401	128967	0.375	15.63
Standard-3	95583	130730	0.731	31.25
Standard-4	201919	141570	1.426	62.50
Standard-5	392115	140334	2.794	125.00
Standard-6	796223	136925	5.815	250.00
Standard-7	1568078	136642	11.476	500.00
Standard-8	3106069	131686	23.587	1000.00
Blank	280	277	1.011	N/A
98-1	3574181	199569	17.909	N/A
98-2	4172132	192247	21.702	N/A
98-3	3685428	191517	19.243	N/A

After AUC determination of solubility samples and internal standard, AUC and area ratios were used to calculate drug concentration using the calibration curve. The area ratios were plotted as a function of the compound concentration,

as shown in Figure 16. The equation of the line was obtained from the regression plot which was further used for calculation of the compound concentration in test samples. The area ratios of test samples were substituted into the equation for y, and solving for x gave the concentration of compound.



**Figure 16:** Plot of area ratio v/s compound concentration for compound **98**

**Calculations:** The equation for calculation of the solubility can be found out from the plot above and is as follows:

$$y = 0.0235x - 0.0554$$

Where y stands for the area ratio and x stands for the concentration, hence the unknown concentration can be calculated as follows

$$x = \frac{(y + 0.0554)}{0.0235}$$

for 98-1,

$$x = \frac{(17.909+0.0554)}{0.0235}$$

$$x = 764.44 \text{ ng/mL}$$

Since the test samples were prepared by four times dilution of the samples, the calculated value of the concentration was multiplied by the dilution factor.

$$x = 764.44 * 4 \text{ ng/mL}$$

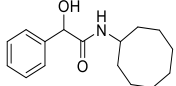
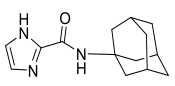
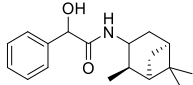
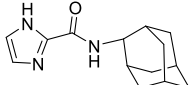
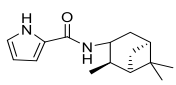
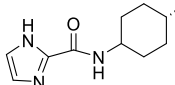
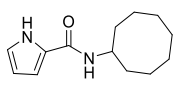
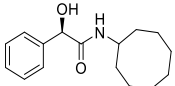
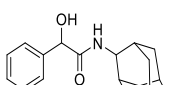
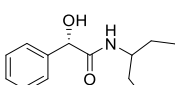
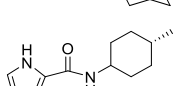
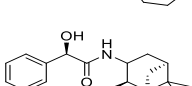
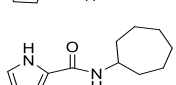
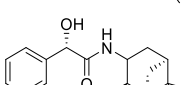
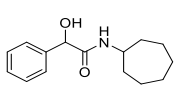
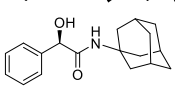
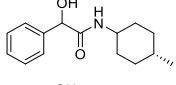
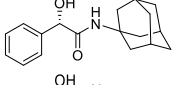
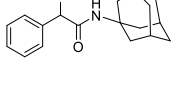
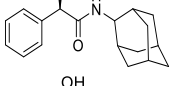
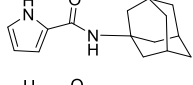
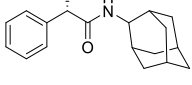
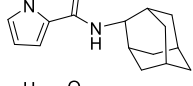
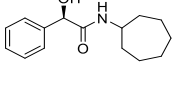
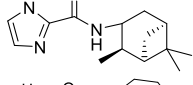
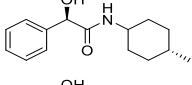
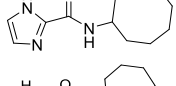
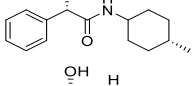
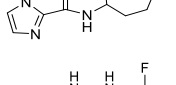
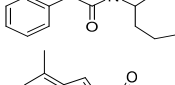

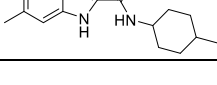
$$x = 3057.78 \text{ ng/mL} \approx 3.058 \text{ } \mu\text{g/mL}$$

Similarly, the concentration was calculated for 98-2 and 98-3 as 3.703  $\mu\text{g/mL}$  and 3.285  $\mu\text{g/mL}$ , respectively.

On averaging and calculating the standard deviation for this value, the result for the kinetic aqueous solubility of compound **98** was found to be  $3.4 \pm 0.3 \text{ } \mu\text{g/mL}$ . All of the 30 compounds synthesized were tested for their kinetic aqueous solubility. The values for the aqueous solubility each of the compounds was calculated as explained above and the results are tabulated in Table 16. It was observed that the racemic mandelic acid analogs (e.g.: Table 16: compounds **77**, **101**, **102**) showed a 1000-fold increase in aqueous solubility as compared to the urea and IC analogs with the same head group. However, the pure enantiomeric forms (e.g.: Table 16: compounds **121**, **122**, **127**) showed a 10 to 100-fold improvement in aqueous solubility. The pyrrole-2-carboxamides and the imidazole-2-carboxamides showed aqueous solubility profiles similar to each other (e.g.: Table 16: compounds **88**, **98**, **108**). Their aqueous solubility improved as compared to the previous classes, but they possessed lower solubility compared to the mandelic acid analogs. Compound **77** was found to have the highest kinetic aqueous solubility of  $182 \pm 15.5 \text{ } \mu\text{g/mL}$  but it had a modest MIC value of  $32 \text{ } \mu\text{g/mL}$  against *M. tb*, whereas, compound **88** was found to have the best MIC value of  $2 \text{ } \mu\text{g/mL}$  against *M. tb* but it had a fairly low aqueous kinetic solubility of  $9.8 \pm 2.4$

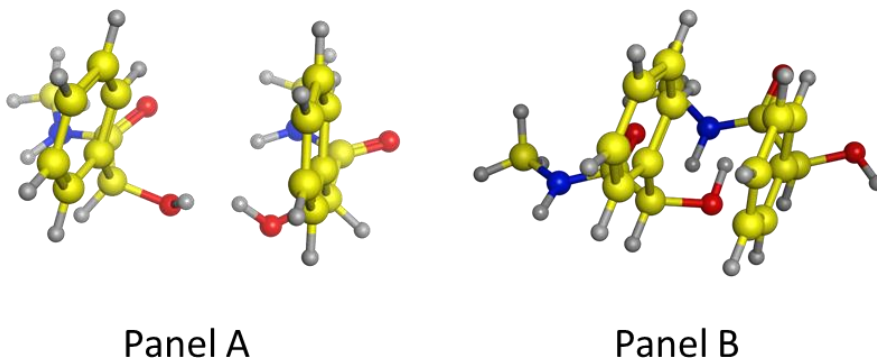
$\mu\text{g/mL}$ . This is a common trend seen in TB drug discovery, since the mycobacterial cell wall is highly lipophilic where the drugs need to penetrate this barrier. Lipophilic compounds more easily penetrate the cell wall and tend to be more active anti-*M. tb* agents, however, this tends to negatively impact the aqueous solubility profile. On the other hand, hydrophilic compounds show better aqueous solubility profiles, but are unable to penetrate the cell wall and reach the site of action and hence are found to be inactive against mycobacteria. Verapamil was used as the standard to validate the method, reported value is  $38 \mu\text{g/mL}$ . [62] The kinetic solubility observed by our method is  $37 \pm 5 \mu\text{g/mL}$ .

**Table 16:** Results for the kinetic aqueous solubility assay

No	Compound	Aqueous Solubility ( $\mu\text{g/mL}$ )	No	Compound	Aqueous Solubility ( $\mu\text{g/mL}$ )
77		182 $\pm$ 15.5	110		11.2 $\pm$ 0.3
78		17.8 $\pm$ 1.2	111		15.5 $\pm$ 0.2
88		9.8 $\pm$ 2.4	112		11.3 $\pm$ 4.8
89		7.2 $\pm$ 0.7	117		28.9 $\pm$ 0.3
95		31.2 $\pm$ 1	118		25.5 $\pm$ 0.9
96		15.1 $\pm$ 2.8	119		32.1 $\pm$ 1.2
98		3.4 $\pm$ 0.3	120		6.4 $\pm$ 0.2
101		144.5 $\pm$ 0.4	121		73.9 $\pm$ 1.8
102		114.3 $\pm$ 3.5	122		49.2 $\pm$ 2.3
103		45.1 $\pm$ 1	123		42.9 $\pm$ 0.9
104		3.9 $\pm$ 0.5	124		37.2 $\pm$ 1.1
105		3.8 $\pm$ 0.1	125		44.6 $\pm$ 0.9
106		26.8 $\pm$ 2.5	126		7.9 $\pm$ 0.3
108		8.3 $\pm$ 1.4	127		57.5 $\pm$ 1.9
109		19.3 $\pm$ 0.4	128		17.5 $\pm$ 0.1
63		<0.1	65		<1

The free hydroxyl group found in the mandelic acids, is beneficial for enhancing its aqueous solubility. In the case of the racemic mandelic acid analogs, the aqueous solubility was enhanced greater as compared to the chirally pure enantiomeric forms. The chirally pure enantiomeric forms also showed enhanced solubility, but the enhancement observed was lower than that observed with the racemic analogs. The lattice energy in the chirally pure compounds may be higher than that of their racemic counterparts, due to the close molecular packing, as shown in panel B of Figure 17. This tighter molecular packing makes it difficult for the water molecules to break these intermolecular interactions.[67] This may be studied further with the help of X-ray crystallography to understand better the crystal packing of the molecules. The tighter packing may be the reason for the lower kinetic solubility observed. Also, due to the lower solubility, there may be lesser amount of compound in solution in the MIC experiments leading to lower MIC values as seen with the pure chiral mandelic acid analogs. In case of the mandelic acid analogs with the (1R,2R,3R,5S)-(-)-isopinocampheyl head group, the enhancement of aqueous solubility was not significant, this may be due to the high lipophilicity associated with the head group. In case of the mandelic acid analogs with the 2-adamantyl head group, aqueous solubility values observed were fairly similar for the racemic as well as the chirally pure compounds, however the racemic analog, **95**, was found to be active against *M. tb* and *M. abscessus*. The reason behind this may also be the high lattice energy associated with the chirally pure compounds. However, it is very difficult to precisely quantify or predict the

aqueous solubility due to the complicated solubilization process and solid phase chemistry of drug candidates.[57]



**Figure 17:** Closer molecular packing seen in chirally pure compounds  
**Panel A:** Racemic mandelic acid analog  
**Panel B:** Chirally pure mandelic acid analog  
**Carbon:** Yellow, **Oxygen:** Red, **Nitrogen:** Blue, **Polar hydrogen:** White

Not surprisingly, in case of the PC series, as the size of the aliphatic ring of the head group decreased, the kinetic aqueous solubility increased as seen with the trans-4-methyl cyclohexyl ring (e.g.: Table 16: compound **96**) versus the cycloheptyl and adamantyl rings (e.g.: Table 16: compounds **98, 104, 105**). The imidazole-2-carboxamide series showed similar results for solubility, ranging between 10 to 20  $\mu\text{g/mL}$ , for all the head groups with an exception of (1R,2R,3R,5S)-(-)-isopinocampheyl head group (e.g.: Table 16: compound **106**), which had the highest solubility amongst the imidazole-2-carboxamide series and the cyclooctyl head group (e.g.: Table 16: compound **108**), which had the lowest solubility amongst the imidazole-2-carboxamide series. Overall, the compounds with lower cLogP values, within a particular mini-series were found to have higher aqueous solubility values. As per FDA guidelines, for a compound to be used as an active pharmaceutical ingredient in a solid- oral dosage form it is required to

have an aqueous solubility of 30 to 100 mg/mL.[59] Hence, the improvement of compound solubility thereby its oral bio-availability remains one of the most challenging aspects of drug development process especially for oral-drug delivery system.[61]

### **3.4. Permeability assay**

Every cell is essentially made up of cytoplasm (the contents of the cell) and a cell membrane. The cell membrane, also known as the plasma membrane, is a bilayer of lipids and proteins that surrounds a cell and separates the cytoplasm from its surrounding environment.[68] Phospholipids are a main component of the cell membrane.[69] These lipid molecules are typically made up of a phosphate group head and two fatty acyl tails. The plasma membranes of animal cells contain four major phospholipids (phosphatidylcholine, phosphatidylethanolamine, phosphatidylserine, and sphingomyelin), which together account for more than half of the lipids in most membranes.[68] It is selectively permeable, which means that it only lets certain molecules enter and exit the cell.[69] It can also control the amount of some substances that go into or out of the cell. Small molecules that are nonpolar (have no charge) can cross the membrane easily through diffusion, but ions (charged molecules) and larger molecules typically cannot.[68]

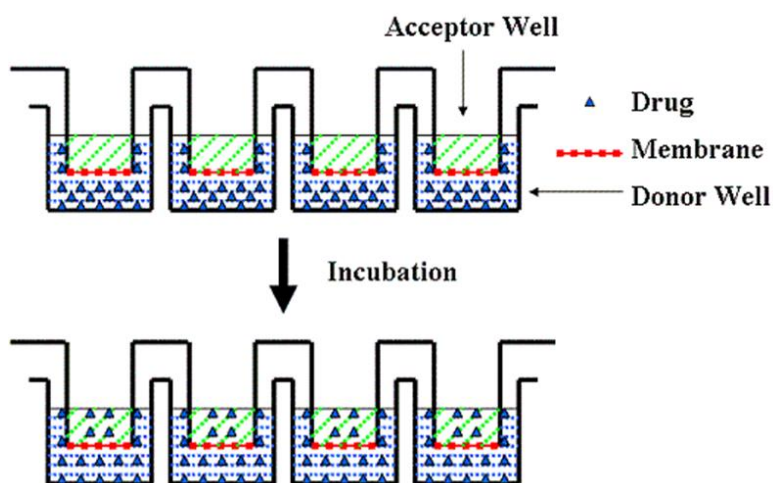
To reach its site of action, a drug needs to cross the cell membrane or permeate from one site to another. Permeation is the movement of a drug molecule into and within the biological environment such as body tissues.[70] Permeability across biological membranes is a key factor in the absorption and distribution of

drugs. Poor permeability can lead to poor absorption across the gastrointestinal mucosa or poor distribution throughout the body.[71]

Main mechanisms of drug permeation are passive diffusion, carrier mediated transport and pinocytosis.[72] Passive diffusion is when drugs cross the cell membranes along the concentration and electrical gradient without expenditure of energy according to Fick's Law, and is the predominant permeability mechanism.[73]

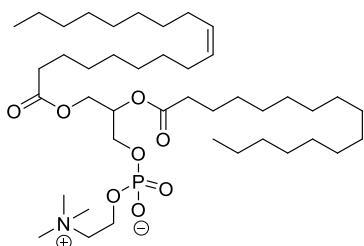
Parallel artificial membrane permeability assay (PAMPA) is widely used as an *in vitro* passive diffusion permeability model using a synthetic phospholipid membrane and has a high correlation with the *in vivo* permeability studies ( $R_2 = 0.87$ ).[74] Thus, the drug permeability through an artificial membrane provides an indication of *in vivo* drug absorption and distribution. PAMPA may serve as a pre-screening tool for permeability to address GI permeability for compounds that are intended to be formulated as oral dosage forms. This model uses a 96-well filter-based donor plate that is placed upon a 96-well acceptor plate. The compound of interest is allowed to passively permeate through the membrane from the donor to the acceptor plate (Figure 18). Drugs with high permeability through the membrane will have increased acceptor concentrations. Certain compounds have a higher affinity for the lipids in the membrane and are retained in the membrane, in which case, a decrease in donor concentrations will not result in increased acceptor concentrations. The fraction of compound retained in the membrane is labeled the R-value and can be calculated as explained below, in equation 2. Low R values

suggest a lower tendency for accumulation in the biological membranes and consequently a lower accumulation in fatty tissues. [70]



**Figure 18:** Drug passive diffusion from donor to acceptor plates through an artificial membrane in PAMPA setup (Modified from membrane A, Assays P. MultiScreen Filter Plates for PAMPA. Small.[75] )

The polyvinylidene fluoride (PVDF) filter was converted to an artificial membrane by the application of 1% w/v lecithin in dodecane. Lecithin is a mixture of amphiphilic phospholipids that have hydrophilic heads and lipophilic tails (Figure 19). Mimicking membrane phospholipids in mammals, the amphiphilic molecules in lecithin are arranged uniformly over the filter support forming a membrane-like phospholipid bilayer.[76] Lucifer yellow is impermeable in this assay and was used to confirm membrane integrity.

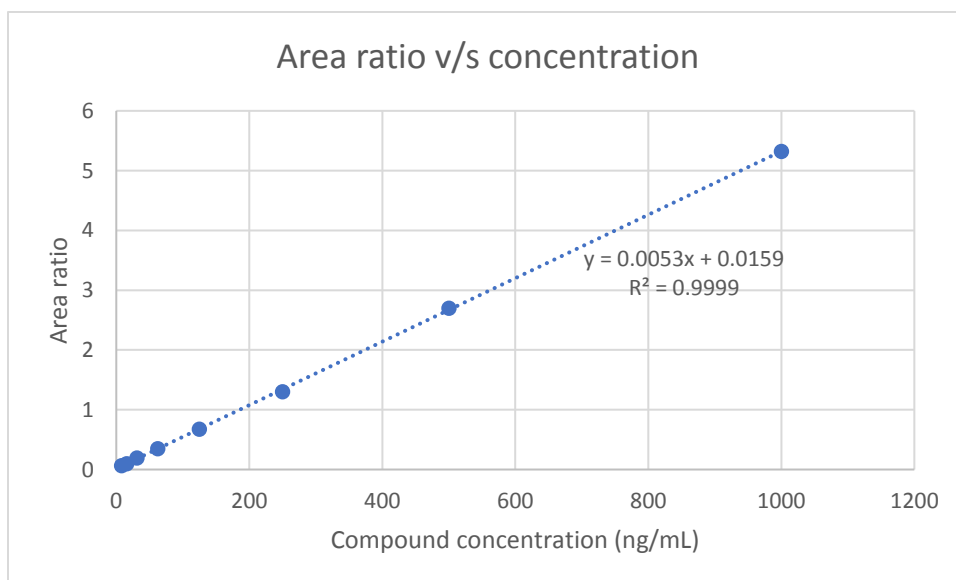


**Figure 19:** An example of a phosphatidylcholine, a type of phospholipid in lecithin

The compound-buffer solution with a concentration of 12.5 µg/mL containing lucifer yellow was placed in the donor well and PBS (pH 7.4) was placed in the acceptor well. The plate was sealed with the donor plate inserted into the acceptor place and incubated for 16 hours at 37 °C. An aliquot from each well was taken and reconstituted with equal volumes of methanol containing internal standard (warfarin), hence a 2-fold dilution was performed. The reconstituted sample was then quantified using LC-MS-MS. The equilibrium concentration was analyzed by mixing the contents of the donor and acceptor wells and diluting it by half with methanol containing warfarin. The calculations for one representative compound, **95**, are shown herein. The results obtained from the LC-MS-MS are AUCs for compounds and internal standards, from which the area ratios are calculated (Table 17). The area ratios are plotted as a function of concentration (Figure 20) and the linear equation obtained from the plot is used to predict the concentration present in the sample.

**Table 17:** Actual and calculated concentrations, AUC and area ratios for compound **95**

Sample Name	AUC for compound	AUC for internal standard	Area ratio	Actual concentration (ng/mL)
Standard-1	50269	750609	0.067	7.82
Standard-2	75698	767309	0.099	15.63
Standard-3	145848	750715	0.194	31.25
Standard-4	261563	756013	0.346	62.5
Standard-5	525017	779467	0.674	125
Standard-6	1029864	791179	1.302	250
Standard-7	2021615	748825	2.7	500
Standard-8	4042308	759915	5.319	1000
Blank	144536	7070	20.443	N/A
Donor-1	3679463	376372	9.776	N/A
Donor-2	3673091	424276	8.657	N/A
Donor-3	3773662	409118	9.224	N/A
Donor-4	3570791	448468	7.968	N/A
Acceptor-1	2208768	389307	5.674	N/A
Acceptor-2	2371016	401799	6.513	N/A
Acceptor-3	2563511	401799	6.38	N/A
Acceptor-4	2431879	400520	6.072	N/A
Equilibrium	4106561	415371	9.886	N/A



**Figure 20:** Plot of area ratio as a function of compound concentration for **95**

The area ratios of test samples were substituted into the equation, obtained from the calibration curve.

**Calculations:** The equation for calculation of the compound concentration can be found out from the plot above and is as follows:

$$y = 0.0053x + 0.0159$$

Where y stands for the area ratio and x stands for the concentration, hence the unknown concentration can be calculated as follows:

$$x = \frac{(y - 0.0159)}{0.0053}$$

for donor-1,

$$x = \frac{(9.776 - 0.0159)}{0.0053}$$

$$x = 1841.5 \text{ ng/mL}$$

Since the test samples were prepared by 2-fold dilution of the samples, the calculated value of the concentration was multiplied by the dilution factor, hence the actual concentration is obtained by multiplying by 2.

$$x = 1841.5 * 2 \text{ ng/mL}$$

$$x = 3683 \text{ ng/mL} = 3.683 \mu\text{g/mL}$$

The concentration was calculated for the other donor samples and the average donor concentration was calculated as  $3.65 \pm 0.29 \mu\text{g/mL}$ . Similarly, the compound concentration was calculated for the acceptor well and the average was  $2.31 \pm 0.14 \mu\text{g/mL}$ . The calculated equilibrium concentration was found to be  $3.72 \mu\text{g/mL}$ .

Using these values the apparent permeability ( $P_e$ ) was calculated with the help of Equation 1. [70]

**Equation 1:** Apparent permeability ( $P_e$ ) calculation.

$$P_e = \left[ \frac{V_D \times V_A}{(V_D + V_A) \times Area \times Time} \right] \times \left\{ -\ln \left[ 1 - \frac{C_A(t)}{C_{eq}} \right] \right\}$$

Where ( $V_D$ ) is the volume in the donor compartment (0.15 mL), ( $V_A$ ) is the volume in the acceptor compartment (0.3 mL), ( $Area$ ) is the area of the membrane (0.3 cm<sup>2</sup>), ( $Time$ ) is the incubation time in seconds (57600 s), ( $C_A(t)$ ) is the concentration of the acceptor compartment after incubation (for compound **95**, calculated to be 2.31 µg/mL), and ( $C_{eq}$ ) is the equilibrium concentration (for compound **95**, calculated to be 3.72 µg/mL). Substituting these values in the above equation for **95**, the apparent permeability was found to be  $5.64 \times 10^{-6}$  cm/s.

The fraction of the compound retained in the membrane ( $R$ ) is calculated using equation 2.

**Equation 2:** Compound retention in the membrane ( $R$ ) calculation

$$R = 1 - \left[ \frac{C_D(t)}{C_D(0)} \right] - \left\{ \left( \frac{V_A}{V_D} \right) \times \left[ \frac{C_A(t)}{C_D(0)} \right] \right\}$$

Where ( $C_D(0)$ ) and ( $C_D(t)$ ) are the concentrations in the donor compartment before (12.5 µg/mL) and after incubation (for compound **95**, calculated to be 3.65 µg/mL). Substituting these values in the above equation for **95**, the compound retained in the membrane was 0.361. The  $R$ -value is indicative of the fraction of compound retained in the membrane and lies between 0 and 1. If a compound has a  $R$ -value close to 1, it means most of the compound is retained in the membrane and only

a small fraction of compound penetrates through the membrane. On the other hand, a R- value close to 0 means that the compound is highly permeable and diffuses through the membrane easily and only a small fraction of drug is retained in the membrane. As observed from the above calculations, with a R- value of 0.361, compound **95** was found to be moderately retained in the membrane .

Active compounds that were found to have MIC values of 32 µg/mL or below against *M. tb*, were further studied for their permeability. Hence, seven out of the 30 compounds described in Chapter 2, were evaluated by PAMPA. Calculations were performed as explained above for compound **95**. As per BD biosciences, in the PAMPA set-up, if  $P_e > 4.0 \times 10^{-6}$  cm/s it corresponds to high permeability and if  $P_e < 4.0 \times 10^{-6}$  cm/s then it corresponds to low permeability. [77]

**Table 18:** Acceptor, donor and drug equilibrium concentrations of active compounds that have been used for the calculation of the apparent permeability ( $P_e$ ) and the fraction retained in the membrane (R)

No	Acceptor concentration* (µg/mL)	Donor concentration* (µg/mL)	Drug equilibrium concentration (µg/mL)	$P_e \times 10^{-6}$ (cm/s)	R
<b>88</b>	3.04	4.68	6.70	3.49	0.140
<b>89</b>	3.98	5.69	6.72	5.18	0.026
<b>95</b>	2.31	3.35	3.72	5.64	0.361
<b>96</b>	2.86	4.48	4.03	7.17	0.184
<b>98</b>	1.63	2.31	2.36	6.74	0.554
<b>104</b>	4.64	6.43	8.69	4.42	0.371
<b>105</b>	3.28	5.15	6.41	4.15	0.062
<b>Verapamil</b>	1.86	0.92	1.91	11.75	0.620

\*N=4

All analogs are permeable and can move across the membrane. However, as observed in Table 18 all of the compounds have high permeability except **88**. Compound **88**, which is a PC with the (1R,2R,3R,5S)-(-)-isopinocampheyl head

group has the lowest permeability at  $3.49 \times 10^{-6}$  cm/s. However, **88** has the best anti-mycobacterial potency in the series. The compounds **95**, **104** and **105** with the adamantyl head groups had good permeability in the range of  $4.15 \times 10^{-6}$  cm/s -  $5.64 \times 10^{-6}$  cm/s. Compound **89** which is a PC with a cyclooctyl head group also showed good permeability at  $5.18 \times 10^{-6}$  cm/s. Compound **96**, a PC with a trans-4-methyl cyclohexyl head group has the highest permeability of  $7.17 \times 10^{-6}$  cm/s amongst the series of compounds tested. Compound **98**, which has a cycloheptyl group as its head group and belongs to the PC series, also had a very high permeability of  $6.74 \times 10^{-6}$  cm/s. Hence, the head groups such as the cycloheptyl and the trans-4-methyl cyclohexyl, that had the least bulk associated with them, among the compounds tested, were found to have the highest permeability. Hence, less bulky head groups may be beneficial for permeability. Since all of the PCs tested had a high permeability, with an exception of compound **88**, this indicates that the presence of a hetero-atom such as a nitrogen, as a part of the aromatic ring possesses good permeability. Compound **95**, which is a racemic mandelic acid analog, was also highly permeable, hence the aromatic ring may have only little influence on the permeability profile of the compounds. Compound **104** had the lowest cLogP value amongst the series of compounds tested, but it showed good permeability with a value that was in the middle of the spectrum of results observed. On the other hand, compound **88** had the second highest cLogP value, amongst the series of compounds tested, compound **95** being the highest. However, the permeability of compound **88** was the least amongst the series. Hence, the permeability values of the compounds are not directly proportional to

their cLogP values. Verapamil was used as the standard for validation of our method. The reported values for permeability of verapamil are  $11.5 \pm 3.21 * 10^{-6}$  cm/s and the values observed are  $11.75 * 10^{-6}$  cm/s.[78]

The R value, is the fraction of compound retained in the membrane. Moderately high R-values are required for the compound to concentrate at its site of action, but very high R-values could impede absorption and distribution before making it to the mycobacterial cell. However, most of the other compounds have a low R value, which indicates that only a small amount of compound is retained in the cell membrane. Higher permeability and lower membrane retention mean that the compounds are able to cross the lipophilic biological membrane with a decreased propensity of lipid accumulation. However, the lipid content in the mycobacteria is very high and the PAMPA assay does not test for such highly lipophilic membranes and hence the R- values may not be accurately extrapolated to the concentration of compound that might be retained in the mycobacterial membrane.

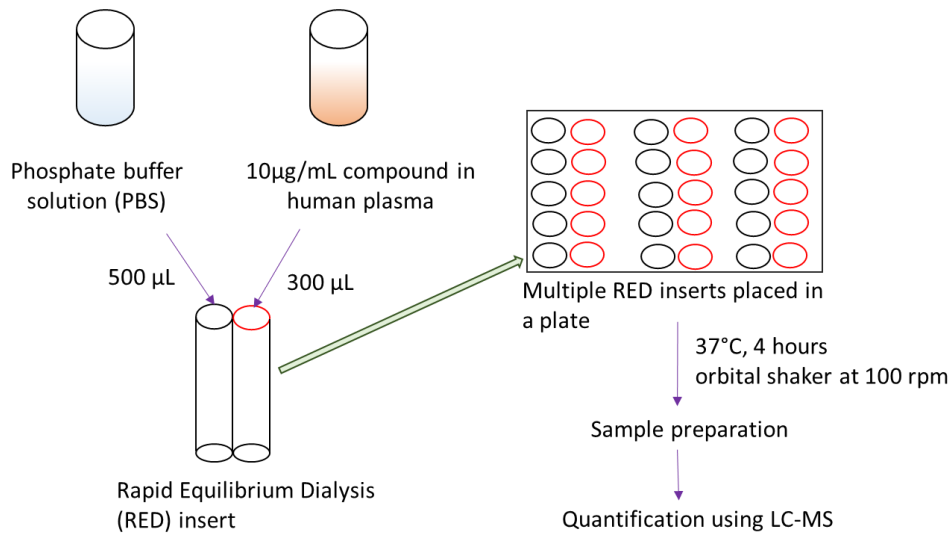
### **3.5. Protein binding assay**

Most drugs bind to proteins or other biological materials, such as albumin;  $\alpha_1$ -acid glycoprotein; lipoproteins;  $\alpha$ -,  $\beta$ -, and  $\gamma$ -globulins; and erythrocytes that are found ubiquitously found in blood plasma. Usually, drug distribution takes place through the transport of compound by binding to plasma and tissues proteins.[79] Only unbound drug is available for passive diffusion to extravascular or tissue sites and typically determines drug concentration at the active site and thus its efficacy.[79] Using a plasma protein binding assay, we can estimate the fraction of

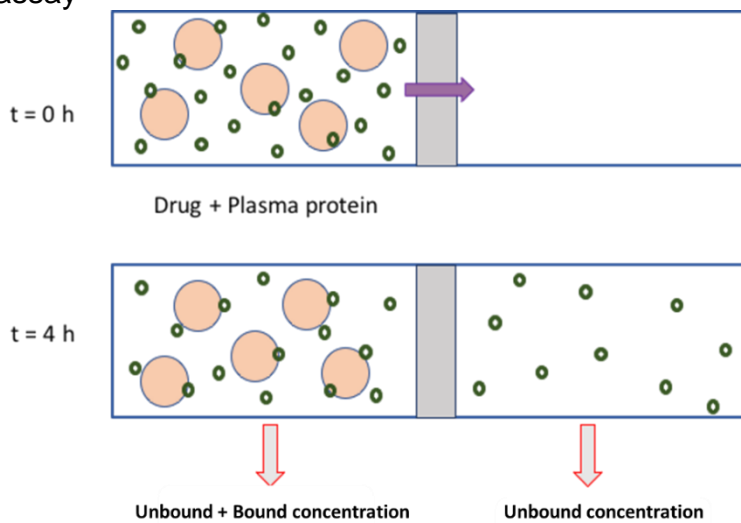
drug bound to the human plasma proteins and the unbound free drug.[80] Besides distribution, binding to plasma proteins also affects drug metabolism and elimination, since both hepatic uptake and glomerular filtration are directly proportional to the free drug fraction present in the plasma.[81] Currently marketed drugs, show varied plasma protein binding patterns. Drugs that have a high degree of plasma protein binding (>95 %) are more likely to be displaced by another drug with a greater affinity for the same binding site.[79] This is the reason behind most of the drug-drug interactions seen between highly plasma protein bound drugs. The efficacy of the drugs can also be compromised due to high plasma binding since lower amounts of the free drug will be available for binding at their target. However, clearance of the drug is reduced due to high plasma binding since the drug is not available to bind to metabolic enzymes.[82]

Equilibrium dialysis is an accurate and reliable method for determining protein binding affinities to chemical or biological substances of low molecular weight.[83] Rapid equilibrium dialysis (RED) is widely used for *in vitro* human plasma protein binding testing. This technique uses RED inserts which are composed of high-density polypropylene and each insert is comprised of two side-by-side chambers separated by a vertical cylinder of dialysis membrane with varying molecular-weight cutoffs.[84] The procedure conducted for equilibrium dialysis is explained herein (Figure 21). Stock solution of each compound was prepared in DMSO and it was diluted in human plasma. One chamber of the RED insert contained human plasma spiked with the compound solution, whereas the other chamber contained phosphate buffer solution, pH 7.4. These inserts were sealed and mixed using an

orbital shaker, after protein precipitation free drug concentration was quantified using the LC-MS/MS. As shown in Figure 22, the compound bound to the protein cannot diffuse through membranes because of the high molecular weight of the protein which makes them impermeable through the dialysis tubing. The free drug diffuses across the membrane, into the buffer chamber, till an equilibrium is attained between the free drug concentrations in both the chambers.



**Figure 21:** Equilibrium dialysis experiment for human plasma protein binding assay

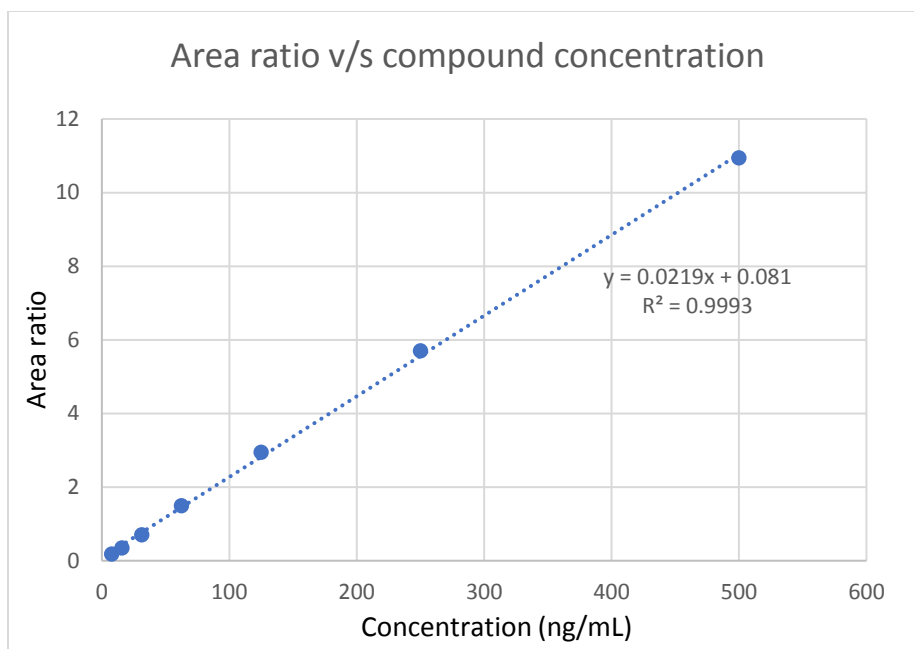


**Figure 22:** Free drug crossing dialysis membrane and drug concentrations in both chambers

The calculations for one representative compound, **89**, are shown herein. The results obtained from the LC-MS/MS are AUCs for compounds and internal standards, from which the area ratios are calculated (Table 19). The area ratios were plotted as a function of concentration (Figure 23) and the linear equation obtained from the plot was further used to predict the concentration present in the sample.

**Table 19:** Actual and calculated concentrations, AUC and area ratios for compound **89**

Sample Name	AUC for compound	AUC for internal standard	Area ratio	Actual concentration (ng/mL)
Standard-1	386426	2111060	0.183	7.82
Standard-2	741731	2117480	0.35	15.63
Standard-3	1770810	2095459	0.702	31.25
Standard-4	3118048	2091600	1.491	62.5
Standard-5	6218193	2110380	2.946	125
Standard-6	12137633	2127947	5.704	250
Standard-7	22838614	2086998	10.943	500
Blank	1473	5734	0.257	N/A
Plasma-1	10990210	37368	294.106	N/A
Plasma-2	13111987	38061	344.496	N/A
Plasma-3	13111987	34803	394.75	N/A
Buffer-1	1257790	35225	35.708	N/A
Buffer-2	1358084	35777	37.96	N/A
Buffer-3	1500061	34145	43.933	N/A



**Figure 23:** Plot of area ratio as a function of compound concentration for **89**

The area ratios of test samples were substituted into the equation, obtained from the calibration curve.

**Calculations:** The equation for calculation of the concentration of compound **89** can be found out from the plot above and is as follows:

$$y = 0.0219x + 0.081$$

Where y stands for the area ratio and x stands for the concentration, hence the unknown concentration can be calculated as follows

$$x = \frac{(y - 0.081)}{0.0219}$$

for plasma-1,

$$x = \frac{(294.106 - 0.081)}{0.0219}$$

$$x = 13425.8 \text{ ng/mL}$$

The test samples were prepared by 8 fold dilution of the samples, hence the calculated value of the concentration was multiplied by the dilution factor. The actual solubility is obtained by multiplying by 8.

$$x = 13425.8 * 8 \text{ ng/mL}$$

$$x = 107406.4 \text{ ng/mL} = 107.46 \text{ } \mu\text{g/mL}$$

The concentration was calculated for the other plasma samples and the average plasma chamber concentration was calculated as  $125.79 \pm 18.41 \text{ } \mu\text{g/mL}$ .

Similarly, the compound concentration in the buffer samples were calculated and averaged to obtain the average concentration of the buffer chamber as  $14.29 \text{ } \mu\text{g/mL}$ . The percentage of the test compound bound to plasma was calculated on following equations:

**Equation 3:** Equation for calculation of percentage of free drug

$$\% \text{ Free} = \frac{[\text{Buffer Chamber Compound Concentraion}]}{[\text{Plasma Chamber Compound Concentraion}]} \times 100$$

$$\% \text{ Free} = \frac{14.29}{125.79} \times 100 = 11.36$$

**Equation 4:** Equation for calculation of percentage of bound drug

$$\% \text{ Bound} = 100 - \% \text{ Free}$$

$$\% \text{ Bound} = 100 - 11.36 = 88.64$$

The percentage of **89** bound to plasma was found to be 88.64.

Active compounds that were found to have MIC values of  $32 \text{ } \mu\text{g/mL}$  or below against *M. tb*, were further studied for their human plasma protein binding. Therefore, seven out of the 30 compounds described in Chapter 2, were evaluated

by equilibrium dialysis. Calculations were performed as explained above for compound **89**.

**Table 20:** Percentage of compound bound to plasma proteins, unbound and bound concentrations of compounds tested for protein binding

No	Unbound concentration* (µg/mL)	fraction	Bound concentration* (µg/mL)	fraction	% Protein bound
<b>88</b>	1.50		30.33		95.04
<b>89</b>	1.80		15.86		88.64
<b>95</b>	2.33		25.93		91.02
<b>96</b>	2.18		12.53		82.64
<b>98</b>	8.28		38.15		78.29
<b>104</b>	0.93		11.64		95.04
<b>105</b>	6.96		70.96		88.62
<b>Verapamil</b>	4.14		32.41		87.23

\*N=3

All of 7 compounds tested were highly protein bound, as shown in Table 20. Verapamil was used as a standard for validation of the method. Verapamil was used as a control and 87.23% of verapamil was determined to be protein bound, similar to reported literature of 88-92% protein binding.[85] The compounds can be grouped into three categories based on their protein binding patterns. The first category comprises of compounds within the range of 70-80 percent protein binding. Compound **98**, a PC with the cycloheptyl head group, is the only compound in this category with the lowest percentage of protein binding, of 78.29. The second category of compounds comprises of the compounds within the range of 80-90 percent protein binding. PCs **89** (cyclooctyl analog), **96** (trans-4-methyl analog) and **105** (2-adamantyl analog) belong to this category with moderately high protein binding percentages. The head groups on these are the cyclooctyl, trans-4-methyl cyclohexyl and the 2-adamantyl group respectively. In spite of the varying bulk associated with them, these three compounds showed similar results for

protein binding. Hence, the bulk of the head groups may not have a great influence on the protein binding of the compound. The third category of compounds are the highly protein bound compounds with a percentage of protein binding greater than 90 percent. Compounds **88** (PC with the (1R,2R,3R,5S)-(-)-isopinocampheyl head group), **95** (2-adamantyl racemic mandelic acid analog) and **104** (PC with the 1-adamantyl head group) belong to this category. The cLogP values associated with these compounds are 2.21, 2.47 and 1.55 respectively. These compounds were found to have high protein binding irrespective of the difference in their lipophilicities and hence the change in cLogP values may not be directly proportional to the change in protein binding patterns. Compound **95** is a racemic mandelic acid analog, whereas the other two compounds are PCs. Since all these have high protein binding, the aromatic side chain may have a minimal effect on protein binding patterns.

### **3.6. Metabolic stability assay**

Metabolism describes the chemical reactions that change drugs into compounds which are subsequently eliminated. The products of these chemical reactions are called metabolites. Drugs can be metabolized by oxidation, reduction, hydrolysis, hydration, conjugation, condensation, or isomerization reactions. The enzymes involved in metabolism are present in many tissues but the majority are concentrated in the liver. Hence, the liver is the principal site of drug metabolism. First-pass metabolism, which generally occurs with lipophilic drugs or lipophilic functional groups, generating more polar metabolites in

preparation for excretion or Phase II conjugation reactions.[86] First-pass metabolism is an important factor that affects the oral bioavailability of drugs. Poor metabolic stability often is a major liability for a lead series and often needs improvement.[64] Metabolic stability is defined as the percentage of parent compound lost over time in the presence of a metabolically active test system.[87] By understanding the metabolic stability of compounds early in discovery, compounds can be prioritized for progression into pharmacokinetic studies.[87] Metabolic stability results aid in the calculation of the secondary pharmacokinetic parameters such as bioavailability and half-life when other data on volume of distribution and fraction absorbed are available.[88] These parameters are important in defining the drug pharmacokinetic and toxicological profiles.

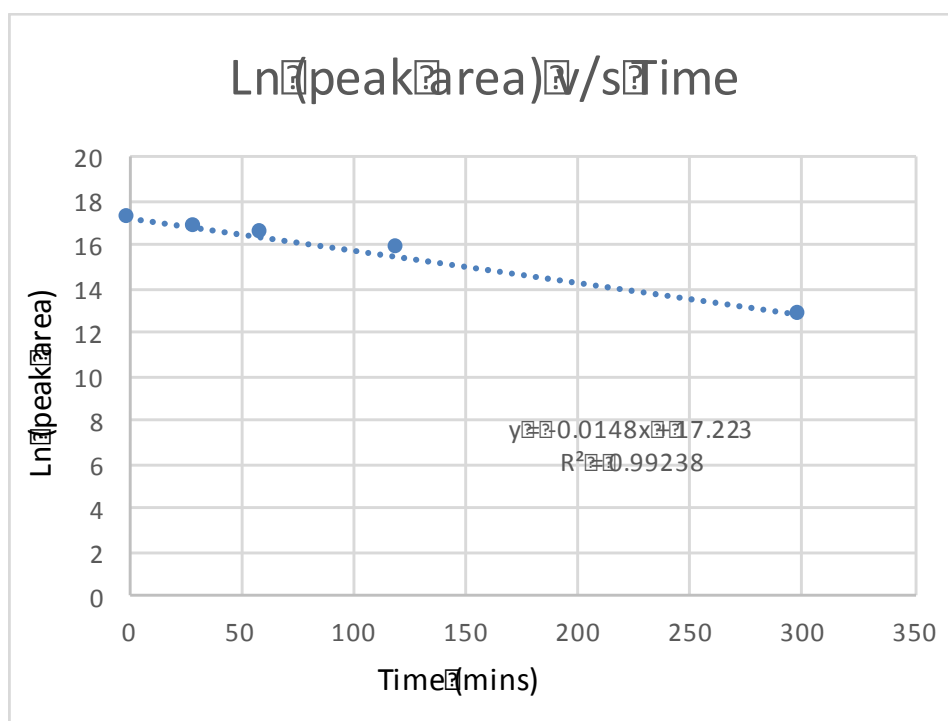
Metabolic stability is commonly determined using either liver microsomes or the liver S9 enzyme fraction. Liver microsomes contain only the endoplasmic reticulum subcellular fraction, containing most notably cytochrome P450's (CYPs) and uridine 5'-diphospho-glucuronosyltransferase (UGTs).[87] The S9 fraction contains all the metabolizing enzymes in liver microsomes plus some additional enzymes found in the cytosol. In the S9 fraction, the microsomal enzymes are present at 20% to 25% of their concentrations in liver microsomes, The S9 fraction accesses extra-microsomal enzymes, such as sulfotransferase, alcohol dehydrogenase, and N-acetyltransferase.[87] It is especially useful for compounds having moieties that are prone to metabolic reactions catalysed by extra-microsomal enzymes.

The S9 fractions require exogenous cofactors such as  $\beta$ -Nicotinamide adenine dinucleotide phosphate-regenerating system (NADPH; Phase I oxidation), uridine 5'-diphospho- $\alpha$ -D-glucuronic acid (UDPGA; Phase II glucuronidation), glutathione (GSH; Phase II), and 3'-phosphoadenosine-5'-phosphosulphate (PAPS; Phase II sulfation) for activity.[87] For the scope of this project, metabolic stability of the compounds to phase I oxidation is investigated. Hence, nicotinamide adenine dinucleotide phosphate (NADPH) is the co-factor used for activating the enzymes in the S9 fraction. Metabolism differs in animal models versus humans. The initial preclinical evaluation is conducted typically in mice, therefore mouse metabolic profiles were monitored. Mouse metabolic profiles also prove to be high-throughput assays, which are beneficial during drug discovery.

The assay was carried out as follows. The compound-DMSO solution at a concentration of 50  $\mu$ g/mL was added to the S9 fraction along with NADPH and the mixture was incubated at 37°C. Aliquots were collected at specific time points and quantified using the LC-MS/MS after dilution and protein precipitation. The calculation of the half-life is described below, for one of the representative compounds. The peak areas of the compound **95** were averaged and are tabulated in Table 21 below. The natural log of peak areas was plotted as a function of time (Figure 24).

**Table 21:** Time, peak areas and natural log of the peak areas for compound **95**

Time (minutes)	Area of peak for compound	Ln (peak area)
0	26678292	17.099
30	18166427	16.715
60	12970960	16.378
120	6610899	15.704
300	325853	12.694



**Figure 24:** Plot of Ln (peak area) v/s time for compound **95**

For first-order reactions, the slope of the line obtained from the plot of natural log of the peak areas versus time gives the elimination rate constant as shown in equation 3.

**Equation 5:** Equation for calculation of the elimination rate constant ( $k$ ) for first-order reactions

$$\text{Elimination rate constant } (k) = -(\text{gradient or slope})$$

Since the metabolism of all the compounds tested depends on the initial concentration of the compound, it follows first-order kinetics. The half-life of a first-order reaction can be calculated using the elimination rate constant as shown in equation 5. The half-lives of all the 7 compounds are measured similarly and are reported in Table 22 below.

**Equation 6:** Equation for calculation of half-life, for first-order reactions:

$$\text{Half life} \left( t_{\frac{1}{2}} \right) = \frac{0.693}{k}$$

For **95**, k is 0.0148 and the half life is calculated as:

$$\text{Half life} \left( t_{\frac{1}{2}} \right) = \frac{0.693}{0.0148} = 46.82 \text{ mins}$$

**Table 22:** Half-lives of compounds after incubating with mouse S9 liver fraction

No	Half-life ( $t_{1/2}$ ) mins	North No.	Half-life ( $t_{1/2}$ ) mins
<b>88</b>	34	<b>98</b>	154
<b>89</b>	85	<b>104</b>	25
<b>95</b>	47	<b>105</b>	84
<b>96</b>	112	<b>Verapamil</b>	277

\*N=3

To further understand the metabolic stability of the active compounds with MIC values of 32 µg/mL or below against *M. tb*, seven hits out of the 30 compounds described in Chapter 2, were evaluated for their half-lives, using mouse liver S9 enzymes. Calculations were performed as explained above for compound **95** and results are tabulated in Table 22 above. As seen in Table 22, compounds **88** and **104**, which were structurally PCs with the (1R,2R,3R,5S)-(-)-isopinocampheyl and the 1-adamantyl head groups, respectively, were metabolically labile and had shorter half-lives of 35 and 25 minutes, respectively. On the other hand,

compounds **96** (PC with a trans-4-methyl head group) and **98** (PC with a cycloheptyl head group), showed good metabolic stability and had moderate half-lives of 112 and 154 minutes, respectively. The previous class of ureas, tested for their metabolic stability, were found to have half-lives ranging from 30 minutes to 132 minutes. [42] All these compounds are PCs, with an exception of compound **95**, which is a mandelic acid analog. In spite of the similarities in their aromatic ring they have differing half-lives, which could be modulated by the bulky aliphatic head groups. Compounds **96** and **98** have 7-carbon head groups and hence have the least bulk associated with them as compared to the other 8 and 10- carbon head groups. As the bulk on the head group increased, the half-life of the compound reduced as observed with compound **104**, which contains a 10-carbon head group. The aromatic rings of the compounds may also have multiple sites which act as a target for metabolism, thus reducing their half-life. Verapamil was used as the standard for validation of the method. The reported range for the half-life of verapamil is 200 to 400 minutes.[89] Our observed value, 277 minutes, lies within this range and hence our method is validated. Generally, for mice liver enzymes, for a compound to be metabolically stable, it is required to have 70% or less drug metabolized in 90 minutes.[90] Hence, most novel compounds discussed herein are metabolically stable, with an exception of compounds **88** and **104**. Half-lives of these compounds may be improved by identifying the metabolites and the metabolically labile sites. Thus, prodrugs can be synthesized or substituted analogs maybe synthesized to block the metabolically labile sites and hence increase the half-life of the compound.

### **3.7. Experimental section**

**3.7.1. Materials and instrumentation.** An Exion HPLC system (Applied Biosystems, Foster City, CA, USA) coupled with AB Sciex API 5500 Q Trap with an electrospray ionization (ESI) source (Applied Biosystems, Foster City, CA, USA) was used. The LC-MS/MS system was controlled by Analyst 1.6.3 software. LC-MS. The LC-MS/MS system was equipped with an Acquity BEH C18 column (1.7  $\mu\text{m}$ ), flow rate of 0.5 mL/min and a isocratic run of 50% solvent A (water with 0.1% formic acid) and 50% solvent B (acetonitrile with 0.1% formic acid).

**3.7.2. Kinetic solubility determination.** Compounds were initially prepared by dissolving them into DMSO at a final concentration of 10 mg/mL. Stock drug plates were prepared by adding 30  $\mu\text{L}$  of 10 mg/mL DMSO stocks to each well in a 96-well plate. For reference plates, compounds were diluted 600-fold in system solution buffer (SSB, pH=7.4; pION INC, Woburn, MA) and methanol (1:1, v/v) containing 500ng/mL of warfarin, used as an internal standard. Concentrations were assessed by LC-MS. For sample plates, compounds were diluted 100-fold in system solution buffer, incubated at room temperature for 6 h to allow the compounds to be fully stable. Fractions were collected from the sample plate, and were centrifuged at 13,000 r.p.m for 10 minutes. Supernatant was diluted 4-fold with a 1:1 v/v solution of methanol and water, containing 500ng of warfarin, and concentration determined via LC/MS. The concentrations were determined using a six-point calibration with appropriate dilution of samples with a concentration

range of 7.8 – 1000 ng/mL. Calculation was carried out by graphical methods and all compounds were tested in triplicates.

**3.7.3. PAMPA Permeability determination.** Compounds were initially prepared by dissolving them into DMSO at a final concentration of 10 mg/mL. A 1% solution of lecithin in dodecane was prepared and sonicated to ensure complete dissolution. The PAMPA membrane was generated by adding 5  $\mu$ L of the 1% lecithin in dodecane solution to each filter. Compound solutions were prepared to a final concentration of 12.5  $\mu$ g/mL containing 50  $\mu$ g/mL of Lucifer yellow in 5% DMSO in phosphate buffered saline (PBS). To each well of the donor plate (top), 150  $\mu$ L of compound solution was added (N = 4). To each well of the acceptor plate (bottom), 300  $\mu$ L of 5% DMSO in PBS was added. The drug-filled donor plate was placed into the acceptor plate ensuring the underside of the membrane was in contact with the solution in the acceptor plate. Sealing tape was placed on the top of the donor plate and incubated for 16 hours at 37 °C. After incubation, 100  $\mu$ L aliquots from each well in the donor plate and 200  $\mu$ L aliquots from each well in the acceptor plate were taken and reconstituted with equal volumes of methanol containing internal standard (500ng/mL warfarin). The concentration was determined using LC-MS quantification method. To determine the drug equilibrium concentration, 150  $\mu$ L of the donor plate solution and 300  $\mu$ L of the acceptor plate solution were mixed and diluted with equal volume of methanol containing internal standard. The concentrations were determined using an eight-point calibration with appropriate dilution of samples with a concentration range of 7.8 – 1000 ng/mL.

**3.7.4. Human plasma protein binding determination.** Compounds were initially

prepared by dissolving them into DMSO at a final concentration of 10 mg/mL. Dulbecco's phosphate buffered saline (DPBS; pH 7.4) was obtained from Invitrogen (Carlsbad, CA), single-use RED (rapid equilibrium dialysis) device was obtained from Thermo scientific (Rockford, IL) and human plasma was obtained from Innovative Research INC (Novi, Michigan, IL). Sample preparation for plasma protein binding was modified from Waters' method.[91] Teflon base plates with the RED inserts (molecular weight cut-off (MWCO) = 8,000) were used without any pre-conditioning of the membrane inserts. Human plasma was thawed and centrifuged at 1000 rpm for two minutes to remove any particulates. Each compound was prepared at 10 µg/mL in human plasma. These samples were prepared by adding one µL of drug stock to 1000 µL of human plasma. Spiked plasma solutions (300 µL) were placed into the sample chamber (indicated by the red ring) and 500 µL of DPBS into the adjacent chamber. The plate was sealed and incubated at 37°C on an orbital shaker (100 rpm) for 4 hours. After incubation, the seal was removed from the RED plate and the volume of the insert was inspected to ensure minimal volume change. Aliquots (50 µL) were removed from each side of the insert and dispensed into a 96-well deep plate. An equal volume of blank plasma or DPBS was added to the required wells to create analytically identical sample matrices. To each sample, 300 µL of methanol containing the internal standard (500ng/mL warfarin) was added. All the plates were sealed and mixed well at 600 rpm for 1 min and were centrifuged at 4000 rpm for 10 minutes. The supernatants (200 µL) were transferred to analytical plates for analysis by LC/MS. LC/MS conditions were described in the materials and instrumentation

section above. The concentrations were determined using a six-point calibration with appropriate dilution of samples with a concentration range of 7.8 – 1000 ng/mL. The test compound concentrations were quantified in both buffer and plasma chambers via peak areas relative to the internal standard. The percentage of the test compound bound to plasma was calculated on following equations:

**Equation 3:** Equation for calculation of percentage of free drug

$$\% \text{ Free} = \frac{[\text{Buffer Chamber Compound Concentration}]}{[\text{Plasma Chamber Compound Concentration}]} \times 100$$

**Equation 4:** Equation for calculation of percentage of bound drug

$$\% \text{ Bound} = 100 - \% \text{ Free}$$

**3.7.5. S9 metabolic stability testing.** Metabolic stability of compounds was assessed in the mouse liver S9 fraction. Briefly 5µg/mL of compound was incubated with 1 mg/mL mouse liver S9 fraction supplemented with 1 mg/mL nicotinamide adenine dinucleotide phosphate (NADPH) in Dulbecco's phosphate buffered saline at 37°C. At designated time points (i.e. 0, 0.5, 1, 2, 5hr), 100 µL samples were collected and quenched immediately with 300µL acetonitrile containing 1µg/mL internal standard. Samples were vortexed for 30 seconds and centrifuged at 15,000 rpm for 10min. Supernatant was assessed by LC/MS.

## **Chapter 4: Summary and Future Directions**

#### 4.1. Conclusion

Bioisosteric replacements made to the IC scaffold generated five mini-series of novel compounds. Major structural changes revolved around the aromatic group to discover compounds with maintained anti-TB activity while improving solubility and permeability of the analogs. These compounds were designed to decrease the cLogP values, in order to study the influence of cLogP values on the physicochemical and *in vitro* pharmacokinetic properties associated with the compounds. The aromatic groups tested in each miniseries were pyrrole, imidazole and mandelic acid (racemic, pure R and pure S enantiomers). To optimize anti-*M. tb* activity, known bulky aliphatic groups were added to the amide nitrogen. The bulky aliphatic groups chosen to form a mini-series were the head groups that showed best activity in the previous classes, trans-4-methylcyclohexyl, cycloheptyl, cyclooctyl, 1-adamantyl, 2-adamantyl and (1R,2R,3R,5S)-(-)-isopinocampheyl groups.

All the PC compounds i.e. **88**, **89**, **96**, **98**, **104**, **105** and the 2-adamantyl racemic mandelic acid analog, **95**, were found to be modestly active against *M. tb* with MIC values less than or equal to 32 µg/mL as opposed to the sub-µg/mL level potency observed with IC. This may be due to the inability of the compounds to penetrate the lipophilic mycobacterial cell wall and reach its site of action, due to the decreased cLogP values and lower lipophilicity of the new scaffolds. However, compound **88** (PC with the (1R,2R,3R,5S)-(-)-isopinocampheyl head group) had the best anti-TB activity, with an MIC of 2 µg/mL, amongst the entire series of compounds synthesized. Hence, on a molecular level, the deletion of the benzene

ring of the IC caused a potency drop but the compounds were still active against *M. tb*. The imidazole-2-carboxamide compounds were found to be inactive within the range of concentrations tested where *M. tb* MIC values were greater than 32 µg/mL. This may be due to the addition of an extra heteroatom to the aromatic ring, which proved to be detrimental for anti-mycobacterial activity. On changing the H-bond donor group from an NH to an OH in the mandelic acid series, there was a significant loss of activity, with an exception of compound **95** which was found to be active against *M. tb* at 32 µg/mL. A more specific H-bond donor such as the NH group might be required for binding at the receptor site that might be one of the reasons behind the loss in activity observed in the mandelic acid analogs.

All compounds showed significantly enhanced kinetic aqueous solubility, this was predicted by the decrease in cLogP values as compared to the IC. Compounds **77, 101, 102, 103, 122, 123, 124, 125, 127**, which are mandelic acid analogs showed a 100 to 1000-fold increase in aqueous solubility with values between 37 to 183 µg/mL. Compound **77**, a cyclooctyl racemic mandelic acid derivative had the highest aqueous solubility amongst the series tested. The aqueous solubility of all the PC compounds i.e. **88, 89, 96, 98, 104, 105** and the 2-adamantyl racemic mandelic acid analog, **95**, increased 10-50 times as compared to the previous generations. These compounds had the best potency in the series, with *M. tb* MICs of 32 µg/mL for all of these with an exception of compound **88**, which had an *M. tb* MIC of 2 µg/mL. However, the aqueous solubility was not substantially improved. It is apparent that when the solubility is increased, compounds start losing their anti-TB activity and, therefore, anti-TB activity and

solubility tend to have an inverse relationship. As per FDA guidelines, for a compound to be used as an active pharmaceutical ingredient in a solid oral dosage form it is recommended to have an aqueous solubility of 30 to 100 mg/mL.[59] Hence, the improvement of compound solubility thereby its oral bio-availability remains one of the most challenging aspects of drug development process especially for oral-drug delivery system.[61] Table 23 summarizes the results of all the assays conducted on the compounds active against *M. tb*.

**Table 23:** A summary of *M. tb* MIC, cLog P, solubility, plasma protein binding, half-life using mice liver enzymes,  $P_e$ , and fraction retained in the membrane (R) for active compounds from the mini-series

No	MIC against <i>M. tb</i> ( $\mu\text{g/mL}$ )	cLogP	Kinetic aqueous solubility ( $\mu\text{g/mL}$ )	Percent plasma protein binding	Half-life (mins)	$P_e \times 10^{-6}$ (cm/s)	R
<b>88</b>	2	2.21	9.8 $\pm$ 2.4	95.04	34	3.49	0.140
<b>89</b>	32	2.10	7.2 $\pm$ 0.7	88.62	85	5.18	0.026
<b>95</b>	32	2.47	31.2 $\pm$ 1	91.02	47	5.64	0.361
<b>96</b>	32	1.60	15.1 $\pm$ 2.8	82.64	112	7.17	0.184
<b>98</b>	32	1.68	3.4 $\pm$ 0.3	78.29	154	6.74	0.554
<b>104</b>	32	1.55	3.9 $\pm$ 0.5	95.04	25	4.42	0.371
<b>105</b>	32	1.73	3.8 $\pm$ 0.1	88.62	84	4.15	0.062

Compound **88** ((1R,2R,3R,5S)-(-)-isopinocampheyl PC) had the lowest permeability,  $3.49 \times 10^{-6}$  cm/s, amongst the series whereas compounds **95** (2-adamantyl racemic mandelic acid analog) and **96** (trans-4-methyl cyclohexyl PC) not only show improved solubility, they also have a high permeability, with a  $P_e$  value of  $5.64 \times 10^{-6}$  cm/s and  $7.17 \times 10^{-6}$  cm/s, respectively, and low fractions of compounds are retained in the membrane, with an R-value of 0.361 and 0.184, respectively. This suggests that the compounds are highly permeable and are not retained in cellular membranes. Since MmpL3 is a transporter protein in the

membrane, the compounds need to be retained in the membrane. The low R-values are indicators that the compound doesn't concentrate at its site of action and hence, the anti-mycobacterial activity, of the newer series of compounds, may have been reduced. Higher permeability and lower membrane retention means that the compounds are able to cross the lipophilic biological membrane with a decreased propensity of lipid accumulation. However, the lipid content in the mycobacteria is very high and the PAMPA assay does not test for such highly lipophilic membranes and hence the R-values may not be accurately extrapolated to the concentration of compound that might be retained in the mycobacterial membrane.

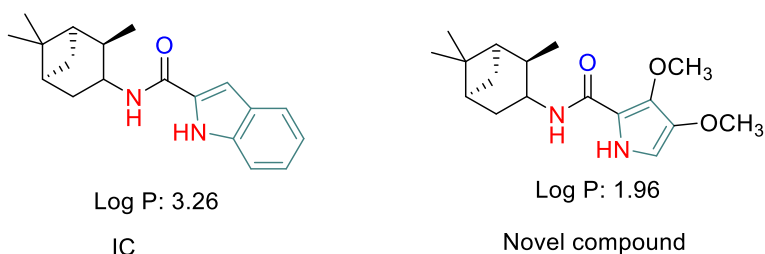
Human plasma protein binding and mouse liver S9 metabolic stability assays were conducted. Compound **98**, a PC with the cycloheptyl head group, was found to have the lowest percentage of protein binding, of 78.29, amongst the series of compounds tested. Compounds **88**, **95** and **104** were highly protein bound compounds with a percentage of protein binding greater than 90 percent. The cLogP values associated with these compounds are 2.21, 2.47 and 1.55 respectively. These compounds were found to have high protein binding irrespective of the difference in their lipophilicities and hence the change in cLogP values may not be directly proportional to the change in protein binding patterns. Compounds containing varying aromatic rings were assayed and all compounds were found to be highly protein bound. Hence, protein binding patterns may be independent of the variation on the aromatic ring. Compounds **96** (trans-4-methyl cyclohexyl PC) and **98** (cycloheptyl PC) showed good metabolic stability and had

moderate half-lives of 112 and 154 minutes, respectively. On the other hand, compounds **88** ((1R,2R,3R,5S)-(-) isopinocampheyl PC) and **104** (1-adamantyl PC) were metabolically labile and had shorter half-lives of 35 and 25 minutes, respectively. The variations of the head groups play a major role in the metabolic behaviors observed. Metabolically labile sites on these compounds need to be identified and thus, prodrugs can be synthesized or substituted analogs maybe synthesized to block the metabolically labile sites and hence increase the half-life of the compound.

The active compounds from these mini-series of compounds have good *in vitro* pharmacokinetic properties. As far as the activity of these compounds is concerned, the anti-TB potency of compound **88**, with an MIC of 2 µg/mL is better as compared to ethambutol, a currently marketed anti-TB drug with an MIC of 3-5 µg/mL.[53] The aqueous solubility of **95**, of 31.2±1 µg/mL, is found to be close to the aqueous solubility of rifampicin, a currently marketed anti-TB drug with an aqueous solubility of 41.3 µg/mL.[92] Therefore, the PC series is an interesting series for future development of novel anti-TB therapeutics. Since these compounds have an improved pharmacokinetic profile and are active against *M. tb*, this supports my hypothesis.

In order to optimize the activity of the compounds, the most active mini-series can be further studied. Substitutions to the pyrrole scaffold may be tried. The (1R,2R,3R,5S)-(-) isopinocampheyl head group provided the best activity and substitutions explored on the pyrrole ring with this head group is warranted. An example of a potential compound which might have good anti-TB activity along

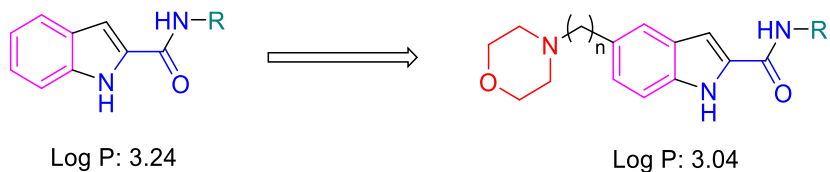
with an improved pharmacokinetic profile is shown in Figure 25. As the aqueous solubility of the compounds was found to increase with a decrease in the cLogP values, this compound may have a greater aqueous solubility. The substitutions on the pyrrole ring may prevent the metabolism due to aromatic hydroxylation and hence increase the half-life for the compound. The permeability profiles may be reasonable due to the lipophilicity associated with the compound. Protein binding values for the PC series were varied and hence the protein binding for this compound cannot be predicted.



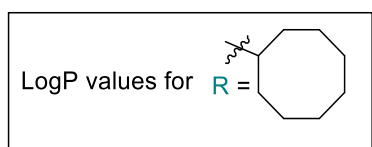
**Figure 25:** Potential compound for synthesis with a reduced cLogP as compared to an IC with the same head group

The current series of compounds showed improved aqueous solubility. However, they had shortcomings with respect to their potency. The IC class has the most potent compounds and to compensate for the potency loss with the current series, alternative classes of compounds can be designed using the indole amides as a primary scaffold. The aqueous solubility of the ICs can be improved by addition of solubilizing group linkers, which may decrease the cLogP and hence enhance hydrophilicity. An example of an indole-linked compound with a **morpholine** group is shown below, and bulky aliphatic groups are represented as the **R** group. Morpholine and morpholino analogs are routinely used as solubilizing groups.[93] A variety of other solubilizing groups (as shown in Figure 27 below)

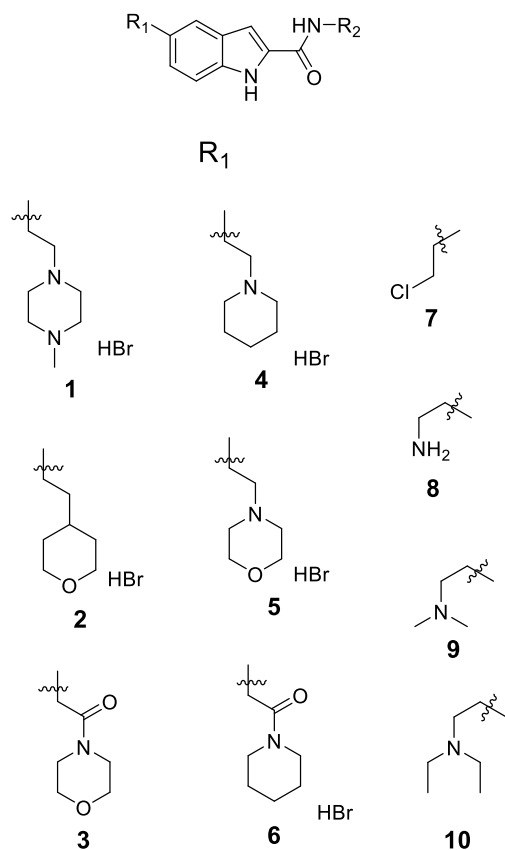
can be linked to the aromatic indole ring and hence two points of variation can be achieved. Since the indole scaffold is retained, the compounds are expected to be highly potent against mycobacteria. The other *in vitro* pharmacokinetic properties are also expected to be enhanced due to the additional solubilizing groups.



Indole-2-carboxamide    Indole-2-carboxamide linked to a solubilizing group

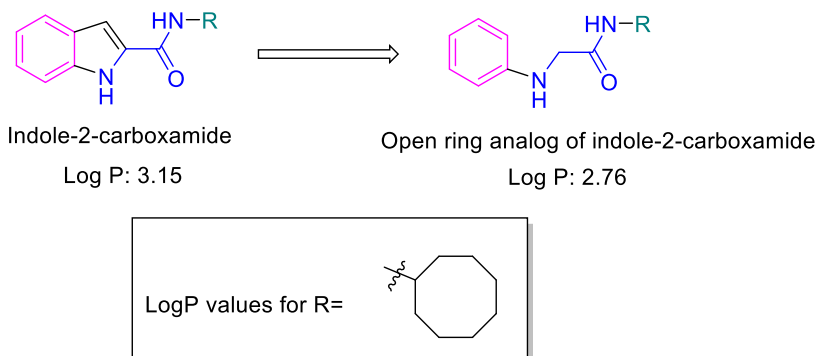


**Figure 26:** Example of a solubilizing group on IC where  $n = 0, 1, 2$  or  $3$   $\text{CH}_2$  groups.



**Figure 27:** Different solubilizing groups that can be added to the IC scaffold  
 In addition to the solubilizing group series, open ring indole analogs were

also designed, as shown below, in order to decrease cLogP values while maintaining the pharmacophore of the novel scaffold. A carbon atom is removed from the IC, which results in lower cLogP values with putative improved aqueous solubility as compared to the ICs.



**Figure 28:** Open ring ICs

The antibacterial potency testing and the aqueous solubility assay is very essential for the screening of compounds during initial drug design. However, parameters such as the protein binding, membrane permeability and metabolic stability are secondary characteristics which can be evaluated further based on aqueous solubility and potency profiles.

#### **4.2. Global perspectives**

As discussed earlier, TB is a global epidemic with increasing cases of resistant strains. TB is also the main cause of deaths related to antimicrobial resistance and the leading killer of people with HIV.[3] Developing countries, such as Africa, Ethiopia, Indonesia, Kenya and India are affected greatly by TB. The Centers for Disease Control and Prevention list the *M. tb* resistant strains as a serious threat to the United States.[94] Active compounds with a novel mechanism of action, such as compounds **95** (2-adamantyl racemic mandelic acid analog) and **96** (trans-4-methyl cyclohexyl PC), against the mycobacteria, is the first step in the battle to eliminate TB worldwide. The discovery and subsequent *in vitro* testing of lead compounds is vital for the establishment of a base for the pre-clinical and the clinical studies. Further, the discovery and the approval of new anti-TB compounds, with improved drug profiles should lead to the improvement in the quality of life and reduce the number of people suffering from TB and should cure patients infected with resistant strains of *M. tb*. The newer compounds allow for novel treatment regimen that could improve patient adherence, decrease the number of resistant TB cases, the number of TB deaths and, eventually, end TB.

### **4.3. Future perspectives**

#### **4.3.1 Human metabolic stability testing**

The metabolic stability testing performed as a part of this project was carried out using the S9 fraction containing mouse liver enzymes, including the cytochrome P450 enzymes. The metabolism of compounds in mice is faster than humans and hence the metabolic stability results obtained using mice the liver S9 fraction cannot accurately be extrapolated as the half-lives in humans.[95] However, there is a necessity to understand mouse metabolic profiles since early pre-clinical development often begins with *in vivo* experiments in mice. Since these compounds are intended for administration to humans, testing this series for metabolic stability against human enzymes is would be useful preclinical studies. The results obtained from this study will help analyze the clearance and volume of distribution for these compounds in humans.

#### **4.3.2 Toxicity studies for active compounds**

Cytotoxicity studies are a useful initial step in determining the safety profile of novel compounds. Little to no toxicity is essential for the successful development of an antibiotic. Cytotoxicity studies can be carried out on the active compounds to determine their selectivity towards mycobacteria as compared to human cells. These studies can be carried out on human lung carcinoma cells using the 3-(4,5-Dimethylthiazol-2-yl)-2,5-diphenyltetrazolium bromide (MTT) assay. If a compound is highly selective for *M. tb*, the dose may be increased with minimal adverse effects. Since most of these compounds have a potency of around 32 µg/mL, increased doses might be required. If these compounds are determined to be non-

cytotoxic, they can be potentially used as anti-TB drugs. However, if they are found to be cytotoxic, these compounds will be repurposed as potential anti-cancer agents.

#### **4.3.3 MmpL3 binding assay**

The synthesized compounds are hypothesized to act by binding to the MmpL3 protein present in the mycobacterial membrane. Surface plasmon resonance (SPR) spectroscopy is a rapidly developing technique for the study of ligand binding interactions with membrane proteins, which are the major molecular targets for validated drugs and for current and foreseeable drug discovery.[96] For our application, SPR spectroscopy currently being explored to evaluate the binding of our compounds to the MmpL3 protein. The results obtained by this assay will aid our understanding of the MIC values obtained for these series of compounds. Our compounds are currently being assayed by our collaborators at Oklahoma State University. Preliminary data obtained will help us evaluate the affinity that the compounds have for the MmpL3 protein. If the compounds have high affinity for the protein but poor MIC values were observed by their whole cell assay, this may be a result of poor pharmacokinetics of the compounds. The poor pharmacokinetics of the compounds limit the amount of compound reaching the site of action and hence poor anti-mycobacterial activities are observed. For example, if one of the compounds with an MIC greater than 32  $\mu\text{g}/\text{mL}$  binds with a great affinity at the MmpL3 binding site, it may be due to the poor pharmacokinetics associated with the compounds. On the other hand, if the compound with an MIC

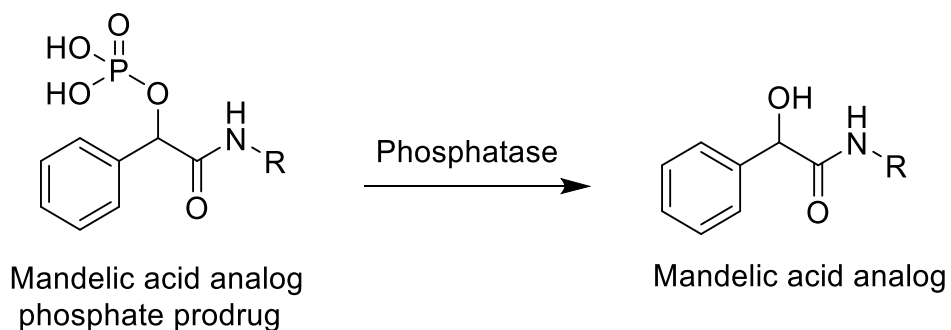
of 32 µg/mL or below does not bind to the MmpL3 binding site, it may have a different mechanism of action for inhibiting mycobacterial growth.

#### 4.3.4 Prodrugs and substituted analogs

As explained above, a few of the synthesized compounds such as compound **104**, a PC with a 1-adamantyl head group and compound **88**, a PC with a (1R,2R,3R,5S)-(-)-isopinocampheyl head group, have a short metabolic half-life which. Hence, to improve metabolic stability, which could increase duration of action, of the compounds showing some anti-mycobacterial activity, prodrugs and substituted analogs can be synthesized. The metabolically labile sites on the compounds need to be identified. This can be investigated by a metabolic screening, using the LC–MS-based metabolomics approach, to obtain the most probable metabolites. Metabolomics is the global analysis of small molecule metabolites in a biological sample by analytic tools.[97] Once the metabolically labile sites are identified, these sites can be protected by halogenated atoms or formation of prodrugs. The compounds may be resynthesized, by coupling substituted analogs of the reagents, wherein the metabolic sites are blocked by bioisosteric replacements.

Prodrugs are bio-reversible derivatives of drug molecules that undergo an enzymatic and/or chemical transformation *in vivo* to release the active parent drug, which can then exert the desired pharmacological effect.[98] The free hydroxyl groups of the mandelic acids can be formulated as phosphate prodrugs which are expected to have vastly improved aqueous solubility as compared to mandelic acid.[99] Phosphatases can activate these into the active mandelic acid analogs,

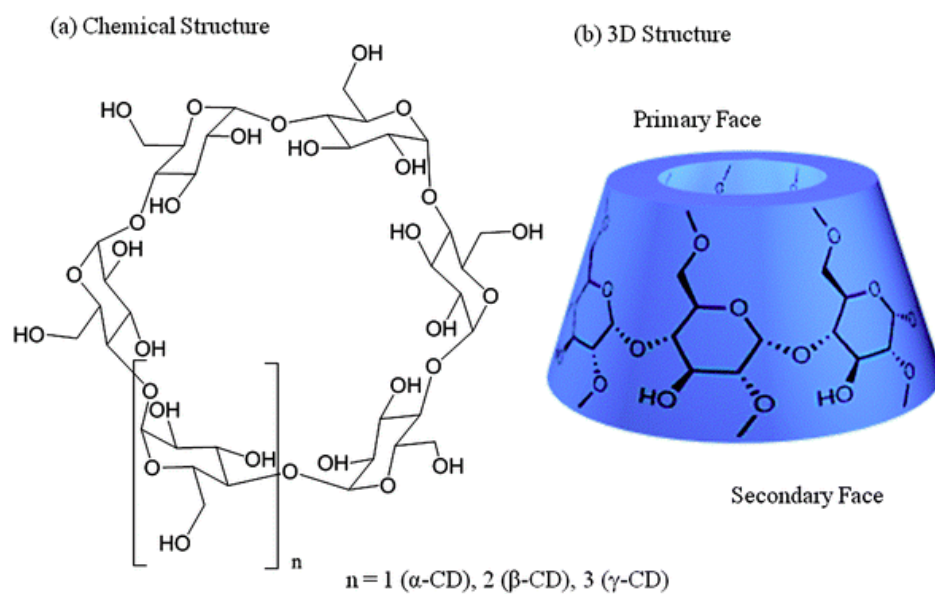
as shown in Figure 26.



**Figure 26:** Phosphate prodrug of mandelic acid analog activation by phosphatase

#### 4.3.5 Formulation and delivery systems

ICs were found to be highly potent in their action but posed problems relating their solubility in aqueous body fluids. Most of the compounds that are found to be active against *M. tb* have high lipophilicity and hence low solubility leading to low oral absorption. Cyclodextrins are polysaccharide macromolecules with a hydrophilic exterior and lipophilic core. Trapping the drugs in cyclodextrin core (Figure 30) forming a cyclodextrin/drug complex makes them hydrophilic and increases the bioavailability. [100].



**Figure 30:** Chemical and 3D structure of cyclodextrins  
*Polym. Chem*, 2010, **1**, 1552-1559

## REFERENCES

1. WHO, *WHO treatment guidelines for drug-resistant tuberculosis (2016 update)*.
2. *Global Tuberculosis Report*. 2015, WHO.
3. *WHO fact sheet*. 2017.
4. Bailo, R., A. Bhatt, and J.A. Ainsa, *Lipid transport in Mycobacterium tuberculosis and its implications in virulence and drug development*. *Biochem Pharmacol*, 2015. **96**(3): p. 159-67.
5. World Health Organization. and Stop TB Initiative (World Health Organization), *Treatment of tuberculosis : guidelines*. 4th ed. 2010, Geneva: World Health Organization. x, 147 p.
6. Wanger, A. and K. Mills, *Testing of Mycobacterium tuberculosis susceptibility to ethambutol, isoniazid, rifampin, and streptomycin by using Etest*. *J Clin Microbiol*, 1996. **34**(7): p. 1672-6.
7. Mathuria, J.P., et al., *Primary and acquired drug resistance patterns of Mycobacterium tuberculosis isolates in India: A multicenter study*. *Journal of Infection and Public Health*, 2013. **6**(6): p. 456-464.
8. Kempker, R.R., et al., *Acquired Drug Resistance in Mycobacterium tuberculosis and Poor Outcomes among Patients with Multidrug-Resistant Tuberculosis*. *Emerging Infectious Diseases*, 2015. **21**(6): p. 992-1001.
9. Long, R., *Drug-resistant tuberculosis*. *Canadian Medical Association Journal*, 2000. **163**(4): p. 425-428.
10. Hazbon, M.H., et al., *Population genetics study of isoniazid resistance mutations and evolution of multidrug-resistant Mycobacterium tuberculosis*. *Antimicrobial Agents and Chemotherapy*, 2006. **50**: p. 2640-2649.
11. North, E.J., M. Jackson, and R.E. Lee, *New approaches to target the mycolic acid biosynthesis pathway for the development of tuberculosis therapeutics*. *Curr Pharm Des*, 2014. **20**(27): p. 4357-78.
12. *Handbook of anti-tuberculosis agents. Introduction*. *Tuberculosis (Edinb)*, 2008. **88**(2): p. 85-6.
13. Arbex, M.A., et al., *Antituberculosis drugs: drug interactions, adverse effects, and use in special situations. Part 1: first-line drugs*. *J Bras Pneumol*, 2010. **36**(5): p. 626-40.
14. North, E.J., M. Jackson, and R.E. Lee, *New Approaches to Target the Mycolic Acid Biosynthesis Pathway for the Development of Tuberculosis Therapeutics*. *Curr Pharm Des*, 2013.
15. Anthony, R.M., A.L. den Hertog, and D. van Soolingen, *'Happy the man, who, studying nature's laws, Thro' known effects can trace the secret cause.'* *Do we have enough pieces to solve the pyrazinamide puzzle?* *J Antimicrob Chemother*, 2018.
16. Graham, D.Y. and A. Shiotani, *New concepts of resistance in the treatment of Helicobacter pylori infections*. *Nat Clin Pract Gastroenterol Hepatol*, 2008. **5**(6): p. 321-31.
17. Ray CG, R.K.e.S., *Medical Microbiology*. 4th Edition ed, ed. M.-H. Medical. 2004.
18. Scheinfeld, N.S. Feb 16, 2016 [cited 2017 1st Dec]; Available from: <https://emedicine.medscape.com/article/1105570-overview>.

19. Chan, E.D. and M.D. Iseman, *Underlying host risk factors for nontuberculous mycobacterial lung disease*. *Semin Respir Crit Care Med*, 2013. **34**(1): p. 110-23.
20. Johnson, M.M. and J.A. Odell, *Nontuberculous mycobacterial pulmonary infections*. *Journal of Thoracic Disease*, 2014. **6**(3): p. 210-220.
21. Mirsaeidi, M., et al., *Nontuberculous Mycobacterial Disease Mortality in the United States, 1999–2010: A Population-Based Comparative Study*. *PLoS ONE*, 2014. **9**(3): p. e91879.
22. Marras, T.K., et al., *Isolation prevalence of pulmonary non-tuberculous mycobacteria in Ontario, 1997–2003*. *Thorax*, 2007. **62**(8): p. 661-666.
23. Jarlier, V. and H. Nikaido, *Mycobacterial cell wall: structure and role in natural resistance to antibiotics*. *FEMS Microbiol Lett*, 1994. **123**(1-2): p. 11-8.
24. Marrakchi, H., M.-A. Lanéelle, and M. Daffé, *Mycolic Acids: Structures, Biosynthesis, and Beyond*. *Chemistry & Biology*, 2014. **21**(1): p. 67-85.
25. Chatterjee, D., *The mycobacterial cell wall: structure, biosynthesis and sites of drug action*. *Current Opinion in Chemical Biology*, 1997. **1**(4): p. 579-588.
26. Li, W., et al., *Novel insights into the mechanism of inhibition of MmpL3, a target of multiple pharmacophores in Mycobacterium tuberculosis*. *Antimicrob Agents Chemother*, 2014. **58**(11): p. 6413-23.
27. Gavalda, S., et al., *The Pks13/FadD32 crosstalk for the biosynthesis of mycolic acids in Mycobacterium tuberculosis*. *J Biol Chem*, 2009. **284**(29): p. 19255-64.
28. Abrahams, K.A. and G.S. Besra, *Mycobacterial cell wall biosynthesis: a multifaceted antibiotic target*. *Parasitology*, 2016: p. 1-18.
29. Stanley, S.A., et al., *Identification of novel inhibitors of M. tuberculosis growth using whole cell based high-throughput screening*. *ACS Chemical Biology*, 2012. **7**(8): p. 1377-1384.
30. Belardinelli, J.M., et al., *Structure-Function Profile of MmpL3, the Essential Mycolic Acid Transporter from Mycobacterium tuberculosis*. *ACS Infect Dis*, 2016. **2**(10): p. 702-713.
31. Székely, R. and S.T. Cole, *Mechanistic insight into mycobacterial MmpL protein function*. *Molecular Microbiology*, 2016. **99**(5): p. 831-834.
32. Jain, M., E.D. Chow, and J.S. Cox, *12 The MmpL Protein Family*, in *The Mycobacterial Cell Envelope*. 2008, American Society of Microbiology.
33. Stec, J., et al., *Indole-2-carboxamide-based MmpL3 Inhibitors Show Exceptional Antitubercular Activity in an Animal Model of Tuberculosis Infection*. *J Med Chem*, 2016. **59**(13): p. 6232-47.
34. Brown, J.R., et al., *The structure-activity relationship of urea derivatives as anti-tuberculosis agents*. *Bioorg Med Chem*, 2011. **19**(18): p. 5585-95.
35. Scherman, M.S., et al., *Screening a library of 1600 adamantyl ureas for anti-Mycobacterium tuberculosis activity in vitro and for better physical chemical properties for bioavailability*. *Bioorganic & Medicinal Chemistry*, 2012. **20**(10): p. 3255-3262.
36. North, E.J., et al., *Design, synthesis and anti-tuberculosis activity of 1-adamantyl-3-heteroaryl ureas with improved in vitro pharmacokinetic properties*. *Bioorganic & Medicinal Chemistry*, 2013. **21**(9): p. 2587-2599.

37. North, J., *Bioisosteric replacement and scaffold hopping*. 2013.
38. Zhao, H., *Scaffold selection and scaffold hopping in lead generation: a medicinal chemistry perspective*. *Drug Discov Today*, 2007. **12**(3-4): p. 149-55.
39. Kondreddi, R.R., et al., *Design, synthesis, and biological evaluation of indole-2-carboxamides: a promising class of antituberculosis agents*. *J Med Chem*, 2013. **56**(21): p. 8849-59.
40. Onajole, O.K., et al., *Preliminary structure-activity relationships and biological evaluation of novel antitubercular indolecarboxamide derivatives against drug-susceptible and drug-resistant Mycobacterium tuberculosis strains*. *Journal of Medicinal Chemistry*, 2013. **56**: p. 4093-4103.
41. Stec, J., et al., *Indole-2-carboxamide-Based MmpL3 Inhibitors Show Exceptional Antitubercular Activity in an Animal Model of Tuberculosis Infection*. *J Med Chem*, 2016.
42. North, E.J., et al., *Design, synthesis and anti-tuberculosis activity of 1-adamantyl-3-heteroaryl ureas with improved in vitro pharmacokinetic properties*. *Bioorg Med Chem*, 2013. **21**(9): p. 2587-99.
43. Franz, N.D., et al., *Design, synthesis and evaluation of indole-2-carboxamides with pan anti-mycobacterial activity*. *Bioorg Med Chem*, 2017.
44. Kondreddi, R.R., et al., *Design, synthesis, and biological evaluation of indole-2-carboxamides: A promising class of antituberculosis agents*. *Journal of Medicinal Chemistry*, 2013. [dx.doi.org/10.1021/jm4012774](https://doi.org/10.1021/jm4012774).
45. North, E.J., *MmpL3 inhibitors*. St. Jude.
46. Lun, S., et al., *Indoleamides are active against drug-resistant Mycobacterium tuberculosis*. *Nature Communications*, 2013. **4**: p. 2907.
47. Jeffrey North, M.J., *Indole-2-carboxamides are Active against an Acute Mycobacterium abscessus Infection Mouse Model*, C. University, Editor. 2018: under review at *Antimicrobial Agents & Chemotherapy*.
48. Meanwell, N.A., *Synopsis of Some Recent Tactical Application of Bioisosteres in Drug Design*. *Journal of Medicinal Chemistry*, 2011. **54**(8): p. 2529-2591.
49. Matta, C.F., A.A. Arabi, and D.F. Weaver, *The bioisosteric similarity of the tetrazole and carboxylate anions: Clues from the topologies of the electrostatic potential and of the electron density*. *European Journal of Medicinal Chemistry*, 2010. **45**(5): p. 1868-1872.
50. Ertl, P., *In silico identification of bioisosteric functional groups*. *Current opinion in drug discovery & development*, 2007. **10**(3): p. 281-288.
51. Lima, L. and E. Barreiro, *Bioisosterism: A Useful Strategy for Molecular Modification and Drug Design*. Vol. 12. 2005. 23-49.
52. Stavrakov, G., et al., *Design of novel camphane-based derivatives with antimycobacterial activity*. *J Mol Graph Model*, 2014. **51**: p. 7-12.
53. Deshpande, D., et al., *Ethambutol Optimal Clinical Dose and Susceptibility Breakpoint Identification by Use of a Novel Pharmacokinetic-Pharmacodynamic Model of Disseminated Intracellular Mycobacterium avium*. *Antimicrobial Agents and Chemotherapy*, 2010. **54**(5): p. 1728-1733.

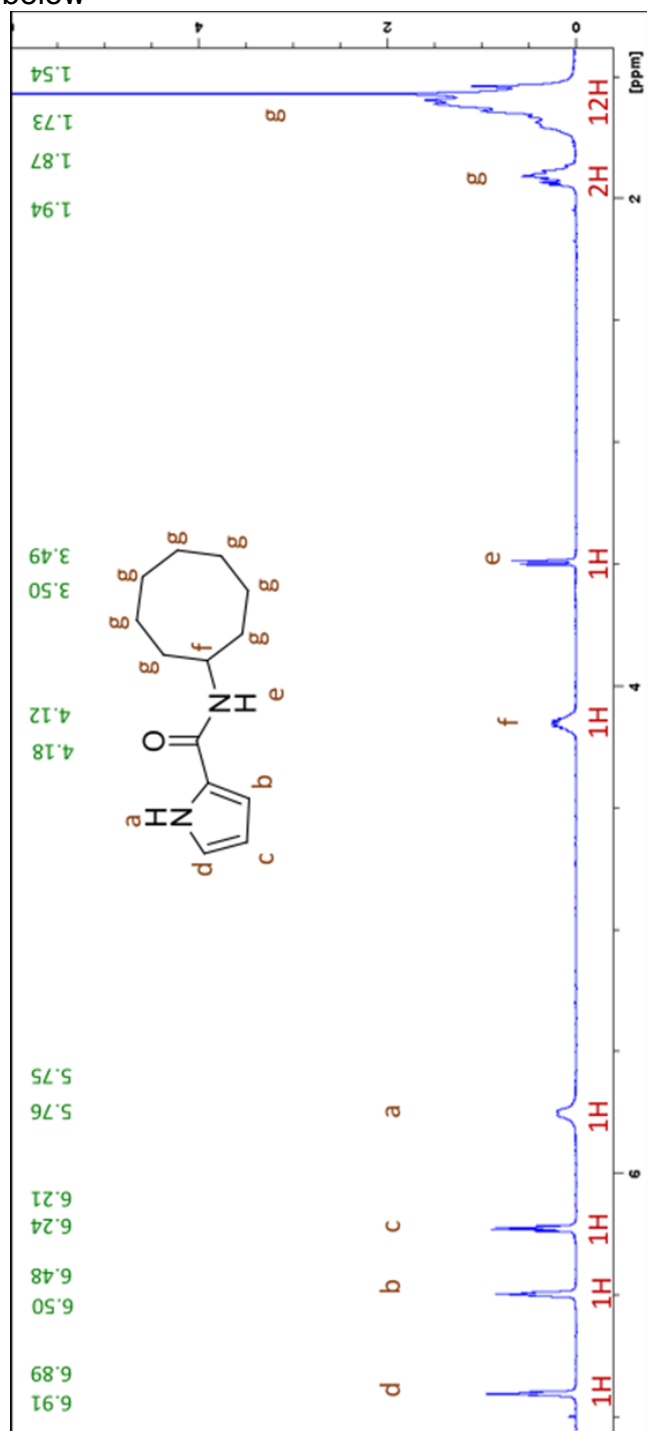
54. Suo, J., et al., *Minimal inhibitory concentrations of isoniazid, rifampin, ethambutol, and streptomycin against Mycobacterium tuberculosis strains isolated before treatment of patients in Taiwan*. Am Rev Respir Dis, 1988. **138**(4): p. 999-1001.
55. Doogue, M.P. and T.M. Polasek, *The ABCD of clinical pharmacokinetics*. Therapeutic Advances in Drug Safety, 2013. **4**(1): p. 5-7.
56. Vugmeyster, Y., J. Harrold, and X. Xu, *Absorption, Distribution, Metabolism, and Excretion (ADME) Studies of Biotherapeutics for Autoimmune and Inflammatory Conditions*. The AAPS Journal, 2012. **14**(4): p. 714-727.
57. Jianling Wang, L.U., *The impact of early ADME profiling on drug discovery and development strategy*. ADME Profiling, 2004.
58. Sakai, J.B., in *Practical Pharmacology for the Pharmacy Technician*. 2008.
59. *Guidelines for Industry: FDA*.
60. Discovery, Q. [cited 2018 20th Feb]; Available from: <http://quintaradiscovery.com/adme/physicochemical-properties/kinetic-solubility/>.
61. Savjani, K.T., A.K. Gajjar, and J.K. Savjani, *Drug Solubility: Importance and Enhancement Techniques*. ISRN Pharmaceutics, 2012. **2012**: p. 195727.
62. *Aqueous Solubility*. 2013, Cerep. p. 4.
63. Brittain, H.G., *Thermodynamic vs. Kinetic Solubility: Knowing Which is Which*. 2014.
64. Di, E.K.a.L., *Drug-like Properties: Concepts, Structure Design and Methods*. 2008.
65. *Analytical Chemistry: Calibration Curves*, in *JoVE Science Education Database*. 2018: JoVE, Cambridge, MA.
66. *Analytical Chemistry. Internal Standards*, in *JoVE Science Education Database*. 2018: JoVE, Cambridge, MA.
67. Price, S.L., *Predicting crystal structures of organic compounds*. Chem Soc Rev, 2014. **43**(7): p. 2098-111.
68. GM, C., *The Cell: A Molecular Approach*. 2nd edition ed. 2000.
69. Li, L., *Organ*. Biologydictionary.net, Nov 4, 2014.
70. Wohnsland, F. and B. Faller, *High-Throughput Permeability pH Profile and High-Throughput Alkane/Water log P with Artificial Membranes*. Journal of Medicinal Chemistry, 2001. **44**(6): p. 923-930.
71. University, M. *Drug Permeability*. 12/22/2017]; Available from: <https://www.monash.edu/pharm/research/areas/optimisation/capabilities/drug-permeability>.
72. Yano, K., et al., *Mechanisms of membrane transport of poorly soluble drugs: role of micelles in oral absorption processes*. J Pharm Sci, 2010. **99**(3): p. 1336-45.
73. Sangeetha, S., *Mechanisms of drug permeation/ transport*, S. University, Editor.
74. Bermejo, M., et al., *PAMPA--a drug absorption in vitro model 7. Comparing rat in situ, Caco-2, and PAMPA permeability of fluoroquinolones*. Eur J Pharm Sci, 2004. **21**(4): p. 429-41.
75. Lynch, D.S.a.J., *MultiScreen Filter Plates for PAMPA* Millipore, Editor.

76. Schuster, B. and U.B. Sleytr, *Biomimetic interfaces based on S-layer proteins, lipid membranes and functional biomolecules*. Journal of the Royal Society Interface, 2014. **11**(96): p. 20140232.
77. BD, *BD Biosciences*. 2018.
78. Alvarez-Figueroa, M.J., et al., *Evaluation of the Membrane Permeability (PAMPA and Skin) of Benzimidazoles with Potential Cannabinoid Activity and their Relation with the Biopharmaceutics Classification System (BCS)*. AAPS PharmSciTech, 2011. **12**(2): p. 573-578.
79. Palleria, C., et al., *Pharmacokinetic drug-drug interaction and their implication in clinical management*. Journal of Research in Medical Sciences : The Official Journal of Isfahan University of Medical Sciences, 2013. **18**(7): p. 601-610.
80. Asteris. *Plasma Protein Binding*. [cited 2017 10th Oct]; Available from: <http://www.asteris-app.com/technical-info/adme-properties/plasmaproteinbinding.htm>.
81. Ascenzi, P., et al., *Clinical relevance of drug binding to plasma proteins*. Journal of Molecular Structure, 2014. **1077**: p. 4-13.
82. *Distribution and Plasma Protein Binding*. [cited 2017 15th Oct]; Available from: <https://www.cambridgemedchemconsulting.com/resources/ADME/distribution.html>.
83. Kastritis, P.L. and A.M.J.J. Bonvin, *On the binding affinity of macromolecular interactions: daring to ask why proteins interact*. Journal of the Royal Society Interface, 2013. **10**(79): p. 20120835.
84. ThermoScientific, *RED protocol*.
85. Cerep, *Protein-binding and blood partitioning*. July 2013.
86. Pond, S.M. and T.N. Tozer, *First-pass elimination. Basic concepts and clinical consequences*. Clin Pharmacokinet, 1984. **9**(1): p. 1-25.
87. Richardson, S.J., et al., *Efficiency in Drug Discovery: Liver S9 Fraction Assay As a Screen for Metabolic Stability*. Drug Metabolism Letters, 2016. **10**(2): p. 83-90.
88. Masimirembwa, C.M., U. Bredberg, and T.B. Andersson, *Metabolic Stability for Drug Discovery and Development*. Clinical Pharmacokinetics, 2003. **42**(6): p. 515-528.
89. Gupta, S., S. Tyagi, and W.R. Bishai, *Verapamil Increases the Bactericidal Activity of Bedaquiline against Mycobacterium tuberculosis in a Mouse Model*. Antimicrobial Agents and Chemotherapy, 2015. **59**(1): p. 673-676.
90. Patten, C., *Strategies for In Vitro Metabolic Stability Testing*. B D Biosciences, 2009.
91. Waters, N.J., et al., *Validation of a rapid equilibrium dialysis approach for the measurement of plasma protein binding*. Journal of pharmaceutical sciences, 2008. **97**(10): p. 4586-4595.
92. *Rifampin*. Tuberculosis, 2008. **88**(2): p. 151-154.
93. Budha, N.R., et al., *Pharmacokinetically-Guided Lead Optimization of Nitrofuranylamine Anti-Tuberculosis Agents*. The AAPS Journal, 2008. **10**(1): p. 157-165.
94. U.S. Department of Health and Human Services, C.f.D.C.a.P., *Antibiotic Resistance Threats in the United States*. 2013.

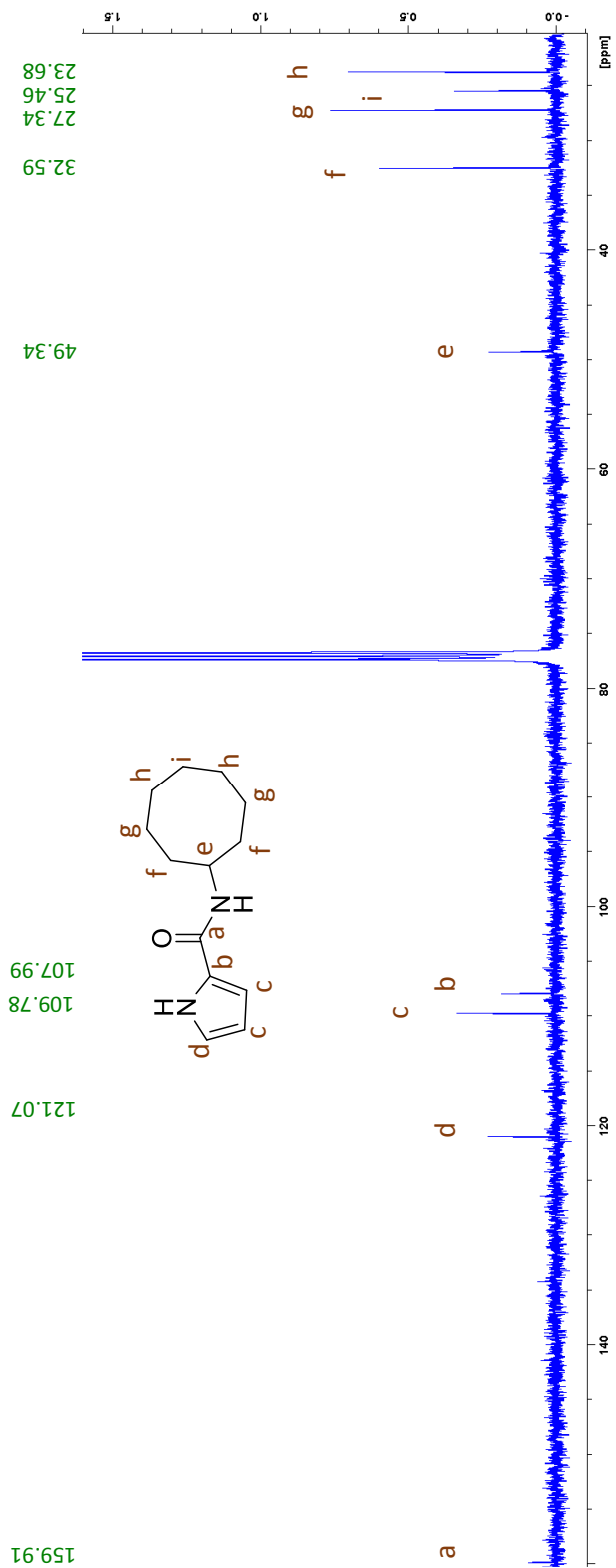
95. Perlman, R.L., *Mouse models of human disease: An evolutionary perspective*. Evolution, Medicine, and Public Health, 2016. **2016**(1): p. 170-176.
96. Patching, S.G., *Surface plasmon resonance spectroscopy for characterisation of membrane protein–ligand interactions and its potential for drug discovery*. Biochimica et Biophysica Acta (BBA) - Biomembranes, 2014. **1838**(1, Part A): p. 43-55.
97. Li, F., F.J. Gonzalez, and X. Ma, *LC–MS-based metabolomics in profiling of drug metabolism and bioactivation*. Acta Pharmaceutica Sinica B, 2012. **2**(2): p. 118-125.
98. Rautio, J., et al., *Prodrugs: design and clinical applications*. Nature Reviews Drug Discovery, 2008. **7**: p. 255.
99. Huttunen, K.M., H. Raunio, and J. Rautio, *Prodrugs—from Serendipity to Rational Design*. Pharmacological Reviews, 2011. **63**(3): p. 750.
100. Zhou, J. and H. Ritter, *Cyclodextrin functionalized polymers as drug delivery systems*. Polymer Chemistry, 2010. **1**(10): p. 1552-1559.

## APPENDIX

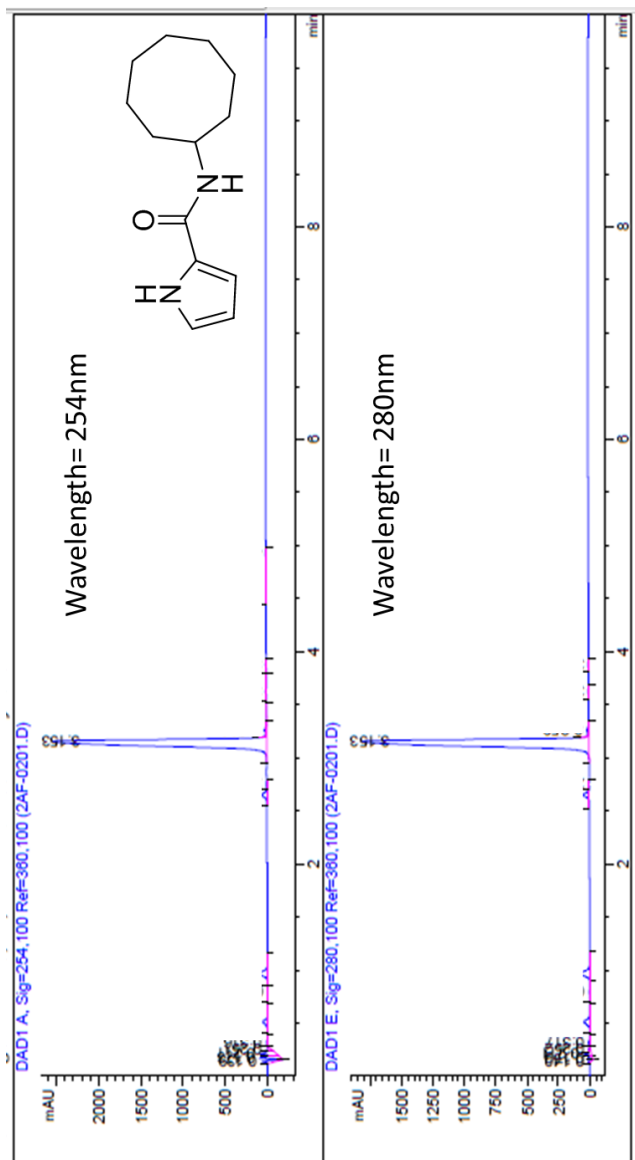
Characterization of representative compounds from each miniseries is shown below



**Figure 31:** Proton NMR spectra for compound **89** (Pyrrole-2-carboxamide)  
<sup>1</sup>H NMR (CDCl<sub>3</sub>-d)  $\delta$  = 1.54-1.73 (m, 12H), 1.87-1.94 (m, 2H), 3.49-3.50 (d,  $J$  = 5 Hz, 1H), 4.12-4.18 (m, 1H), 5.75-5.76 (m, 1H), 6.21-6.24 (d,  $J$  = 7 Hz, 1H), 6.48-6.50 (d,  $J$  = 7 Hz, 1H), 6.89- 6.91 (t,  $J$  = 5 Hz, 1H)

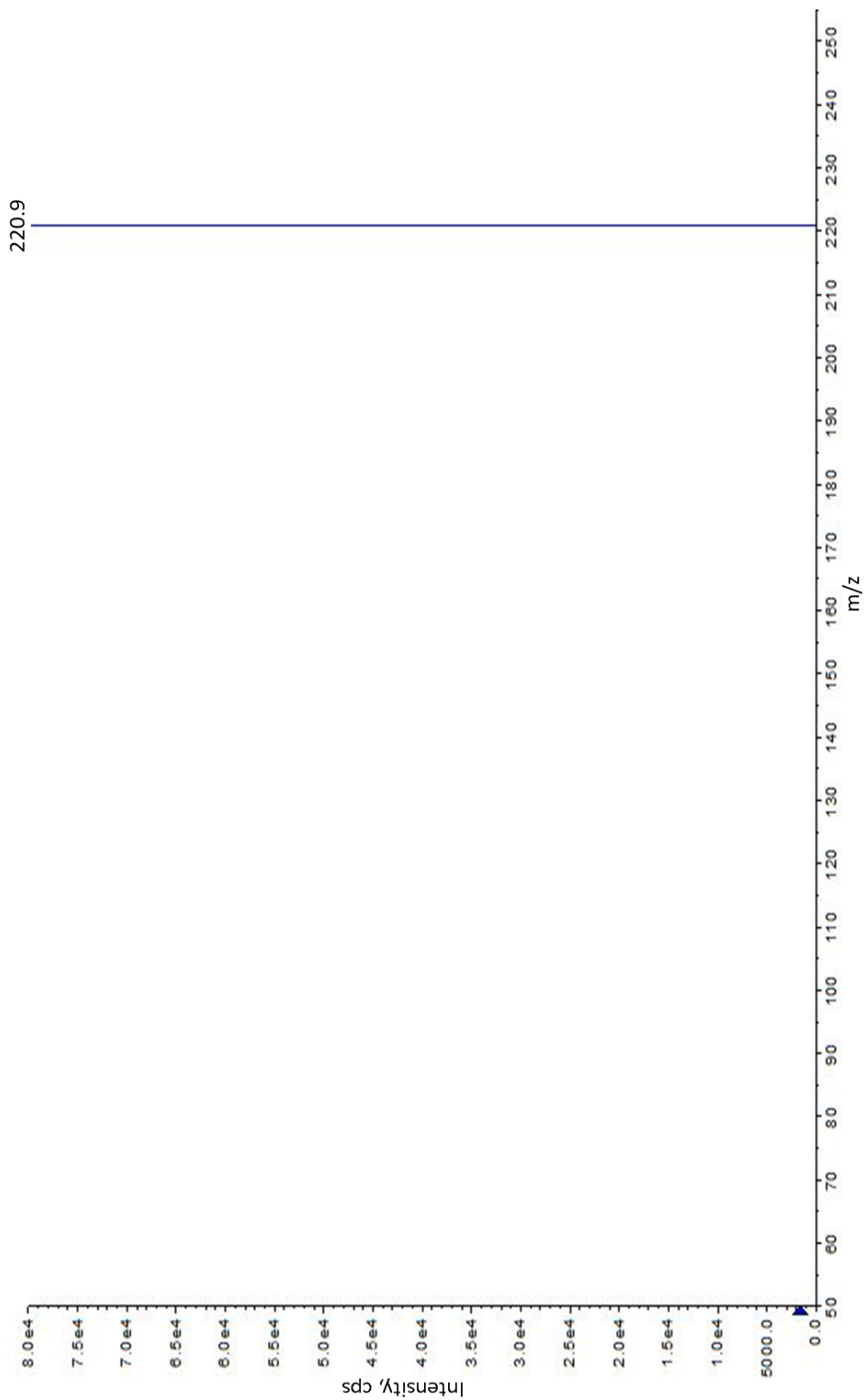


**Figure 32:** Carbon NMR spectra for compound **89**  
 $^{13}\text{C}$  NMR ( $\text{CDCl}_3\text{-d}$ )  $\delta$  = 23.68, 25.46, 27.34, 32.59, 49.34, 107.99, 109.78, 121.07, 159.91

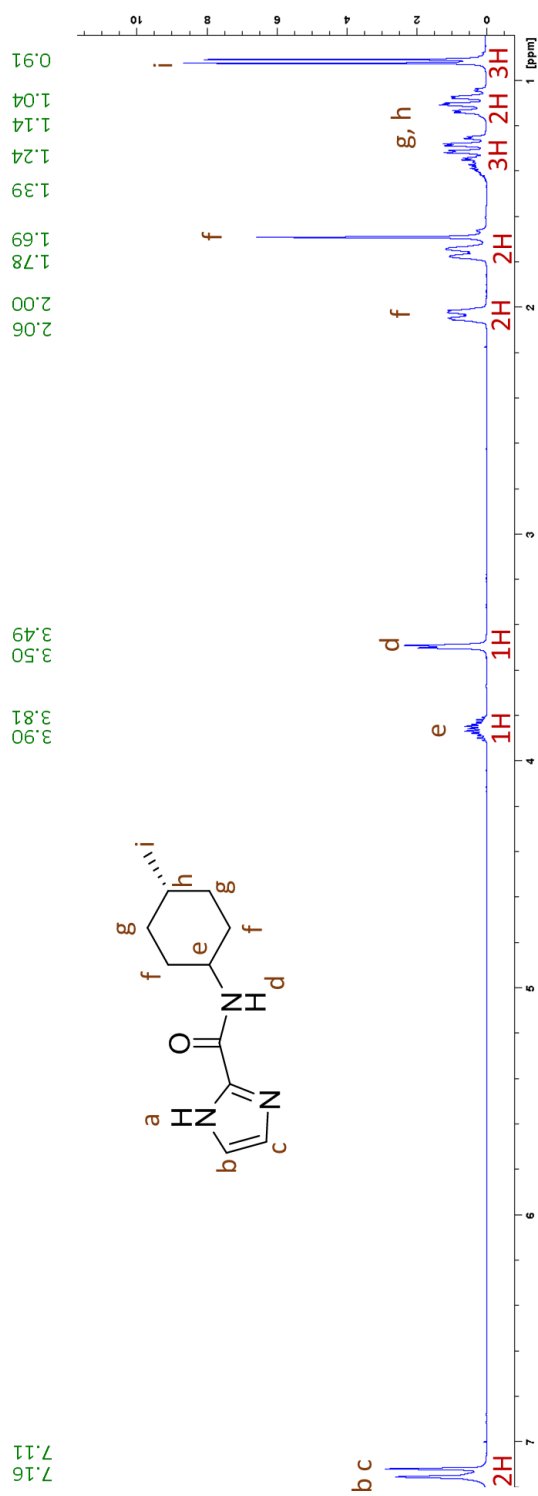


Parameters	
Mobile Phase	a) Water + 1% FA b) ACN + 1% FA
Column	50 x 3.0 mm C18 Kinetex
Flow Rate	1 mL/min
Run Time	10 minutes
Injection Volume	10 µl
Retention time	3.15 minutes
Gradient	20%- 70% ACN
Detector	Photo Diode Array (PDA)

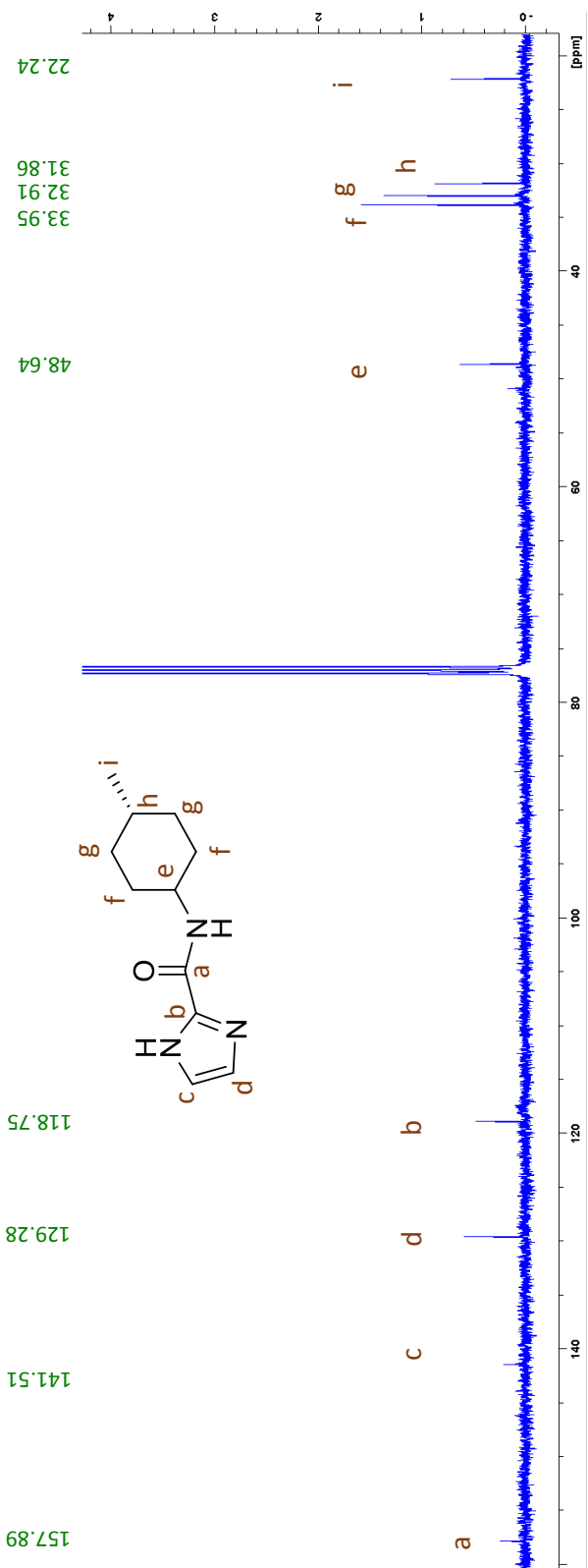
**Figure 33:** HPLC chromatogram and parameters for compound 89



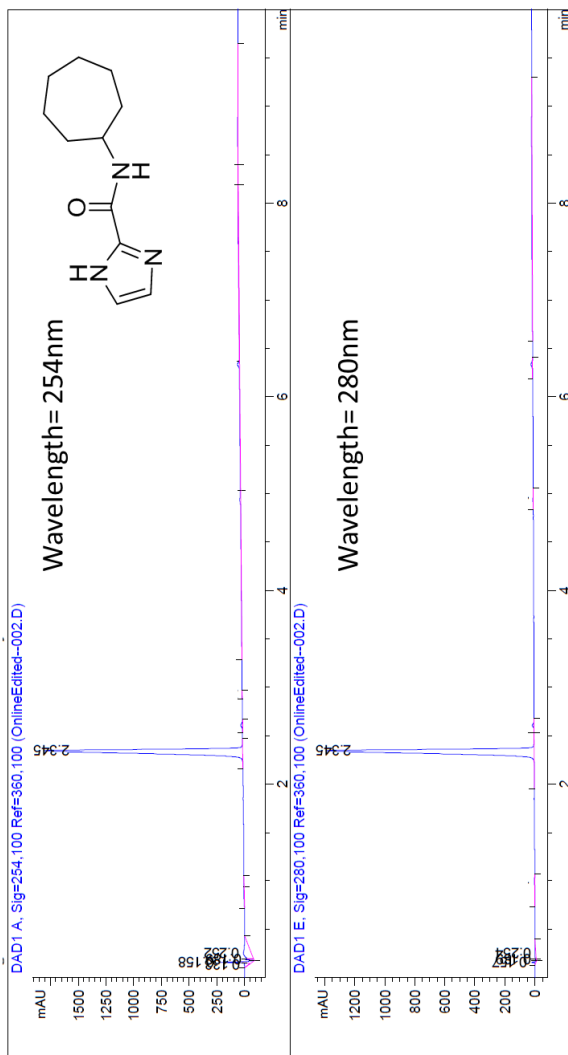
**Figure 34:** Mass spectra for compound **89**  
ESI-MS calculated for  $C_{13}H_{20}N_2O$ : 221.3, found: 220.9  $[M+H]^+$



**Figure 35:** Proton NMR spectra for compound **112** (Imidazole-2-carboxamide)  
<sup>1</sup>H NMR (CDCl<sub>3</sub>-d)  $\delta$  = 0.91 (d,  $J$  = 7 Hz, 3H), 1.04-1.14 (m, 2H), 1.24-1.39 (m, 3H), 1.69-1.78 (m, 2H), 2.00-2.06 (m, 2H), 3.49-3.50 (m, 1H), 3.81-3.90 (m,  $J$  = 4 Hz, 1H), 7.11 (s, 1H), 7.16 (s, 1H)

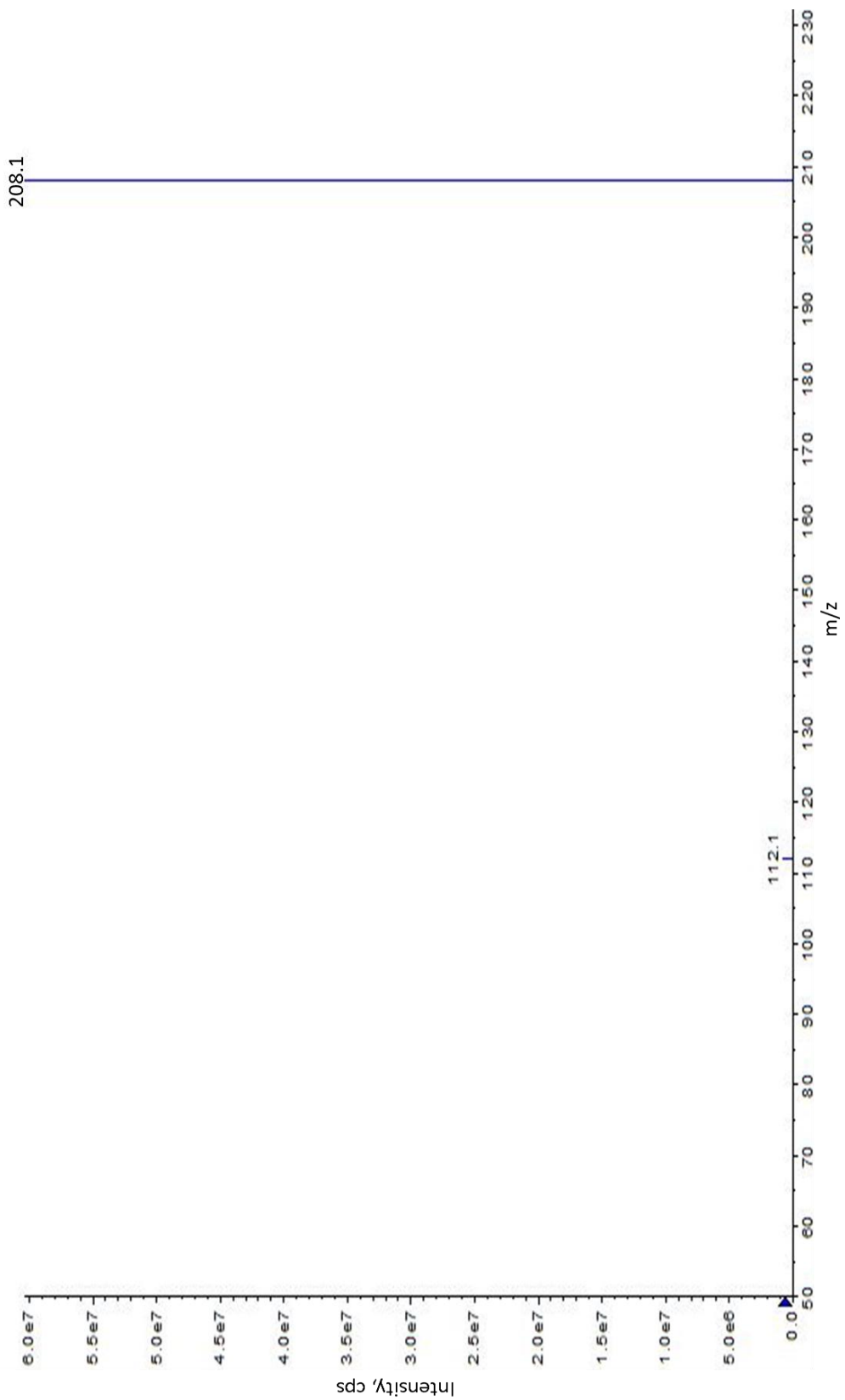


**Figure 36:** Carbon NMR spectra for compound **112**  
 $^{13}\text{C}$  NMR ( $\text{CDCl}_3\text{-d}$ )  $\delta$  = 22.24, 31.86, 32.91, 33.95, 48.64, 118.75, 129.28, 141.51, 157.89

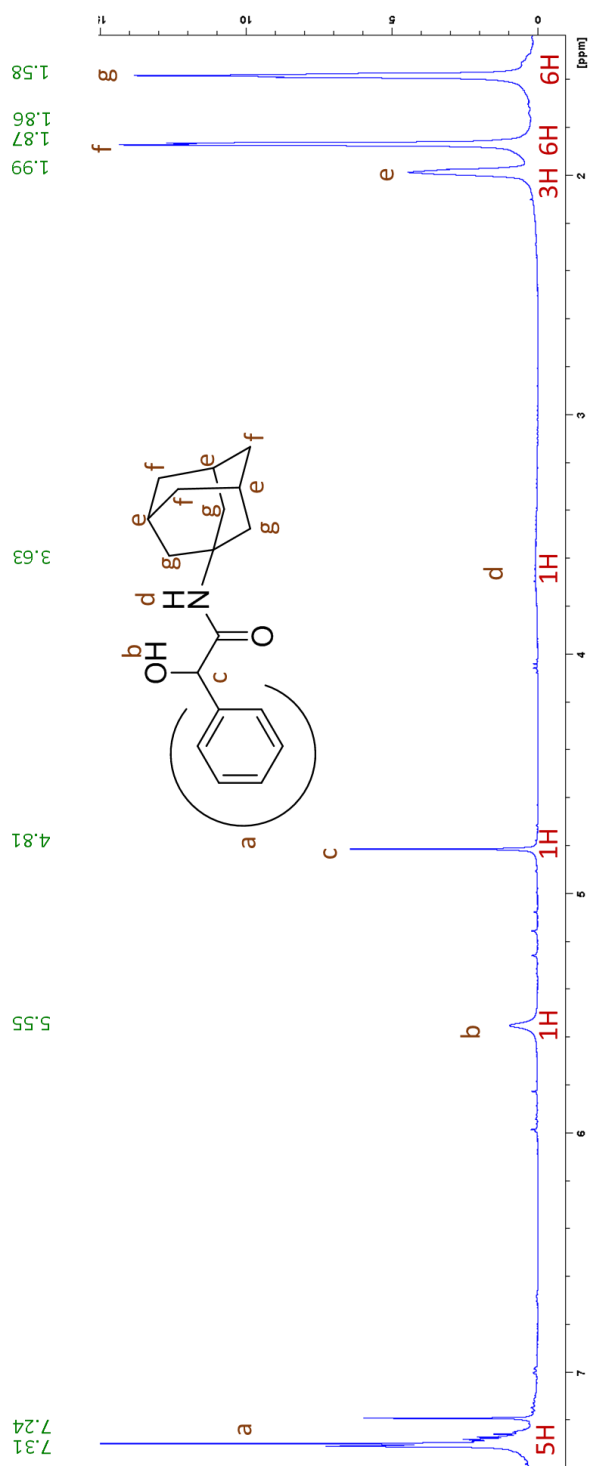


Parameters	
Mobile Phase	a) Water + 1% FA b) ACN + 1% FA
Column	50 x 3.0 mm C18 Kinetex
Flow Rate	1 mL/min
Run Time	10 minutes
Injection Volume	10 µl
Retention time	2.35 minutes
Gradient	20%- 70% ACN
Detector	Photo Diode Array (PDA)

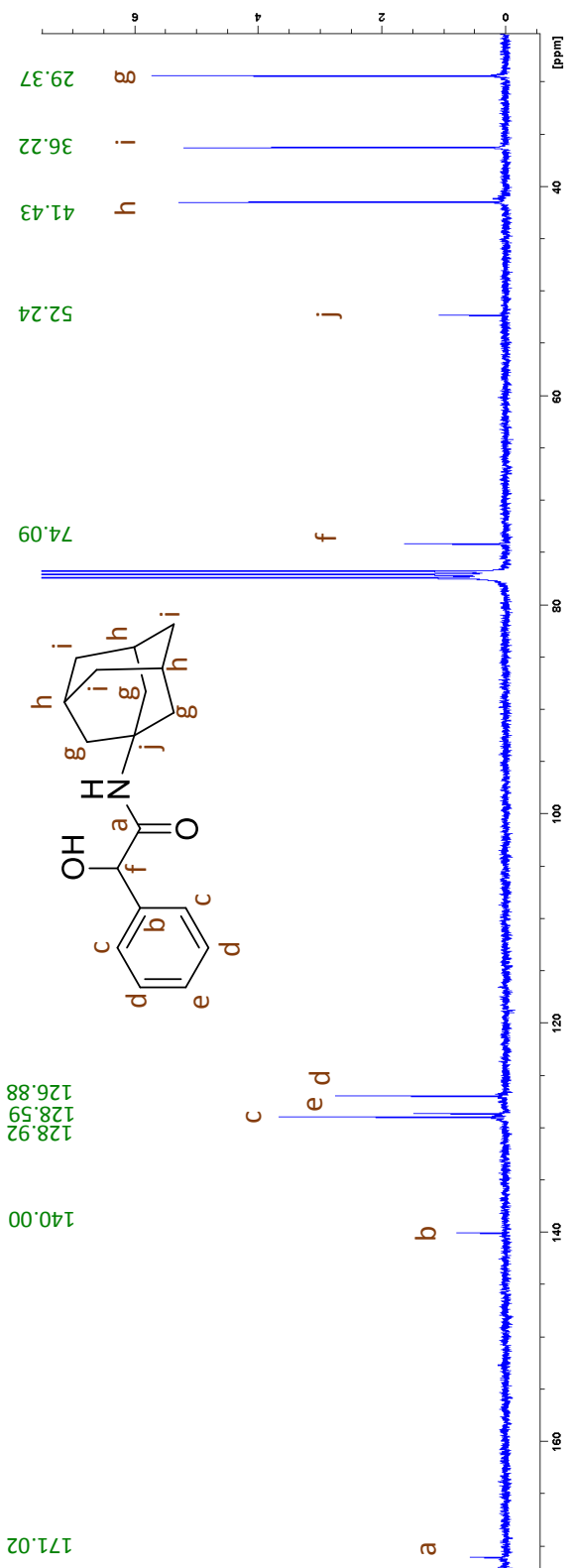
**Figure 36:** HPLC chromatogram and parameters for compound 112



**Figure 38:** Mass spectra for compound **112**  
ESI-MS calculated for  $C_{11}H_{17}N_3O$ : 207.3, found: 208.1  $[M+H]^+$

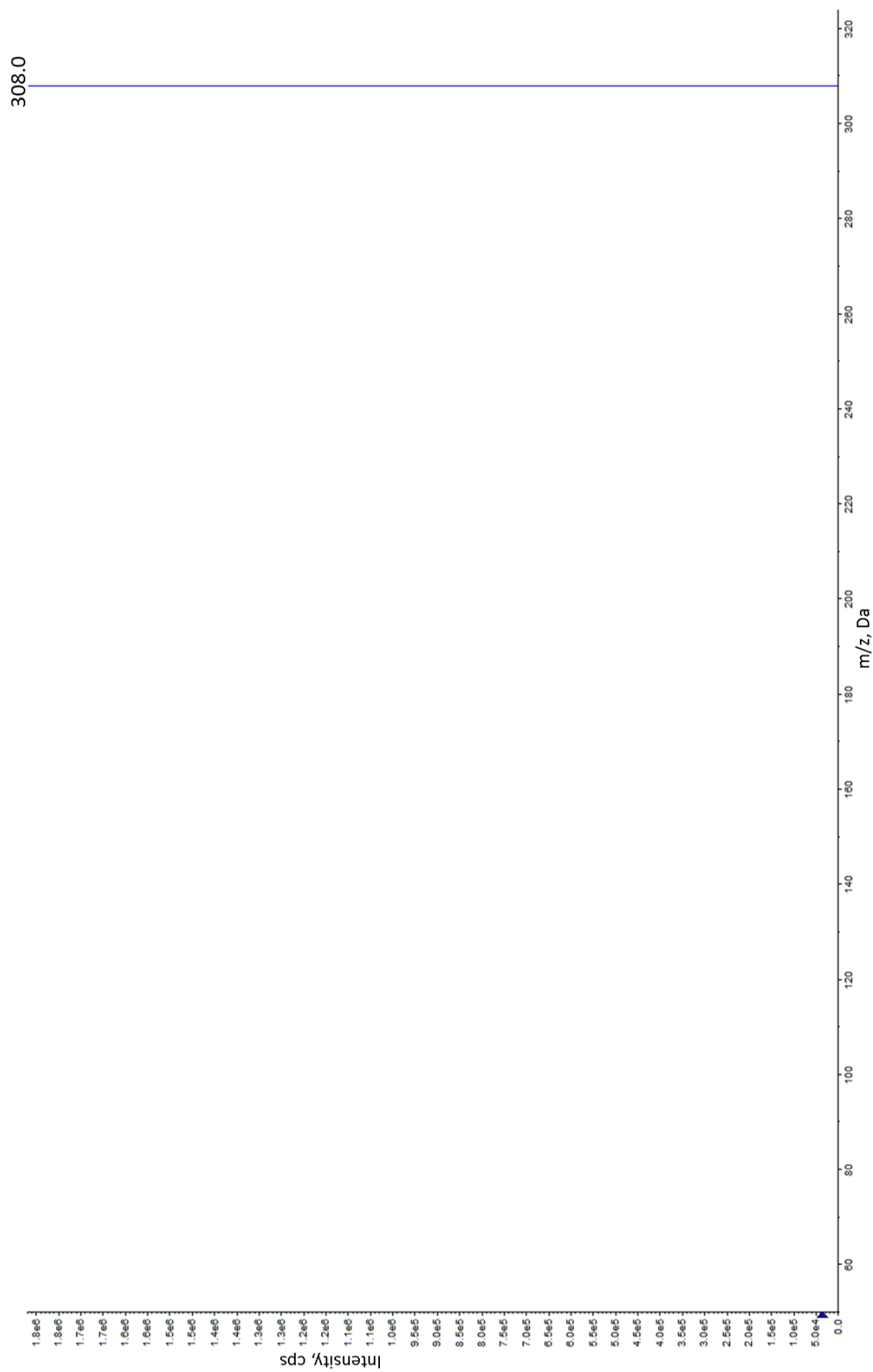


**Figure 39:** Proton NMR spectra for compound **103** (Racemic mandelic acid analog) <sup>1</sup>H NMR (CDCl<sub>3</sub>-d)  $\delta$  = 1.58 (s, 6H), 1.86-1.87 (m, 6H), 1.99 (s, 3H), 3.63 (bs, 1H), 4.81 (s, 1H), 5.55 (s, 1H), 7.24-7.31 (m, 5H)

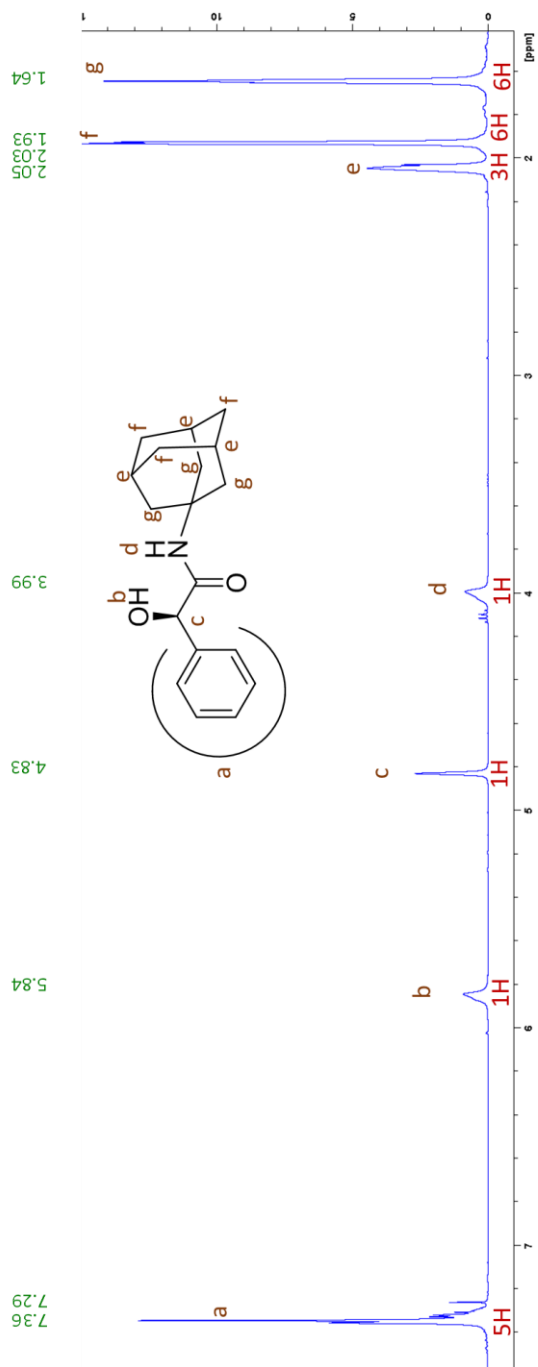


**Figure 40:** Carbon NMR spectra for compound **103**

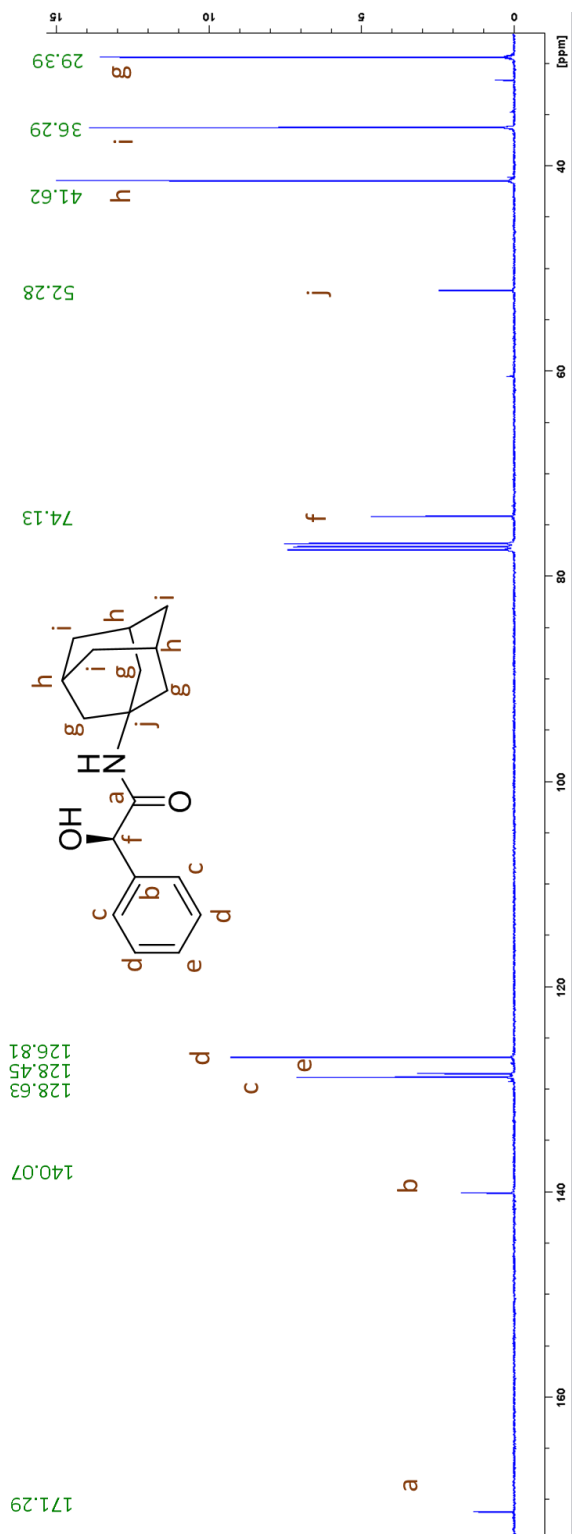
$^{13}\text{C}$  NMR( $\text{CDCl}_3\text{-d}$ )  $\delta$  = 29.37, 36.22, 41.43, 52.24, 74.09, 126.88, 128.59, 128.92, 140.00, 171.02



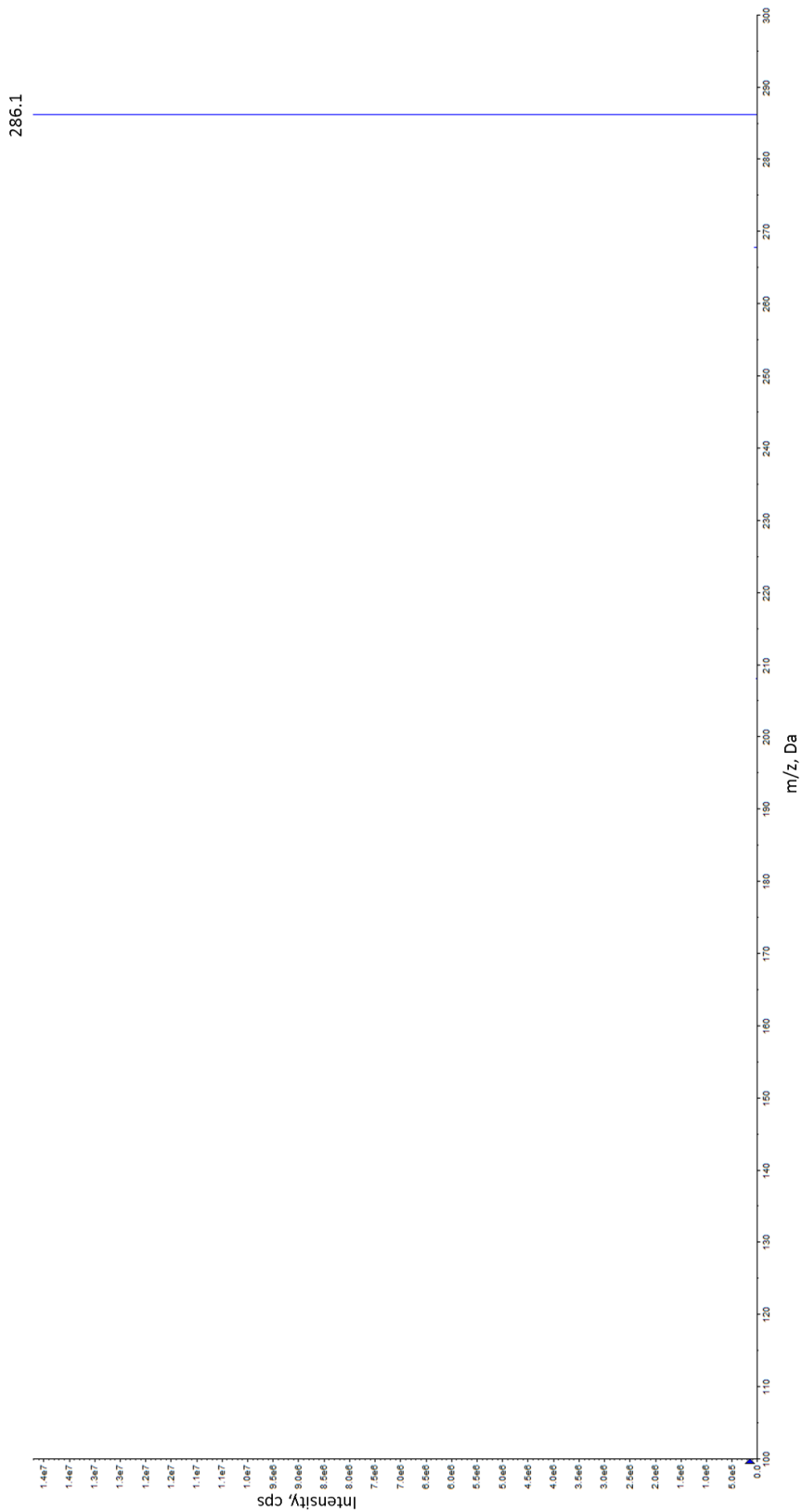
**Figure 41:** Mass spectra for compound **103**,  
ESI-MS calculated for  $C_{18}H_{23}NO_2$ : 287.4, found: 308.0 as  $[M+Na]^+$



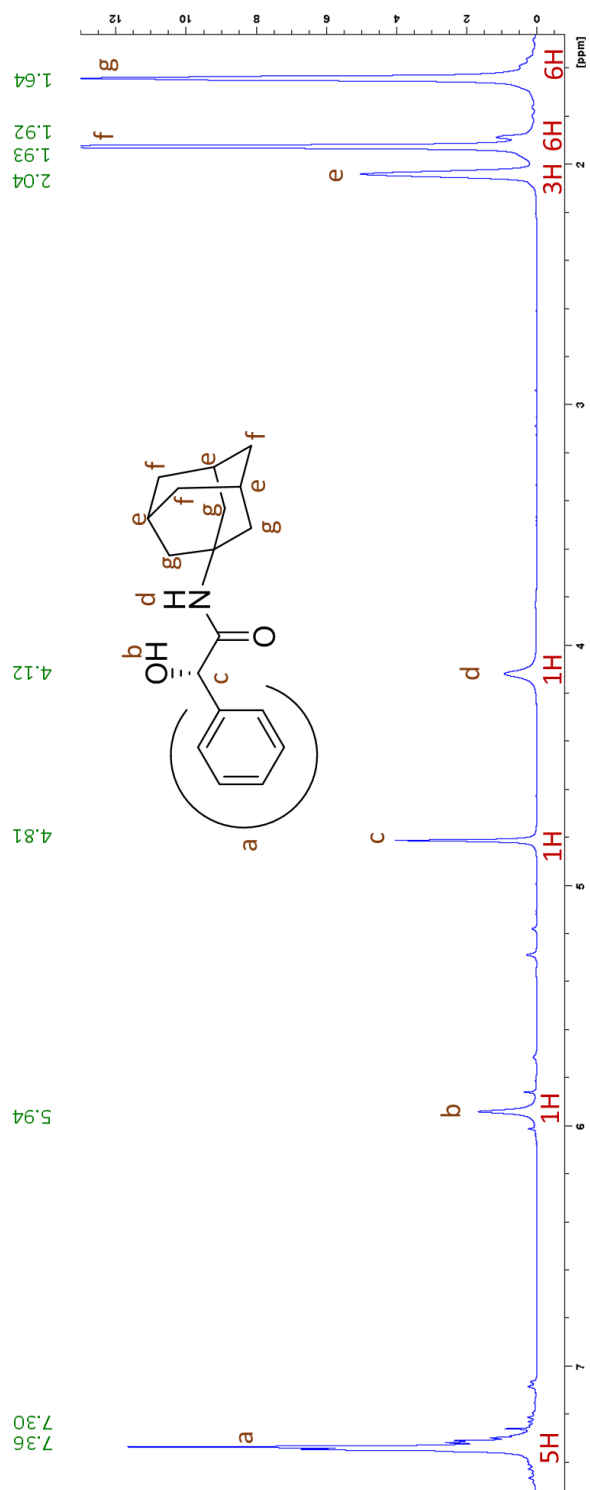
**Figure 42:** Proton NMR spectra for compound **121** (R (-) mandelic acid analog)  
<sup>1</sup>H NMR (CDCl<sub>3</sub>-d) δ = 1.64 (s, 6H), 1.93 (s, 6H), 2.03-2.05 (m, 3H), 3.99 (s, 1H),  
 4.83 (s, 1H), 5.84 (s, 1H), 7.29-7.36 (m, 5H)



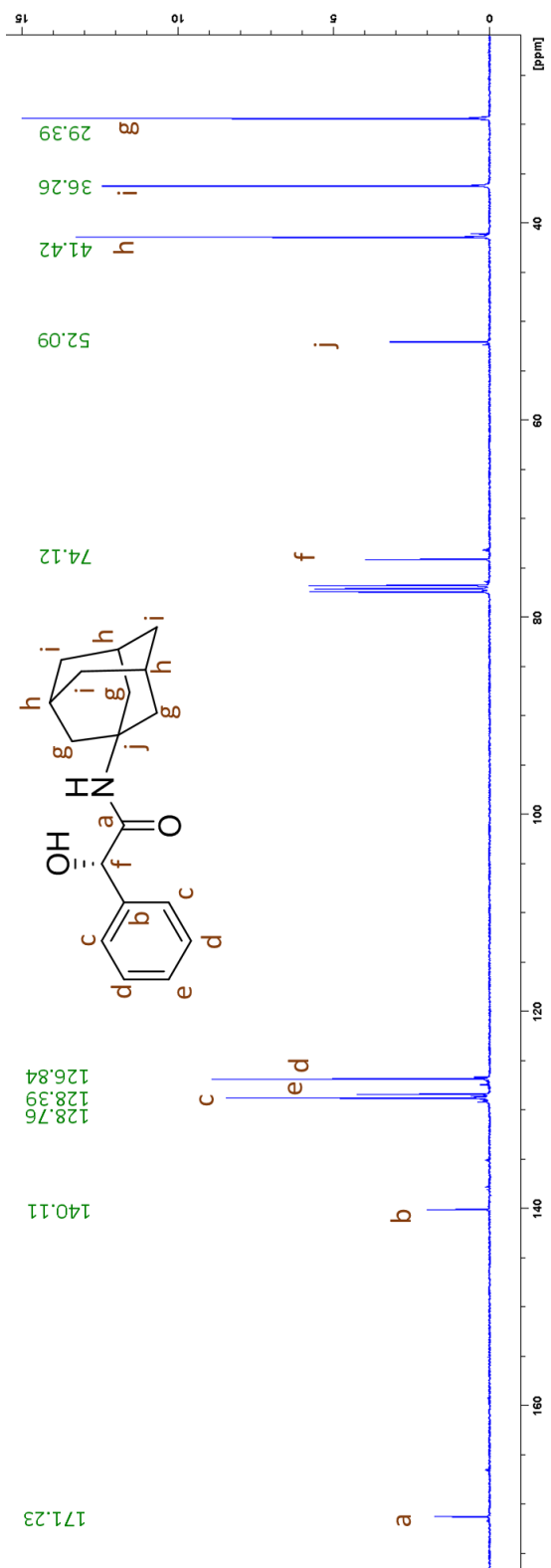
**Figure 43:** Carbon NMR spectra for compound **121**  
 $^{13}\text{C}$  NMR ( $\text{CDCl}_3\text{-d}$ )  $\delta$  = 29.39, 36.29, 41.62, 52.28, 74.13, 126.81, 128.45, 128.63, 140.07, 171.29



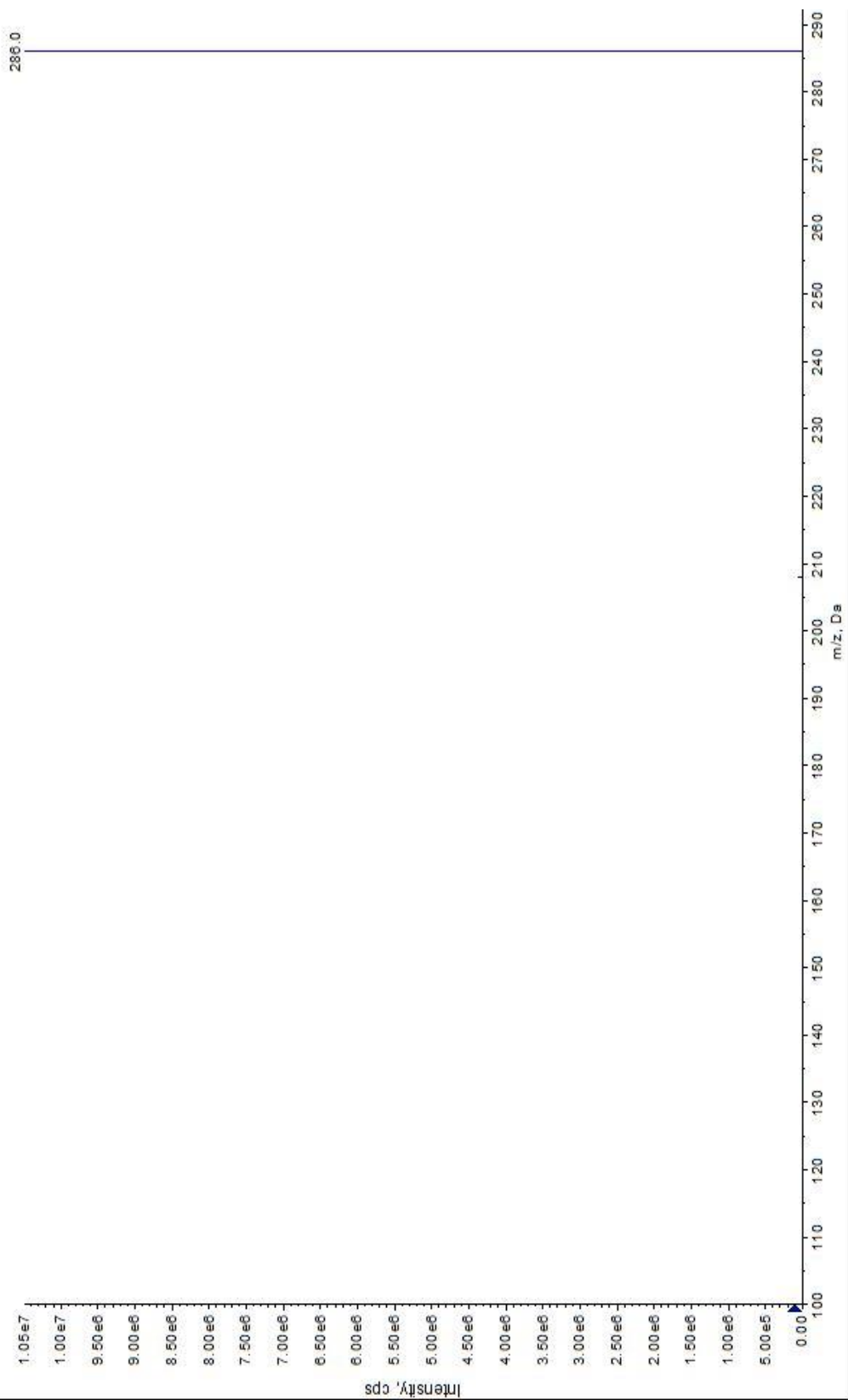
**Figure 44:** Mass spectra for compound **121**, ESI-MS calculated for C<sub>18</sub>H<sub>23</sub>NO<sub>2</sub>: 287.4, found: 286.1 as [M+H]<sup>+</sup>



**Figure 45:** Proton NMR spectra for compound **122** (S (+) mandelic acid analog)  
<sup>1</sup>H NMR (CDCl<sub>3</sub>-d) δ = 1.64 (s, 6H), 1.92-1.93 (m, 6H), 2.04 (s, 3H), 4.12 (s, 1H),  
 4.81 (s, 1H), 5.94 (s, 1H), 7.30-7.36 (m, 5H)



**Figure 46:** Carbon NMR spectra for compound **122**  
<sup>13</sup>C NMR (CDCl<sub>3</sub>-d) δ = 29.39, 36.26, 41.42, 52.09, 74.12, 126.84, 128.39, 128.76, 140.11, 171.23



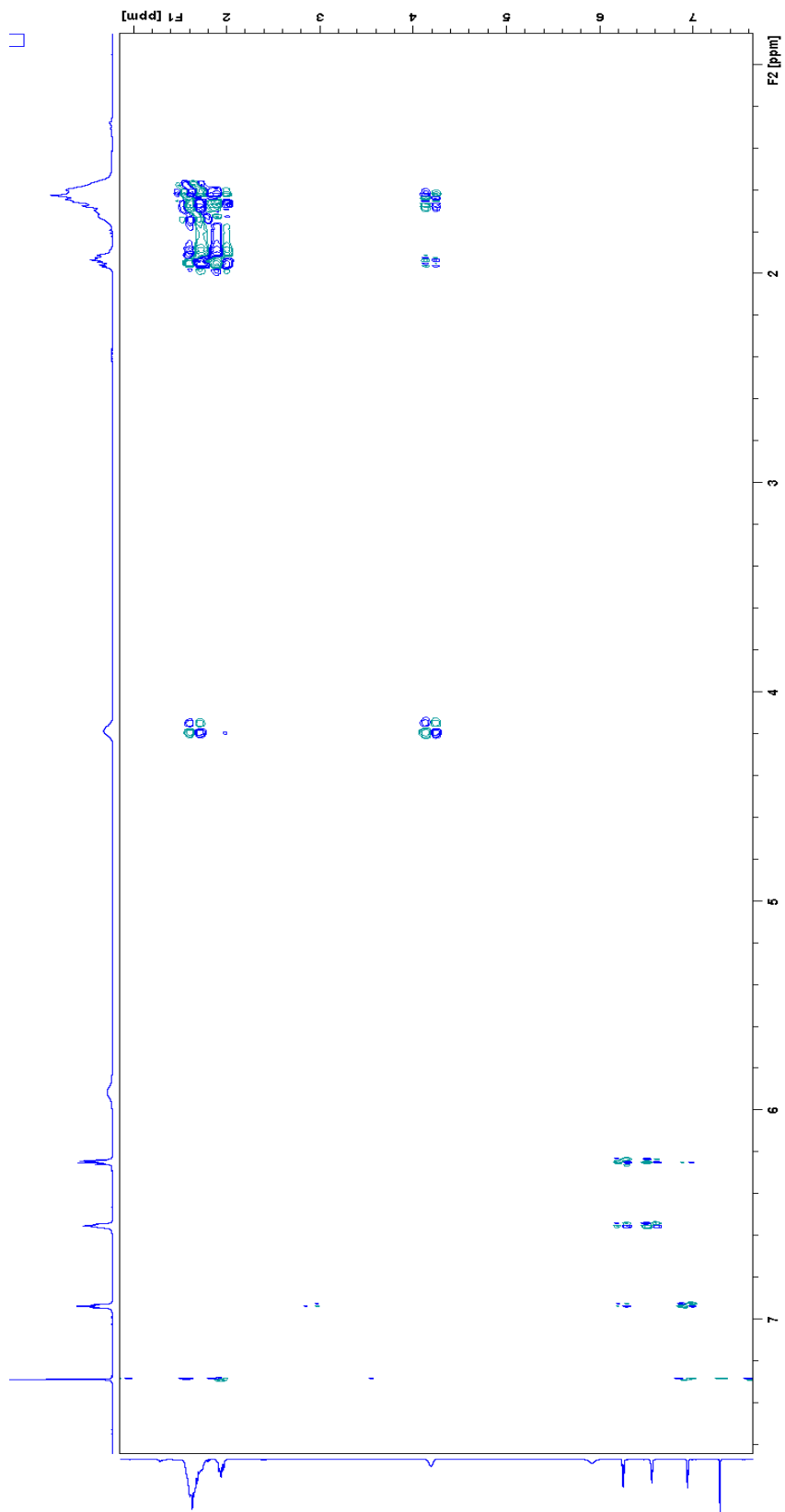
**Figure 47:** Mass spectra for compound **122**  
ESI-MS calculated for  $C_{18}H_{23}NO_2$ : 287.39, found: 286.0 as  $[M+H]^+$

NMR connectivity: One representative compound was analysed for its connectivity using a 1 and 2-dimensional proton NMR. With the help of the 2D NMR and the peak shape and peak splitting observed in the 1D proton NMR, the proton peaks have been assigned to specific protons.

The correlated protons can be identified from the 2D NMR. A proton-proton COSY experiment was run on North 89. Hence, the assignments of the proton peaks made with the help of the 1D NMR can be confirmed and validated with the help of the 2D NMR, shown in Figure 48. 2D NMR helps understanding the connectivity of vicinal protons to one another.

The 2D NMR was analysed after a long period of time and hence there are a few changes in some of the peak sizes in the proton NMR, which may be due to degradation caused over time. Therefore, the 2D analysis was performed for only one representative compound.

The assignments of the protons for the other compounds were carried out based on the 1D NMR for one representative compound from each series. The trend observed was the same within a specific mini-series of compounds.



**Figure 48:** 2D NMR trace for compound **89**.

Analysis for melting points: Differential Scanning Calorimeter (DSC) was used for analysing the purity of the compounds through their melting points. Sharp narrow peaks indicated purity of the compound. The observed melting ranges are tabulated below.

**Table 24:** DSC melting ranges for North compounds

North No.	DSC: Melting range (in °C)
77	No sample left
78	Degradation, No peak
88	155.35-159.83
89	152.05-158.28, broad peak at 209.29-254.17
95	130.48-135.99
96	195.91-204.80, broad peak at 216.98-259.84
98	130.84 -135.84, 181.22-185.89
101	Broad peaks at 93.76-107.45, 234.20-278.02
102	125.01-129.43
103	Broad peak at 97.78-112.47
104	231.47-236.32
105	196.06-201.00
106	181.54-186.31
108	203.74-208.48
109	207.41-212.92
110	No sample left
111	Poor baseline, 146.80-152.10
112	270.38-274.95
117	Oily sample
118	Oily sample
119	Oily sample
120	144.00-151.17, broad peak at 264.09-297.39
121	137.04-145.74, broad peak at 250.39-295.72
122	No sample left
123	149.84-164.93, broad peak at 271.12-325.87
124	Broad peak at 232.65-319.81
125	No sample left
126	96.87-103.42
127	Broad peak at 195.31-234.49
128	No sample left

Sharp melting peaks were observed for most compounds. However, these peaks had an early onset and results were reported for a range of 5 degree Celsius, due to the sensitivity of DSC.

Broad peaks indicative of multiple other endothermic processes including degradation were observed for few of the compounds at higher temperatures.

The melting point experiment could not be performed for a few compounds, **77, 110, 125** and **128**, since not enough sample was available for the experiment.

Compounds **117, 118** and **119** were not tested, since they were of oily consistency.